Final report for AFOSR 2005

Title: Study on Wide-gap Gallium-nitride Based Films and Their Quantum-dots Devices

Contractor (PI): Huey-liang Hwang (PI)

Nano Technology & MEMS Center and Institute of Electronic Engineering, National Tsing Hua University Hsinchu, 300 Taiwan, R. O. C.

E-mail: hlhwang@ee.nthu.edu.tw

Research Team: *Jung-Min Hwang* Ph. D., Brian Yei, kuan-feng Lee

Institute of Electronic Engineering, National Tsing Hua University

E-mail: d889011@alumni.nthu.edu.tw

Report Documentation Page

1. REPORT DATE **05 SEP 2006**	2. REPORT TYPE **Final Report (Technical)**	3. DATES COVERED **23-06-2004 to 01-08-2005**

4. TITLE AND SUBTITLE	5a. CONTRACT NUMBER
Study on Wide-gap Gallium-nitride Films and Their Quantum dots Devices	5b. GRANT NUMBER
	5c. PROGRAM ELEMENT NUMBER
6. AUTHOR(S) **Huey-Liang Hwang**	5d. PROJECT NUMBER
	5e. TASK NUMBER
	5f. WORK UNIT NUMBER

7. PERFORMING ORGANIZATION NAME(S) AND ADDRESS(ES) **National Tsing Hua University,101, Sec. 2, Kuang-fu Road,Hsinchu ,TAIWAN,TW,300**	8. PERFORMING ORGANIZATION REPORT NUMBER **AOARD-044071**

9. SPONSORING/MONITORING AGENCY NAME(S) AND ADDRESS(ES) **The US Resarch Labolatory, AOARD/AFOSR, Unit 45002, APO, AP, 96337-5002**	10. SPONSOR/MONITOR'S ACRONYM(S) **AOARD/AFOSR**
	11. SPONSOR/MONITOR'S REPORT NUMBER(S)

12. DISTRIBUTION/AVAILABILITY STATEMENT
Approved for public release; distribution unlimited

13. SUPPLEMENTARY NOTES

14. ABSTRACT
Wide-gap III-Nitride based white light emission had been proven to yield luminescence efficiency (20-30 Lumen/W) and the III-Nitride devices proved long lifetime (>10khr). It is expected that high efficiency III-Nitride based white light emission will be the major lighting source for daily illumination in the coming decades. In 1998, the world energy consumption of energy is 6.9×10^4 TWh. There had been 2.3×10^3 TWh consumption in illumination with rather inefficiently way. To further largely improve the luminescence efficiency beyond 100 Lumen/W and to increase thermal stability of the III-Nitride based LED, devices in the quantum structure is the viable way to pursuit.

15. SUBJECT TERMS

16. SECURITY CLASSIFICATION OF:			17. LIMITATION OF ABSTRACT	18. NUMBER OF PAGES **12**	19a. NAME OF RESPONSIBLE PERSON
a. REPORT **unclassified**	b. ABSTRACT **unclassified**	c. THIS PAGE **unclassified**			

Chapter 1.

Introduction

1-1. Introduction

Wide-gap III-Nitride based white light emission had been proven to yield luminescence efficiency (20-30 Lumen/W) and the III-Nitride devices proved long lifetime (>10khr). It is expected that high efficiency III-Nitride based white light emission will be the major lighting source for daily illumination in the coming decades. In 1998, the world energy consumption of energy is 6.9×10^4 TWh. There had been 2.3×10^3 TWh consumption in illumination with rather inefficiently way. To further largely improve the luminescence efficiency beyond 100 Lumen/W and to increase thermal stability of the III-Nitride based LED, devices in the quantum structure is the viable way to pursuit.

The efficiency of the conventional wide-gap III-Nitride based white light emission with a multi quantum well (MQW) structure of III-nitride device was typically limited to 20 to 30lm/w due to the low Wall-Plug-Efficiency (WPE) as-depicted as follows

$$\textbf{WPE} = \eta_{in} * \eta_{ext} * \eta_{el}$$

Where WPE is the Wall-Plug-Efficiency, η_{in} is the internal quantum efficiency, η_{ext} is the extraction efficiency, and η_{el} is the electrical efficiency. There are three dominant limiting factors to WPE in the III-nitride device.

1-1-1. the η_{in} issue associated with threading dislocations in the III-Nitride

For fabricating the III-Nitride based LED or laser, the GaN/ $In_xGa_{1-x}N$ multi quantum well (MQW) structure was grown on the GaN. [1] The threading dislocations will penetrate through the MQW from bottom layer of GaN to the top surface of p-GaN. The nanotubes, screws and mix dislocations could penetrate through the InGaN MQW. The recombination center in dislocations will reduce the internal quantum efficiency of the device. The injected electron-hole pair will recombine inside the diffusion length around the dislocation as mentioned above. There had been a special case with the edge dislocation in dislocation penetration. The V-defect is a V-pit with {10-10} plane and initiated from the threading edge dislocation. If p-GaN is post growth at high temperature, these pits will be subsequently filled. [2]. It is found that threading dislocation and V-shaped pits act as the nonradiative recombination centers in InGaN single quantum well structure. It was proposed that the nonstoichiometry and impurity segregation in threading dislocation could produce the gap

state inside InGaN or GaN. From the cathodoluminescence mapping measurement, the minority carrier diffusion length (MCDL) around the dislocation could be calculated. The relationship of dislocation density to luminescence efficiency could be calculated. [3] We calculated the dislocation density as a function of the relative emission efficiency with different diffusion length and different diameter of the non-radiative recombination center. If the dislocation density could be reduced to 10^6-10^7 cm^{-2}, the η_{in} efficiency will be higher than 90%. The traditional growth GaN with buffer layer method could produce the GaN with dislocation density 10^9-10^{10} cm^{-2}, The ELO of GaN method could reach, but the fabrication process was too complex. The high pressure and high temperature synthesis could produce single crystal GaN substrate with ultra low dislocation density ($100cm^{-2}$), but the method was not so efficient for application. We need a new method to prevent the dislocation from reducing the efficiency with simple process and high efficiency for application.

1-1-2. the η_{ext} issue associated with light extraction in the III-Nitride device

The high refractive index of GaN will confine photons inside the semiconductor cavity. The light extraction (n=2.4 at λ=475nm) from the cavity with spontaneous emission will was follow the calculation of $(4n^2)^{-1}$ between GaN and air. The critical angle of the total reflection is ~24.7^o . The low η_{ext} is caused by the light confinement in the light emission device with a high refractive index (n) grown on sapphire substrate. The extraction efficiency of the conventional square device structure is about 16%. The light is extracted from the bottom, edge sidewall and transparent electrode on the top contact.

1-1-3. the η_{el} issue associated with operation voltage in the III-Nitride device

The low η_{el} caused by the high series resistance, which contain the contact resistance, material bulk resistance and spread resistance. The non-uniform current distribution with current crowding effect is due to current transport on the non-conductive sapphire substrate. To discuss the η_{el} issue [4], the GaN/InGaN structure with lateral current path and equivalent circuit model used. The parameters of this structure are shown as follows:

Doping concentration: N_A=3x$10^{18}$$cm^{-3}$, N_D=5x$10^{18}$$cm^{-3}$
Mobilities: μ_p=9cm^2/Vs, μ_n=200cm^2/Vs,
Resistivity :ρ_p=0.2Ωcm, ρ_n=6.3x10^{-3} Ωcm
Specific contact resistance : ρ_c=$10^{-4}$$\Omega cm^2$ for p-type, ρ_c=$10^{-6}$$\Omega cm^2$ for n-type
Layer thickness : t_p=0.2μm for p-type, t_n=2μm for n-type

 The current spreading length (Ls) is indicated as;

Ls=sqrt (($\rho_{c+}\rho_p t_p$)t_n/ρ_n)

From calculation with material parameter and designated device structure, the Ls are equal to 18.2μm. The current density distribution along the x direction is shown as;

$J(x) = J(0) \exp(-x/Ls)$.

If the device scale is smaller than 1 μm, the current density ratio will be higher than 90% and the current crowding effect could be ignored. If we increase the ρ_c, ρ_p, t_p, t_n, the Ls could be increased, but the heat generation of the device will be increased. The transport resistance of n-type layer R_p, p-type layer R_n and p-type contact resistance R_c is shown as follows.

$R_p = \rho_p t_p / L_p\ w$

$R_n = \rho_n L_n / w\ t_n$

$R_c = \rho_c / L_p\ w$

Where L_p is the contact length, L_n is the distance from the center of n-type contact to the center of the p-type contact. w is the device width.

Design of the device geometry could be improved by the thermal generation and current crowding effect. For example, for the device structure A ($L_n=1\mu m$, $L_p=2\mu m$, $w=2\mu m$), the $R_p=100\Omega$, $R_c= 2.5\times10^3\Omega$ and $R_n=15.75\Omega$, and the vertical resistance ($R_v=R_{p+}\ R_c$) is equal to $2.6\times10^3\Omega$. For device structure B ($L_n=3.5\mu m$, $L_p=5\mu m$, $w=100\mu m$), the $R_p=0.8\Omega$, $R_c= 20\Omega$ and $R_n=1.1\Omega$, and the vertical resistance ($R_v=R_{p+}\ R_c$) is equal to $20.8\tilde{\Omega}$

For sample A and B, as w and L_p increase, the emission area in the wafer increases, but the R_v/R_n ratio decreases, and the thermal resistance increases with the flip chip device. From the above discussion, device in smaller structure will produce low operation voltage due to the reduced serial resistance and the current crowding effect. Nano device with flip chip structure could also provide low thermal resistance due to the large surface area contact to the heat sink. Optimization of the structural geometry could help to get the better performance in the electrical, optical and thermal stability of the smaller device.

1-1-4. The WPE issue in the III-Nitride nano device

For the nano-dots structure for LED or laser, the WPE will be largely increased. While the dot size is smaller than 50nm and the dot spacing is smaller than 50nm. The dot density will be higher than $10^{11} cm^{-2}$. which will be higher than the conventional dislocation density $(10^7 \sim 10^9 cm^{-2})$, and the η_{in} will be higher than 90%.

With nano-dots embedded in the activation layer, the spontaneous rate will be enhanced by a Factor and the η_{el} will also be increased, due to the Purcell effect with micro-cavity, as indicated in the equation shown below.

Factor=$3\lambda^3Q/4\pi2V$

Where λ is the wavelength, Q is the quality factor, and V is the cavity volume. The η_{el} could be increased due to the low serial resistance of nano device as discussed above. The η_{ext} could be largely increased to 70% with the photonic crystal structure [5] or rough cavity structure [6] or the nano-dots embedded in the activation layer.

The WPE of the nano dot device could be estimated to 57.9% (λ=450nm, V_{op}=3V, η_{in} =90%, η_{ext} =70%, η_{el}=92%) for blue emission from the GaN based quantum device. The WPE could be estimated to 47.3% (λ=550nm, V_{op}=3V, η_{in} =90%, η_{ext} =70%, η_{el}=75%) for green emission from the GaN based quantum device. The WPE could be estimated to 38.3% (λ=680nm, V_{op}=3V, η_{in} =90%, η_{ext} =70%, η_{el}=61%) for red emission from the GaN based quantum device. If the white light emission was composed with one red, green and blue emission device with the same power intensity, the efficiency could reach 115 Lumen/W by a simple estimation of this white light emission of the nano-dot structure device.

If the dot size is further reduced from10nm to 1nm, the quantum confinement effect will be more pronounced for band gap increase in the III-Nitride based quantum dot device. The Wang's group [7] calculated the eigen-energy of InN quantum dot imbedded in a GaN matrix, the energy transition from the conduction-band minimum (CBM) to the valence-band maximum (VBM) could be changed from 1.9eV (red light) to 2.8eV (blue light) by a change of the dot size from 4nm to 2nm. By Controlling the InN dots size distribution in the activation layer, the emission spectrum could be controlled and the white light emission in a diode could be achieved. The dot size controlled quantum device could produce high Color Rendering Index (CRI), the Rendering average (Ra) could reach 100% by well control the emission spectrum with the dot size control. The color temperature (CT) could also be controlled by the method. Finally we could propose that the size controlled GaN based quantum dot LED for the prospective white light source cold be used to simulate the sun light for higher Lumen/W. From the above discussion, the quantum dot devices could produce high efficiency for the LED application. By controlling the dot size and their compositions, the quantum dots of InGaN or InN could emit light to cover the whole visible spectrum. The quantum dot based white light device could be made in one diode.

1-1-5. Application of the GaN based quantum dot device

The quantum dot array could also be applied for the quantum dot or wire laser. The quantum dot or wire laser has the superior characteristics in theory for the III-Nitride based

device application, for example, include the lower threshold current density, thermal stability, high differential gain, reduced stokes effect by piezoelectric field, sharp line width and high frequency modulation. The quantum dot device have great application potential for the white light source, high density optical data storage with short wavelength laser, optical communication, wireless communication under the ocean with blue laser and bio-technology application with UV laser source.

1-2. Key issues for the nano structure device fabrication

There are two key process issues to affect the quantum dot device performance. One is the etching induced damage. The etching damage creates surface state or interface state on the quantum dots with high surface to volume ratio. These states will capture the injection carrier and then recombine. The process induced damage on surface will reduce the η_{in}. For the device consideration, the high recombination energy loss in the region of high carrier injection will decrease the η_{in} and produce large amount of heat. The cavity will be degraded due to the thermal oxidation. The recombination loss near the activation layer dominates in the diffused minority carrier. There is also the scattering induced energy loss in the side wall with rough etching profile. The etching induced damage will increase the energy loss and increase the temperature of the device. The device efficiency and reliability will be decreased due to the elevated temperature. The damage free etching method then become the essential tools for the nano or quantum device fabrication.

The other issue is the dot size control and position control. It requires high quality facility and high operation skill to control the dots size and position in the fabrication process, for example the electron-beam lithography method or atom manipulated by scanning probe microscopy. There is low through put for mass production at this stage. So the self-assemble quantum dot methods [8] have been recently developed. Although the quantum dots could be grown by control the growth mechanism for mass production. They are poor in the dot size control and distribution control. Without very precise control of the dot size and position, control of the emission wavelength and resonance condition for the quantum dot laser or the device precise characteristic could not be realized. Arakawa's group also developed another method for the position control. To pattern the substrate by photolithography and then to overgrow the dots for the dot position control, in which the dot position could be control well, but the size control was poor.

Our approach for the size controlled quantum dot LED was developed in nano-lithography and damage free etching. The quantum dot device will be fabricated by combination of the nano-masking tools and damage-free etching tools. Nano-masking was applied to determine the dot size and position and the damage-free etching was applied to determine the device structure. Our lab had developed two kinds of nano-mask tools. One is the electrochemical scanning probe microscopy (EC-SPM) lithography and the other is the Electron beam

lithography. We also developed three method of damage free etching for the nano-scale etching. The first one was the photo-assisted cryogenic (PAC) etching, the second are was the photo-assisted wet etching and the third one was the electrochemical atomic force microscopy (EC-AFM) direct etching.

### 1-2-1. Nano-scale masking technology

1-2-1-1. EC-SPM lithography

Scanning Tunneling Microscope (STM), invented in 1982 by Gerd Bining and Heinhrich Rochrer, could, be used in both nano dots making and nano-scale material characterization. The recent development of multiple tips AFM by the MEMS techniques (Calvin F. Quate, Stanford University) provides a tool for the volume production of nano devices. However, the conventional STM approach should be altered, and the STM process could take place in the electrochemical solution enviroment (instead in UHV), otherwise it would hinder the dot fabrication in the industrial scale. EC (Electrochemical)-SPM can therefore meet the challenge for the low-cost, nano structure fabrication and patterning.

The advantages in the use of SPM in electrochemical solution are the concurrent proceeding in the etching, oxidation and electroplating steps. Furthermore, most of the nano structure fabrication tasks could be accomplished by proper manipulations of the EC-SPM, because the electrical, physical and mechanical phenomena are all involved with the additionally incurred electrochemical reactions. Techniques like the Jump-to-contact method (developed by D.M. Kolb) and the Nernst's Equation will be followed.

1-2-1-1-1. Titanium oxidation by EC-STM

There are three cases of oxidation depending on the tip-sample gap and humidity in air. 5nm Ti film was deposited on GaN, and EC-SPM was applied to oxidize Ti into TiOx. After oxidation, the diluted HF solution was used to remove the Ti and then the nano Ti oxide mask was formed. The electrochemical reaction between tip and water is

$$4H^+ + 4e^- \Leftrightarrow 2H_2$$
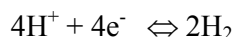
The electrochemical reaction between titanium and water is

$$Ti + 4h^+ + 2H_2O \Leftrightarrow TiO_2 + 4H^+$$

Ti was oxidized with different bias and pulsed duration. The TiOx dot was selectively oxidized at different positions by manipulating the tip of STM. After the tip-sample gap was selected, the pulsed bias was applied. The condition of the applied bias was 4, 5 and 6 volt and the duration was 0.5, 0.01 and 0.005 sec.

The height of TiOx dot was linearly proportional to the applied bias with different duration. The Ti oxidation was related to the ion migration of the O^-, OH^- and positive Ti ions. The applied bias increased electrical field between the tip and sample, high electrical field drift the ion to the interface. While the applied bias was higher that the threshold voltage (2.55~3.5V in our system), the oxidizing agent could be enhanced to diffuse into the Ti and react with Ti to form TiOx. The applied bias will produce electrical field at the tip-sample, the electrical field distribution depends on the geometry of the tip and sample and the electrical field strength depends on the applied bias and the sample material. The electrical field was defocused under the tip and the Ti will be oxidized under the threshold electrical field. While the applied bias was increased, the range of threshold electrical field will increase too. The size of TiOx was linearly proportional to the applied bias. The smallest TiOx size was about 100nm. Shorter pulsed duration or reduced defocus of the electrical field by the insulating coating could reduce the TiOx dot.

1-2-1-1-2. Copper disposition with jump-to-contact method by EC-STM

The in-situ observation of copper deposition and dissolution in solution (5mM$CuSO_4$+0.1N H_2SO_4) could be achieved by controlling the bias direction between HOPG and electrolyte. After the substrate was applied the negative bias, Cu^{2+} start to reduce to Cu atom and is absorbed on the HOPG surface. The Cu dot size was about 20nm. While we applied 100mV positive bias, the Cu nano cluster was dissolved into the electrolyte. The EC-STM scans over the HOPG surface after the dissolution and identify the Cu cluster dissolved. By controlling the substrate bias, in-situ observation of the copper deposition and dissolution could be achieved in the EC-STM system.

In our experiment system, the copper was deposited on the gold film. By applied the pulsed voltage to the z-piezo, the absorbed copper on the tip will be transferred to the gold film. The deposited copper size and height vs. pulsed duration. The copper dot size could be controlled from 150A to 450A by controlling the applied pulsed duration time. With longer duration, more copper atoms could be transferred to the gold substrate. 20nm copper dot array was demonstrated in the 2D and 3D images.

1-2-1-2. Electron beam lithography

The Polymethylmethacrylate (PMMA) was purchased from MicroChem (MCC). It is diluted with chlorobenzene to get the thinnest thickness after coating. The PMMA coating on GaN samples was pre-spinning at 1000rpm for 10 seconds then spun at 3000rpm for 50 seconds. The stable spin thickness of PMMA film was about 100nm. After coating, the sample was Pre-baked at 170^oC for 30min in the oven to enhance the adhesion of PMMA. The probe current (1×10^{-10}A), the injected electron dose ($150\mu C/cm^2$) and electron beam energy (20KeV) was fixed for exposure. After exposure, the sample was developed in metylisobutylketone:

isopropylaceton (MIBK: IPA) (1:1) for 20 seconds. The smallest dimension of PMMA holes array was about 100nm.

1-2-2. Nano-scale etching technology

1-2-2-1. photo-assisted cryogenic etching

Hwang et al. [9] used ArF excimer 193 nm as the light source. The reaction gas was Cl_2. The substrate was cooled by liquid nitrogen. The Taguchi orthogonal design was used for the systematic research. The photon intensity ranged between 390mJ/cm2 and 560mJ/cm2. The substrate temperature ranged between 100K and 373K. The Cl_2 pressure ranged between 10^{-4} torr and $5x10^{-3}$torr. The smooth etching surface with root-mean-square roughness of 1.7nm was achieved at 210K.

The photoluminescence spectrum showed no difference before and after the photon cryogenic etching. At low temperature, chlorine was physisorbed on the GaN surface with long life time before it was desorbed. The condensed layer of chlorine layer reacts with GaN to form $GaCl_x$. The photochemical reaction was liquid nitrogen cooled to avoid the thermal chemical reaction. The volatile products were desorbed by the high energy photon and they were suddenly localized heated by the laser. The photon-control-reaction created a very smooth etching surface by the homogeneous light intensity. The surface became rougher and the Ga vacancy related yellow luminescence appeared at the high etching temperature condition. Damage-free etching was realized with photon cryogenic etching at high etching rate of 84nm/mins.

1-2-2-2. Photo-assisted wet etching

An Hg lamp was served as the UV light source. The electrolyte was the KOH solution. The oxidizer was the $K_2S_2O_8$ solution. Photon was chopped by a chopper. The etching mechanism with Ti and Ti/Pt mask was previously studied, the RMS etching roughness of GaN 0.37nm, [10] which is the world new record. [11~14] we had successfully fabricated a blue light emission device by our chopped photon electro less wet chemical etching. We could successfully etch i-GaN,n-GaN,n-AlGaN,i-InGaN,p-AlGaN and p-GaN in the GaN based MQW structure by our novel method. This is for the first time to break the physical limit of etching the p-type III-nitride materials with any photoelectrochemical etching method. [15]

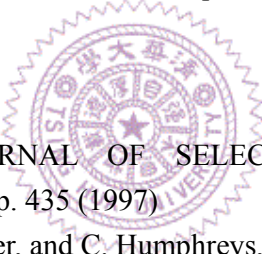### 1-3. III-Nitride based quantum dots device structure

Flip-chip III-Nitride based quantum dot device with the top-down etching method was also adopted. The sample was the double heterojunction (DH) structure with a multi-quantum well activation layer. The device size was determined by the mask formation. After the damage-free etching, an ohmic contact will be applied. By controlling the dot size, the emission wavelength

could be controlled due to the quantum confinement effect. The electrical luminescence wavelength could be shifted from red to the blue region. The high efficiency, quantum dot size-controlled, white light LED could thus be produced.

1-4. Conclusions

We proposed to fabricate the III-nitride quantum dots array by the novel damage-free method for nano-scale etching and the two nano-lithography methods for the structure fabrication, in particular with position, size and distribution control in this project. The EC-SPM method had the ability of dot size control and position control. A scanning tip of the electrochemical scanning probe microscopy (EC-SPM) was used to locally generate the electrochemical environment for the lithography. Three processes were developed. The first one was the direct etching of III-Nitride films by EC-SPM in the KOH solution. The second one was the metal layer oxidation for masking to be covered on the III-nitride epitaxial layer. And, the mask pattern can be transferred by our novel Electrode less photoelectrochemical etching with the chopped UV source techniques without etching damage. The third was the nano mask pattern array formation by electron beam lithography. The quantum dots structure can thus be fabricated. The size reduction and the quantum dot device fabrication are under further research.

Reference:
[1] S. Nakamura, IEEE JOURNAL OF SELECTED TOPICS IN QUANTUM ELECTRONICS, VOL. 3, NO. 2, pp. 435 (1997)
[2] N. Sharma, P. Thomas, D. Tricker, and C. Humphreys, Appl. Phys. Lett. 77, 1274, (2000).
[3] S. J. Henley and D. Cherns, J. Appl. Phys. 93, 3934 (2003)
[4] X. Guo and E. F. Schubert, J. Appl. Phys. 90, 4191 (2001)
[5] T. N. Oder, J. Shakya, J. Y. Lin, and H. X. Jiang, Appl. Phys. Lett. 83, 1231(2003).
[6] T. Fujii, Y. Gao, R. Sharma, E.L. Hu, S.P. DenBaars, and S. Nakamura, Appl. Phys. Lett. 84, 855 (2004).
[7] L.W. Wang, Phys. Rev. B 63, 245107 (2001)
[8] Y Arakawa, IEEE JOURNAL OF SELECTED TOPICS IN QUANTUM ELECTRONICS, VOL. 8, 823 (2002)
[9] J. T. Hsieh, J.M. Hwang, H. L. Hwang and W. H. Hung MRS Internet J. Nitride Semicond. Res. 4S1, G10.6 (1999)
[10] Z. H. Hwang, J. M. Hwang, W. H. Hung and H. L. Hwang, Appl. Phys. Lett. 84, 3759 (2004).
[11] C. Youtsey, I. Adesida,L. T. Romano and G. Bulman, Appl. Phys. Lett. 72, 560 (1998).
[12] B.S. Shelton, T.G. Zhu, M.M. Wong, H.K. Kwon, C.J. Eiting, D.J.H. Lambert, S.P. Turini, and R.D. Dupuis, Electrochem. Solid-State Lett. 3, 87 (2000)
[13] J.A. Bardwell, J.B. Webb, H. Tang, J. Fraser, and S. Moisa, J. Appl. Phys. 89, 4142 (2001).
[14] H. Maher, D. Disanto, G. Soerensen, M.W. Dvorak, T.W. MacElwee, J.B. Webb, and C.R.

Bolognesi, Proc. Int. Workshop on Nitride Semiconductor, 965 (2000).

[15] J.M. Hwanga, K.Y. H, Z.H. Hwang, W.H. Hung, Kei May Lau, H.L. Hwang, Superlattices and Microstructures (in press)

Chapter 2.

Photon-assisted Wet Etching III-Nitride

2.1 Wet etching III-Nitride

The wet etching in III-Nitride and alloy should follow the Arrhenius equation.

$$R = R_0 * e^{-E_a/kT}$$

(2.1.1)   where

R_0 is the successful attempt frequency for breaking of a Ga-N bond and formation of a soluble etch product, E_a is the activation energy, k is the Boltzmann's constant and T is the absolute temperature of the electrolyte. The KOH-based AZ400K developer solution could etch AlN efficiently. [2.1.1] Activation energy was about 15.5 kcal mol^{-1} with high quality AlN growth on Al_2O_3. The KOH and NaOH solutions were found to etch InN a few Å/min at 60°C [2.1.2], but no obvious etching was occurred with crystalline InN. [2.1.1] Etching results of GaN, InN, AlN, InAlN and InGaN with several acid and base solutions below 75°C solution temperature were summarized. [2.1.3] Figure 2.1.1. The etching rate of GaN was ignored with several acid and base solutions below 75°C solution. The InGaN was lift off in the defective site.

Compilation of etching results in acid and base solutions, performed at room temperature (25°C) unless otherwise noted

	GaN	InN	AlN	InAlN	InGaN
Citric acid (75°C)	0	0	0	0	0
Succinic acid (75°C)	0	0	0	0	0
Oxalic acid (75°C)	0	Lifts off	Lifts off	Lifts off	Lifts off
Nitric acid (75°C)	0	Lifts off	0	Lifts off	Lifts off
Phosphoric acid (75°C)	0	0	Oxide removed	Oxide removed	0
Hydrochloric acid (75°C)	0	0	0	0	0
Hydrofluoric acid	0	Lifts off	0	0	Lifts off
Hydriodic acid	0	0	0	0	0
Sulfuric acid (75°C)	0	Lifts off	0	0	0
Hydrogen peroxide	0	0	0	0	0
Potassium iodide	0	0	0	0	0
2% Bromine-methanol	0	0	0	0	0
n-Methyl-2-pyrrolidone	0	0	0	0	0
Sodium hydroxide	0	Lifts off	Lifts off	Lifts off	Lifts off
Potassium hydroxide	0	Lifts off	22.650 Å min^{-1}	0	0
AZ400K Photoresist developer (75°C)	0	Lifts off	~60–10,000 Å min^{-1}	Composition dependent	0
Hydriodic acid/hydrogen peroxide	0	0	0	0	0
Hydrochloric acid/hydrogen peroxide	0	0	0	0	0
Potassium triphosphate (75°C)	0	0	0	0	0
Nitric acid/potassium triphosphate (75°C)	0	Lifts off	0	0	0
Hydrochloric acid/potassium triphosphate (75°C)	0	0	0	0	0
Boric acid (75°C)	0	0	0	0	0
Nitric/boric acid (75°C)	0	Lifts off	0	0	Lifts off
Nitric/boric/hydrogen peroxide	0	Lifts off	0	0	Removes oxide
HCl/H$_2$O$_2$/HNO$_3$	0	Lifts off	0	Lifts off	Lifts off
Potassium tetraborate (75°C)	0	Oxide removal	Oxide removal	Oxide removal	Oxide removal
Sodium tetraborate (75°C)	0	0	0	0	0
Sodium tetraborate/hydrogen peroxide	0	0	0	0	0
Potassium triphosphate (75°C)	0	0	0	0	0
Potassium triphosphate/hydrogen peroxide	0	0	0	0	0

Figure 2.1.1 Summaries of Wet etching III-Nitride at low temperature. The figure is reproduced from J.R. Mileham (1996).

The high activation energy for GaN wet etching in melt KOH was 0.98eV, 50% KOH in ethylene glycol was 0.9eV and H_3PO_4 was 0.9eV. In high temperature of chemical agent, it was able to crystallography etch GaN. The 184 °C molten KOH produce the crystallographic etched surface of {10-1-1} and {10-10}. The 10% KOH in ethylene glycol at 165 °C produce the {10-10} plane. The H_3PO_4 at 132 °C produce the {101-3} and {10-12} planes. The etch rates and observed etching planes for various chemicals was summary in Figure 2.1.2 [2.1.4]

Etch rates and observed etching planes for various chemicals.

Chemical	Temperature (°C)	Etch rate (μm/min)	Etching planes observed
Acetic acid (CH_3COOH)	30	<0.001	None
Hydrochloric acid (HCl)	50	<0.001	None
Nitric acid (HNO_3)	81	<0.001	None
Phosphoric acid (H_3PO_4)	108–195	0.013–3.2	$\{10\bar{1}\bar{2}\},\{10\bar{1}3\}$
Sulphuric acid (H_2SO_4)	93	<0.001	None
Potassium hydroxide (KOH), molten	150–247	0.003–2.3	$\{10\bar{1}0\},\{10\bar{1}\bar{1}\}$
50% KOH in H_2O	83	<0.001	None
10%–50% KOH in ethylene glycol (CH_2OHCH_2OH)	90–182	0.0015–1.3	$\{10\bar{1}0\}$
50% NaOH in H_2O	100	<0.001	None
20% NaOH in ethylene glycol	178	0.67–1.0	None

Figure 2.1.2 Wet etching GaN in high solution temperature. The figure is reproduced from D. A. Stocker (1998).

The attempt frequency is higher in poorer quality material. This is due to the higher density of broken or defective bonds available in grain boundary or threading dislocation. The high temperature solution of KOH or H_3PO_4 could reveal the etching pit at defect site due to the different etching rate (attempt frequency) between defect and crystalline GaN. The molten bases are effective in revealing nano-pipes, mixed-type dislocation and screw dislocation, but the edge type dislocation is impervious to attack. The hot H_3PO_4 could reveal the nano-pipes, but no etching pit at both screw and edge dislocation [2.1.5 – 2.1.7]

Reference

2.1.1   J.R. Mileham, S.J. Pearton, C.R. Abernathy, J.D. MacKenzie, R.J. Shul, and S.P. Kilcoyne, J. Vac. Sci. Technol. A14, 836 (1996).

2.1.2   Q.X. Guo, O. Kato, and A. Yoshida, J. Electrochem. Soc. 139, 2008 (1992).

2.1.3   Note, solid state electronics, Vol.41, No. 12, pp.1947-1951 (1997)

2.1.4   D. A. Stocker, E. F. Schubert, and J. M. Redwing, Appl. Phys. Lett. 73, 2654 (1998).

2.1.5   J.L. Weyher, P.D. Brown, J.L. Rouvie` re, T. Wosinski, A.R.A. Zauner, I. Grzegory, Journal of Crystal Growth, 210 (2000) 151-156

2.1.6   S.K. Hong, B.J. Kim, H.S. Park, Y. Park, S.Y. Yoon and T.I. Kim, Journal of Crystal Growth, 191 (1998) 275-278

2.1.7   P. Visconti, K.M. Jones, M.A. Reshchikov, R. Cingolani, and H. Morkoc, R.J. Molnar, Appl. Phys. Lett. 77, 3532 (2000)

2.2 Electrochemical (EC) etching III-Nitride

To study the EC etching III-Nitride, the sample was immersed in electrolyte. The ohmic contact was deposited on III-Nitride to reduce the voltage dropped between contact and III-Nitride. The Pt electrode was used as cathode. The contact was shielded from the electrolyte by wax. The power supply was connect between Pt electrode and contact on III-Nitride. Before bias applying, the Fermi level was equal between III-Nitride (anode)-electrolyte and electrolyte-Pt (cathode) as shown in Figure 2.2.1

$$2H_2O + 2e^- \rightarrow H_2 + 2OH^-, \quad E^\circ \,(pH = 7) = -0.41\,\text{V versus NHE}$$
$$2H_2O \rightarrow O_2 + 4H^+ + 4e^-, \quad E^\circ \,(pH = 7) = +0.82\,\text{V versus NHE}$$
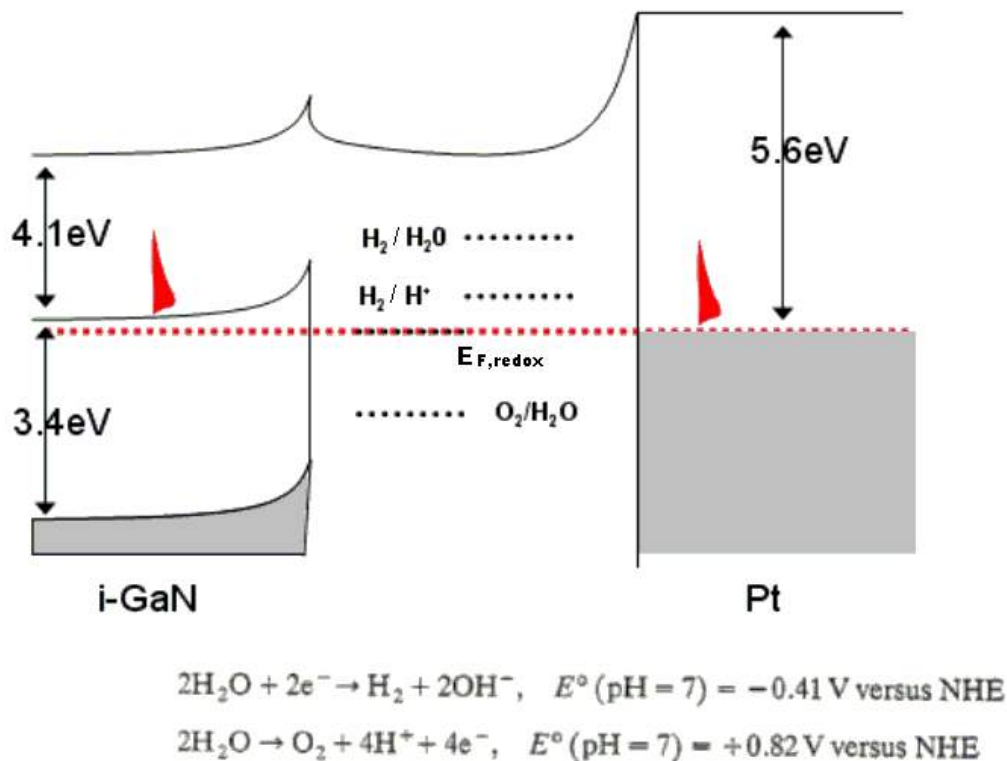
Figure 2.2.1 Band diagram of the electrochemical circuit before bias applied

After the bias applying, the anode will be oxidized or reduced. Pankove et al. [2.2.1] showed the gallium hydroxide form by anodizing the GaN in NaOH electrolyte. The low dissolution rate of gallium hydroxide in NaOH electrolyte blocked the etching GaN. Ohkubo et al. [2.2.2] shown the anodic current density drastically decreased while the oxide form on the GaN surface. The oxide was enhanced dissolved with Cl⁻ ion. The GaN was anodic etched with NaCl/NaOH electrolyte. What is the Cl⁻ ion play in the EC reaction system is still not clear?

Reference

2.2.1 J.I. Pankove, J. Electrochem. Soc. 119 (1972) 1118.

2.2.2 M. Ohkubo, J. Cryst. Growth, 189/190, 734 (1998).

2.3. Photoelectrochemical (PEC) etching III-Nitride

The diagram of photoelectrochemical etching III-Nitride was shown as Figure 2.3.1.
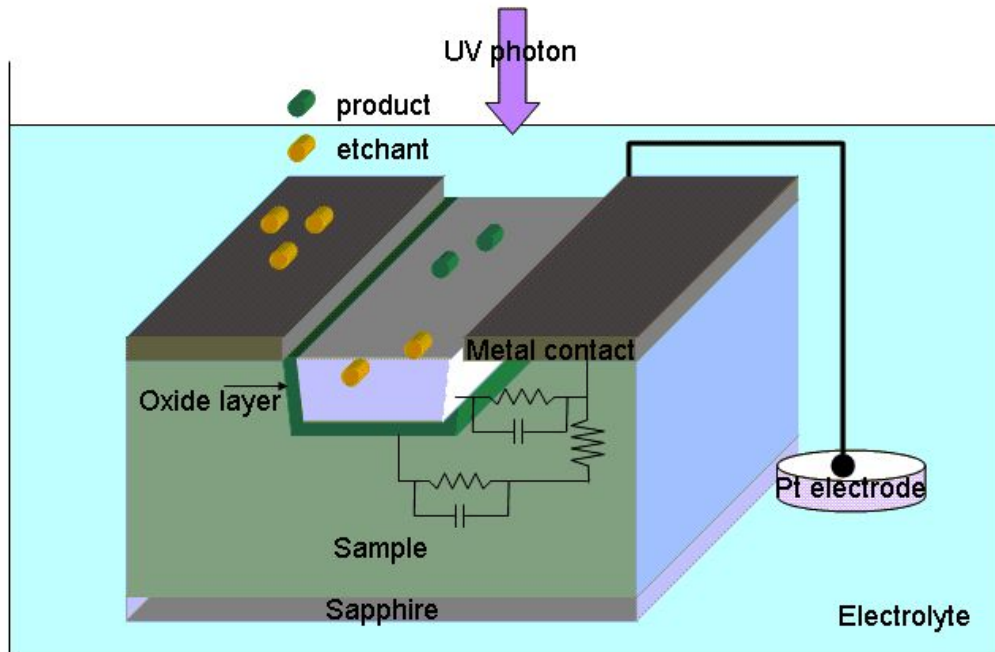
Figure 2.3.1 the diagram of PEC etching III-Nitride

The sample was growth on sapphire. The mask could be metal or other chemical inactive layer deposited on the sample surface. The ohmic contact of metal was deposited on the sample for photocurrent conduction. A Pt electrode was connected to the metal contact by a metal wire. All of the system was immersed into the electroyte inside the Teflon cell. The metal wire was isolated from the electrolyte by coating wax. The electrochemical circuit is formed. The ultraviolet photon source generated by a mercury lamp illuminate on the sample surface. The photon energy was higher than the band gap of the sample. The photon will generate the carriers at the solid and electrolyte interface. The PEC process utilizes photo-generated electron-hole pairs to enhance oxidation and reduction reactions taking place in an electrochemical cell. The band diagram of PEC system with GaN was shown as Figure 2.3.2.
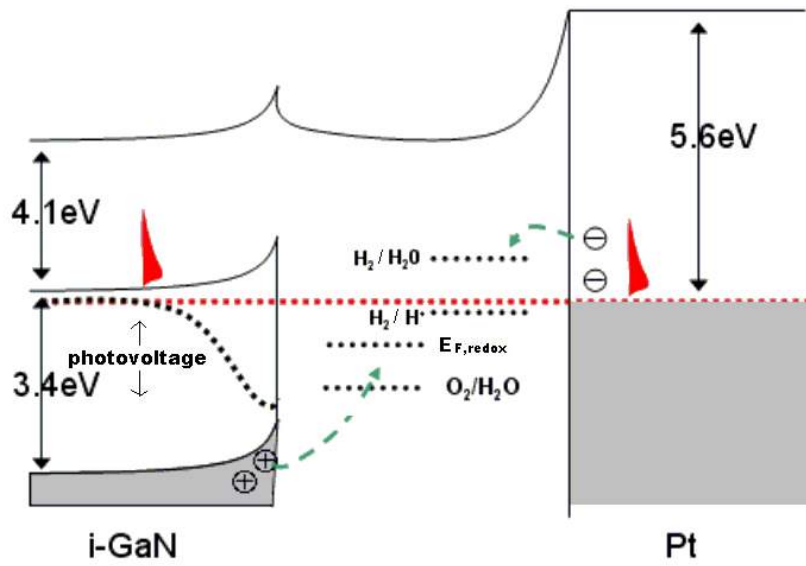
Figure 2.3.2 the band diagram of the PEC circuit with none intentional doped GaN
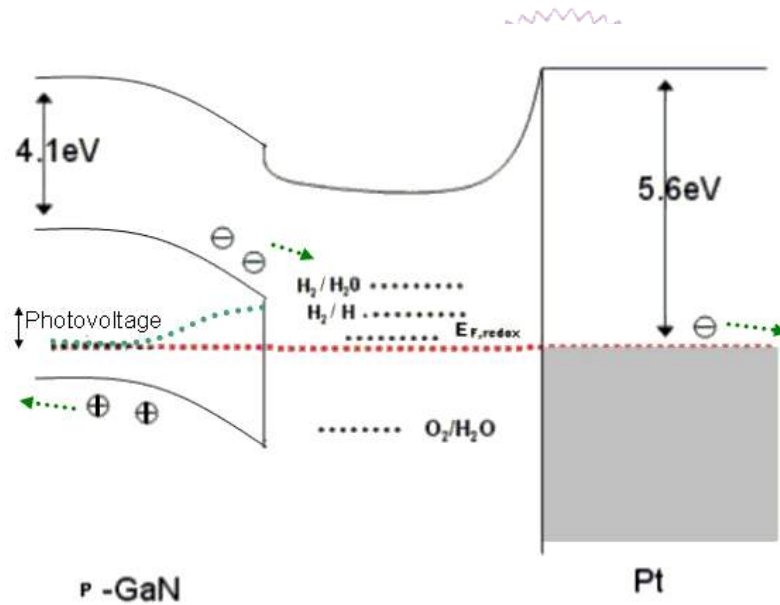
Figure 2.3.3 The band diagram of the PEC circuit with p-type GaN:Mg

The photogenerated holes were swept to the surface between GaN and electrolyte. The GaN was enhanced oxidation with the etchant diffused to the surface. In p-GaN case, the band diagram of PEC system with p-GaN was shown as Figure 2.3.3.

The photogenerated electrons were swept to the surface between GaN and electrolyte. The p-GaN was enhancing reduction. The PEC reaction was strong related to the band edge potentials and band bending of n-type and p-GaN. The flatband potentials as a function of pH could be determinated by impedance analysis or photocurrent measurement. Kocha et al. [2.3.1] found a flatband potential Φ_{FB} = (-0.750-0.055 x pH) V SCE, which for the doping sample (n=1x10^{19} cm^{-3}). Huygens et al. [2.3.2] found a flatband potential of Φ_{FB} = (-0.780-0.060 x pH) V SCE for a GaN sample with (n=2x10^{18} cm^{-3}). Beach et al. [2.3.3] found the conduction band-edge potential Φ_{FB} = (-1.092-0.063 x pH) V vs SCE for p-GaN (p=1x10^{17} cm^{-3}) and Φ_{FB} = (-0.538-0.046 x pH) V vs SCE for n-GaN (n=7x10^{17} cm^{-3}) by photocurrent measurement. By using the impedance spectroscopy measurement, the conduction band-edge potential for n-GaN (n=7x10^{17} cm^{-3}) was Φ_{FB} = (-0.816-0.047 x pH) V vs SCE. The different flatband voltage and V/pH maybe due to the surface state or redox state near the surface. The mechanism was unclear now.

The photogenerated holes were swept to the surface between GaN and electrolyte due to the band bending. The accumulated holes will enhance the gallium oxide and nitrogen gas formation. The chemical reaction is give by

$$2GaN + 6h^+ + 6OH^- --> Ga_2O_3 + 3H_2O + N_2 \qquad (2.3.1)$$
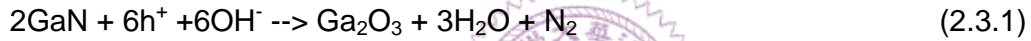
From the Faraday's law, the photocurrent should be proportional to oxidation rate. The relation is give by

$$J_{ph} = \frac{i_{ph}}{A_{cathode}} = (D*V)\frac{N}{W} * \frac{3}{t*A_{cathode}} = \frac{3*D*V*A_{anode}*h}{W} * \frac{1}{A_{cathode}*t} =$$

$$\frac{3*D*V}{W} * \frac{A_{anode}}{A_{cathode}} * \frac{h}{t} = \frac{3*D*V}{W} * \frac{A_{anode}}{A_{cathode}} * R \qquad (2.3.2)$$

The J_{ph} is the photocurrent density. The i_{ph} is the photocurrent. The A_{anode} is the anode etched area. The $A_{cathode}$ is the cathode area contact with the electrolyte. The D is the density of the sample. The V is the etched volume. The charge transfer was 3 per GaN. The h is the etched depth. The t is the etched time. The R is the etched rate. The W is the molecular weight of GaN.

The photocurrent decreased gradually following the oxide thickness increasing to reduce the oxidation rate. [2.3.4] Rotter et al. [2.3.5] study the photo-induced oxidation n-GaN with KOH solution within the PH from 11 to13 by the photocurrent transient. The Ga_2O_3 start to growth whiles the light on. The photocurrent decreased gradually due to the oxide thickness increasing. During the light off duration, the oxide dissolved in KOH solution in dark. The chemical reaction is give by
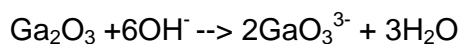
$$Ga_2O_3 + 6OH^- \longrightarrow 2GaO_3^{3-} + 3H_2O \qquad\qquad (2.3.3)$$

The oxide dissolution depended on PH value and dissolution time. Peng et al. [2.3.6] were able to use aqueous H_3PO_4 and KOH solutions with ultraviolet (UV) illumination to etch GaN. The etching rates of GaN were strongly dependent on the pH value of the solutions, peaking at ~1000 - 1200 Å min^{-1} for pH of 1 for H_3PO_4 and 14 for KOH. The photoelectrochemical process was found to create Ga_2O_3 on the GaN surface that was subsequently dissolved by the acid or base solution. The properties were applied to growth gallium oxide by two methods. One is the PEC oxidation GaN during certain low oxide dissolution rate condition with high GaN oxidation rate. [2.3.6] the other method is bias assisted PEC oxidation. The n-GaN was anodized oxidation by bias in H_2O. The gallium oxide was formed due to the low solubility in water. [2.3.7]

The etching of n-type material proceeds through surface oxidation followed by dissolution in aqueous solutions. This process is enhanced by the photogenerated holes by converting surface atoms to higher oxidation states. Increasing absorption of incident optical radiation with energy greater than the band gap energy increase the supply of holes at the surface, thereby enhancing the etch rates. The PEC etching rate vs etching conditions (photon, PH) could be divided into three regions as shown in Figure 2.3.4. In the reaction limit condition region, we could propose the photogenerated holes will transport to electrolyte without oxide blocking. In the diffusion limit condition, the reaction rate will equal to the diffusion rate of etchant to the III-Nitride surface. The gallium oxide was grown in PEC reaction, the etching rate dependence on the oxide growth rate and dissolution rate. The mechanism was two-layer reaction in this condition region.
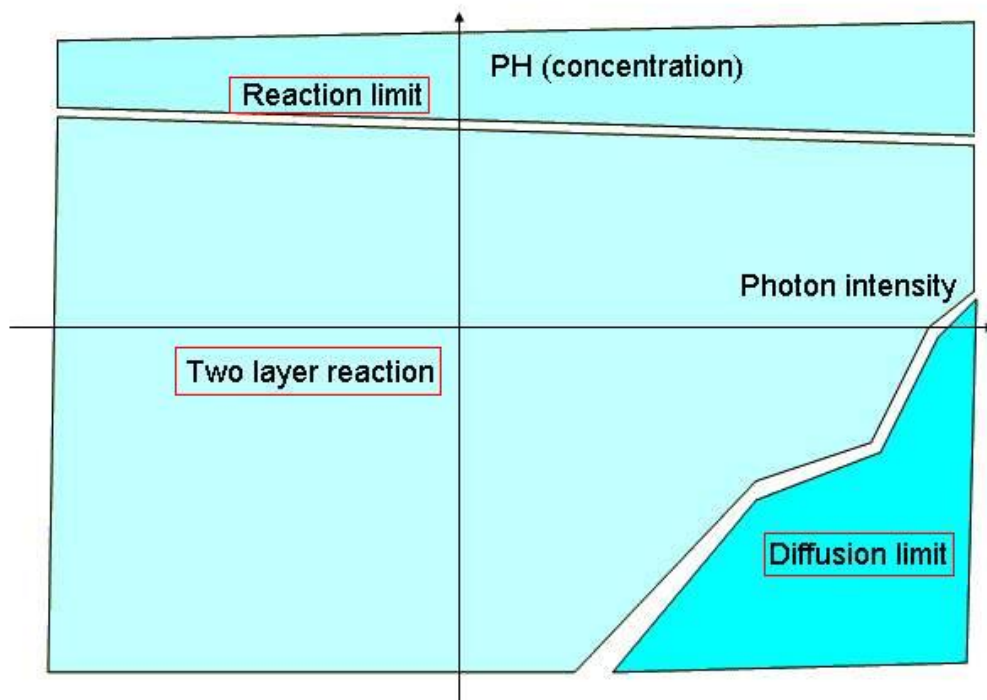
Figure

2.3.4 three regions at different photon intensity and concentration condition.

Reference

2.3.1   S. Kocha, M. W. Peterson, D. J. Arent, J. M. Redwing, M. A. Tischler, and J. A.Turner, J. Electrochem. Soc., 142, L238 (1995)

2.3.2 I. M. Huygens, K. Strubbe, and W. P. Gomes, J. Electrochem. Soc., 147, 1797(2000)

2.3.3 J. D. Beach, R. T. Collins, and J. A. Turnerb, J. Electrochem. Soc., 150 (7) A899-A904 (2003)

2.3.4   M.Ohkubo, Materials Science and Engineering B59 (1999) 355–357

2.3.5   T. Rotter, D. Mistele, J. Stemmer, F. Fedler, J. Aderhold, Graul, V. Schwegler, C. Kirchner, M. Kamp and M. Heuken, Appl. Phys. Lett. 76, 3923 (2000).

2.3.6 L.H. Peng, C.W. Chuang, J.-K. Ho, C.N. Huang and C.Y. Chen, Appl. Phys. Lett. 72, 939 (1998)

2.3.7   J. W. Seo, C. S. Oh, H. S. Jeong, J. W. Yang, K. Y. Lim, C. J. Yoon, and H. J. Lee, Appl. Phys. Lett. 81, 1029 (2002)

2.3.1 PEC etching rate of GaN

--- Reaction limit condition :

The gallium oxide had high solubility in higher PH value region. We propose the photon-generated holes transport to electrolyte without oxide blocking in this condition region. The photon current related to photocurrent could be modeling as equation (3.3.1.1)

$$J_{ph} = q\Phi_0(1 - \frac{e^{-\alpha W}}{1 + L_p})$$

(2.3.1.1)

The q is the electron charge. The Φ_0 is the incident photon flux. The α is the absorption coefficient. The W is the depletion layer width. The L_P is the minority diffusion length. The photonflux is linear proportional to the photocurrent and the photocurrent was equal to the etching rate from equation (2.3.2) The Minsky et al. [2.3.1.1] first demonstrated PEC etching of n-GaN using KOH/H_2O and dilutes HCl solutions. They utilized HeCd laser at 325 nm wavelength for illuminating n-GaN samples at light intensities of ~ 570 mW/cm^2. The GaN sample was connected to a Pt cathode during etching with no external bias applied. Etch rates of ~ 400 nm/min and 40 nm/min were obtained for the KOH and HCl solutions. The ultra high etching rate could be 4mm/min at room temperature with high light intensity. The No etching was observed in the absence of optical illumination. The etching rate was linear proportioned to laser power shown as Figure 2.3.1.1
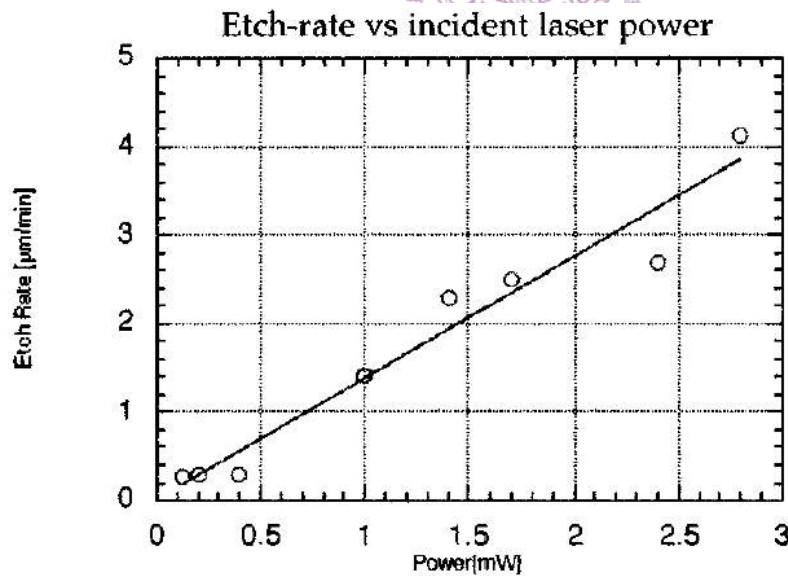
Figure 2.3.1.1 Etch rate for GaN in 45% KOH: H$_2$O (1:3) as a function of incident power. The figure is reproduced from M.S. Minsky (1996).

In low photon intensity region, the etching rate was much smaller than the prediction of equation (2.3.1.1). This was due to the recombination of photogenerated carrier through surface state or defect inside the GaN. The experiment need to be identified in threshold photon intensity of PEC etching GaN.

Rotter et al. [2.3.1.2] found the dissolution potential strong dependence on illumination under He-Cd laser with n-GaN. The photon induced photovoltage will increase while the photon flux increasing. The valency value (z=4) from experiment larger than the theoretical value (z=3) implied that there had the carrier recombination during the etching. By external bias controlling, the dissolution potential could be changed. Seo et al. [2.3.1.3] found that the etching rate will be increased linearly by increasing the external voltage with different electrolyte as shown in Figure 2.3.1.2
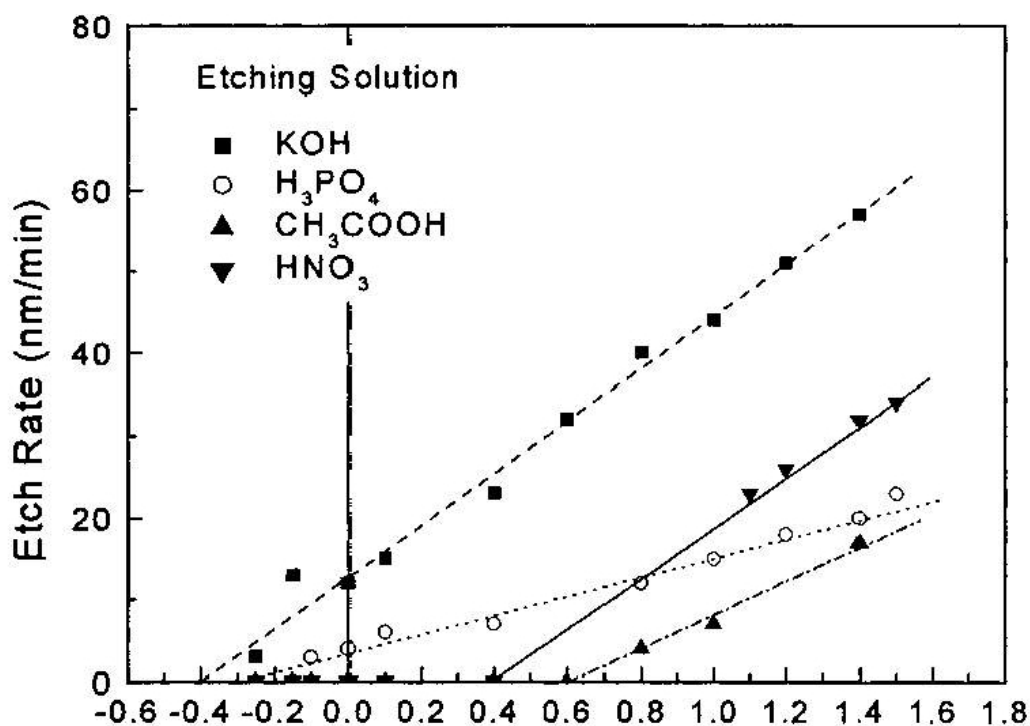
Figure 2.3.1.2 Etch rate for n-GaN on appiled bias form various etching solution under the UV intensity of 90mW/cm^2. The figure is reproduced from J.W. Seo (2001).

The external bias will increase the depletion layer width and the photon current will increase following the equation 4 under reaction limit condition. Seo's experiment results don't follow the equation 4. It needs more research about it. Cho et al. [2.3.1.4] shown the Ea is ~5.1kcal mol^{-1} in PEC etching undoped GaN with 0.01M KOH solution. The **Ea** is ~5.4kcal mol^{-1} in 0.05M KOH with additional 1.5V bias. The **Ea** was reduced to ~0.7kcal mol^{-1} in PEC etching n$^+$ GaN with 0.05M KOH under additional 1.5V bias.

The reaction mechanism between GaN and n$^+$ GaN should be different under 1.5V bias. It needs more research about it.

--- Diffusion limit condition:

While the oxidation rate and oxide dissolution rate are much higher that the etchant diffusion rate. The etching rate will approximate to etchant diffusion rate. Youtsey et al. [2.3.1.5] found that the photocurrent was under reaction limit condition at low photon flux as shown in Figure 2.3.1.3
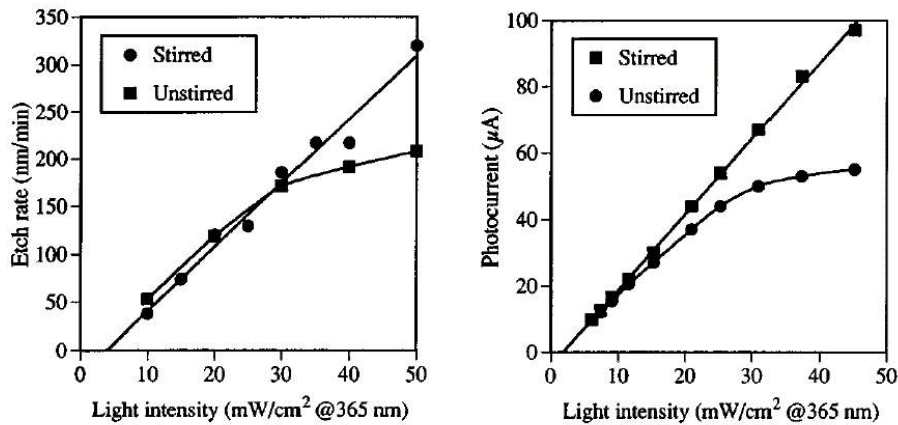
Figure 2.3.1.3 The Light intensity *vs* etch rate and photocurrent in PEC etching GaN. The figure is reproduced from C. Youtsey (1997).

While the high photon flux incident, the photocurrent decreased. The photocurrent and etching rate are related to the etchant diffusion rate. If the electrolyte was stirred, the photocurrent was under reaction limit condition again. Youtsey et al. [2.3.1.6] had also shown the variation of photocurrent with light intensity for different KOH concentrations as Figure 2.3.1.4 (a)
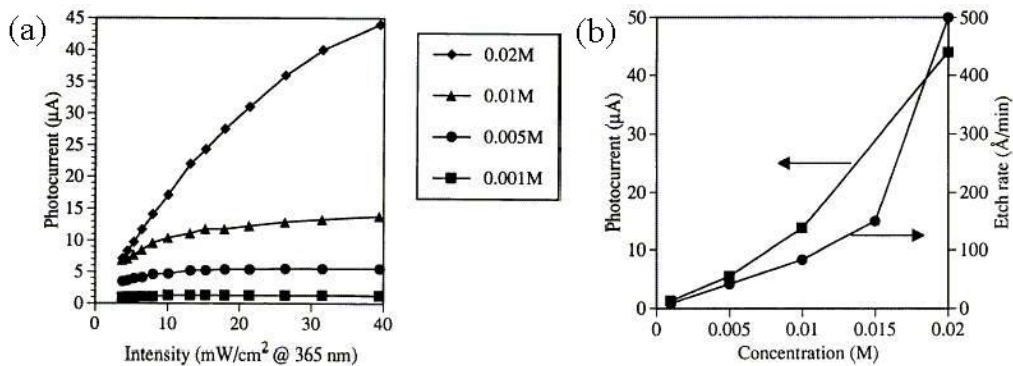
Figure 2.3.1.4 The PEC etching condition (a) Variation of photocurrent with light intensity for different KOH solution concentrations (b) Plot of etch rate as a function of solution concentration under diffusion-limited process conditions. The figure is reproduced from C. Youtsey (1998).

In high photon flux region, the photocurrent was unchanged with increasing photon flux. This is the diffusion limit condition region. From the Fick's diffusion law and Gouy-chapman theory, the photocurrent was proportioned to etchant concentration as equation (2.3.1.2) at the diffusion limit condition.

$$I_{ph} = C_0 C^{\frac{3}{2}}$$

(3.3.1.2)

The C_0 is the constant coefficient. The C is the concentration of etchant. From the calculation based on the Youtsey's data in Figure 2.3.1.4 (b), the C_0 was 14,688 and the comparison between simulation and Youtsey's data was shown in Figure 2.3.1.5
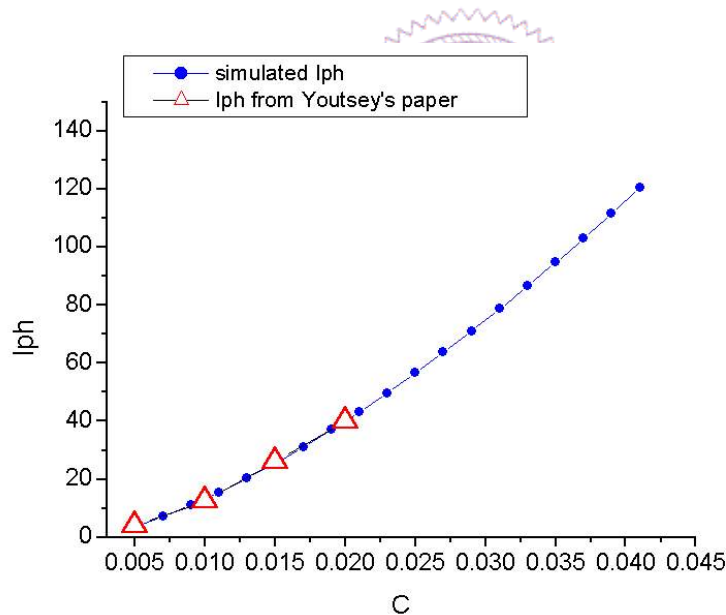
Figure 2.3.1.5 the fitting between C and I$_{ph}$ under diffusion limit condition.

--- Two layer reaction condition:

In this condition region, the etching rate of GaN depended both on the etchant concentration and photon flux. The GaN was enhanced oxidized by incident photon flux. The growth rate of gallium oxide depended on the etchant concentration and photon flux. The oxide dissolution rate although dependence on the etchant

concentration and photon flux. The etching rate was determined by the etchant diffusion rate, oxide growth rate, oxide dissolution rate and production diffusion rate. The mechanism was too complex to modeling.

2.3.2 Profile control of PEC etching GaN

The etch anisotropy obtained during PEC etching arises in part from the collimation of the incident light. During the etching, the gallium oxide growth on the etched sidewall will prevent the lateral etching of the sidewall. The vertical etching profile could be formed.

There had non-uniform lateral profile of the etched depth near the mask. The bulk resistance of the sample produced a different serial resistance and lateral holes distribution near the mask in planar photocurrent transport. The etched profile was deeper near the mask due to the better photocurrent conduction and higher surface hole density. The other factor to produce non-uniform lateral profile was the non-uniform etchant concentration near the mask. Harush et al. [2.3.2.1] research about the effect of mass transfer near the mask The etched profile indicative of accelerated etching near the mask edges (inverted U shape), was observed with low concentrations of the etchant as shown in Figure 2.3.2.1 This etching profile was found to be sensitive to the stirring speed and to the geometric conformation of the wafer. It could be explained by mass transport limited model.
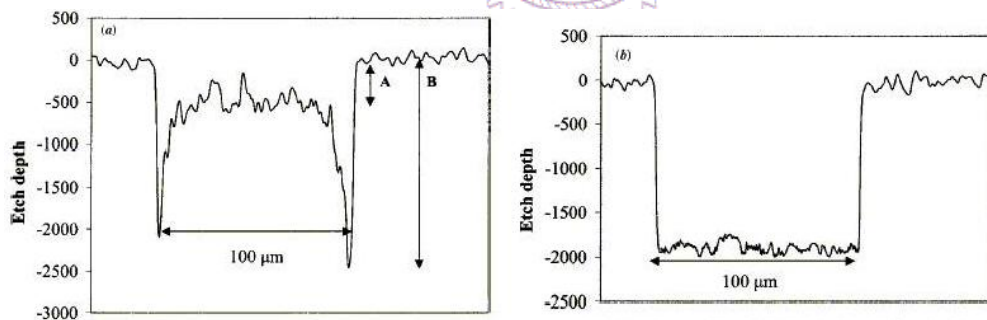
Figure 2.3.2.1 PEC etching profiles of GaN following etching for 50s in an aqueous solution containing (a) 0.02MKOH and (b) 0.6M KOH. The figure is reproduced from E Harush (2002).

2.3.3 Morphology of PEC etching GaN

Youtsey et al. [2.3.1.6] have demonstrated a smooth etched surface with RMS roughness of 1.5nm was obtained on an n^+-GaN sample under a diffusion-limited condition. Shelton et al. [2.3.3.1] shown that there had the narrow range of PEC

etching conditions for smooth etched surface on a n$^+$-GaN sample. The smooth surface with root-mean-square (rms) roughness of ~ 4 nm was obtained. It was also found that this window could be extended by using etch conditions which produced "whisker" growth. Subsequent ultrasonic agitation was applied to remove these whiskers and obtain smoother surfaces with the best rms roughness values being ~0.9 nm.

The dislocation inside GaN with high non-radiation recombination rate will induce the uniform distribution of photogenerated holes in the interface of GaN and electrolyte. The dislocation-induced morphology will produce a rough surface even at diffusion limit condition. Hwang et al. [2.3.3.2] shown the selective etching between the crystalline GaN and it's dislocations by controlling the KOH concentration and the ultraviolet photon intensity in PEC etching. The etch rate of GaN was controlled by the density of photogenerated carriers and the direct chemical reaction between GaN and electrolyte. The dislocation is more chemically reactive than crystalline GaN, whereas crystalline GaN has a higher density of the photogenerated minority carrier than the threading dislocation. The selective etching method was demonstrated as Figure 2.3.3.1
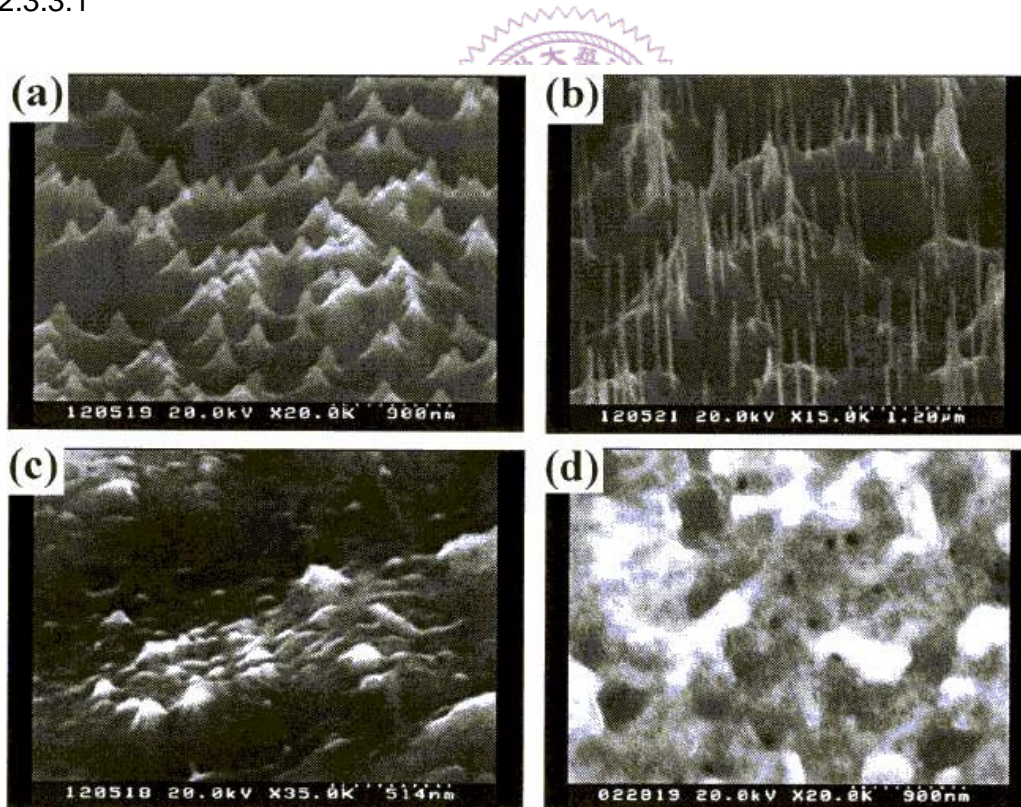
Figure 2.3.3.1 SEM micrographs of PEC etched GaN surfaces etched at (a) power ~ 570 mW/cm2, 0.005M KOH for 30 mins (b) power ~ 570 mW/cm2, 0.01M KOH for 45 mins (c) power ~ 430 mW/cm2, 0.05M KOH for 30 mins (d) power ~ 240 mW/cm2, 0.04M KOH for 30 mins. (From Hwang's group)

Youtsey et al. [2.3.3.3] had identified the etched morphology with whisker was due to the threading dislocation induced morphology as shown in Figure 2.3.3.2
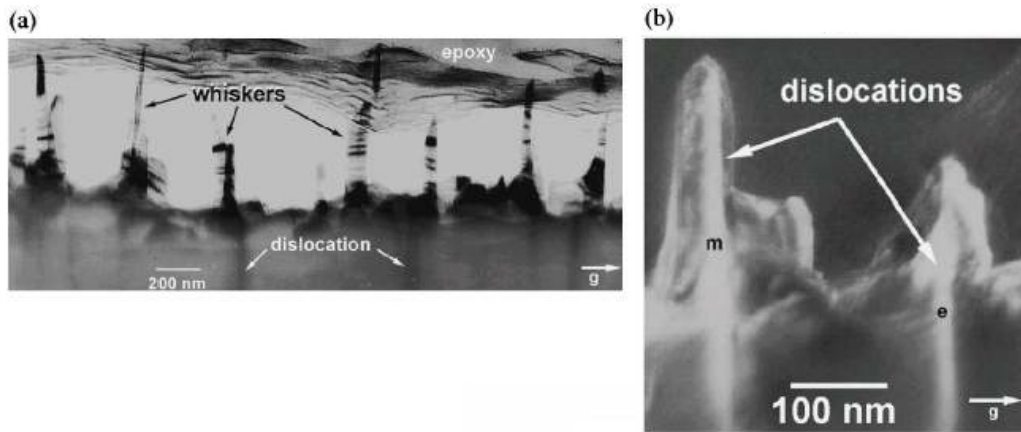
Figure 2.3.3.2 the (a) TEM of the etched GaN film. Visible in this image are the etched whiskers as well as the dislocations in the underlying, unetched GaN film. (b) TEM showing the propagation of dislocations from the unetched GaN film into the etched whiskers. Both mixed (m) and edge (e) dislocations are associated with whisker formation in this image. The figure is reproduced from C. Youtsey (1998).

Ko et al. [2.3.3.4] found that the PEC etching at high pH =14.35 of KOH prefer to chemical etching and depends on the crystal orientation. The PEC etching at pH=0.39 of H_3PO_4 prefer to reveal the dislocation sites.

Hwang et al. [2.3.3.5] develop a boiled KOH post treatment method to smooth the PEC etched sidewall and surface. The boiled KOH will etch stop at {10-10} face and (0001) face. The PEC etched surface before and after smoothing by boiled KOH was shown in Figure 2.3.3.3. A facet sidewall and smooth etching surface was achieved after post-treatment.
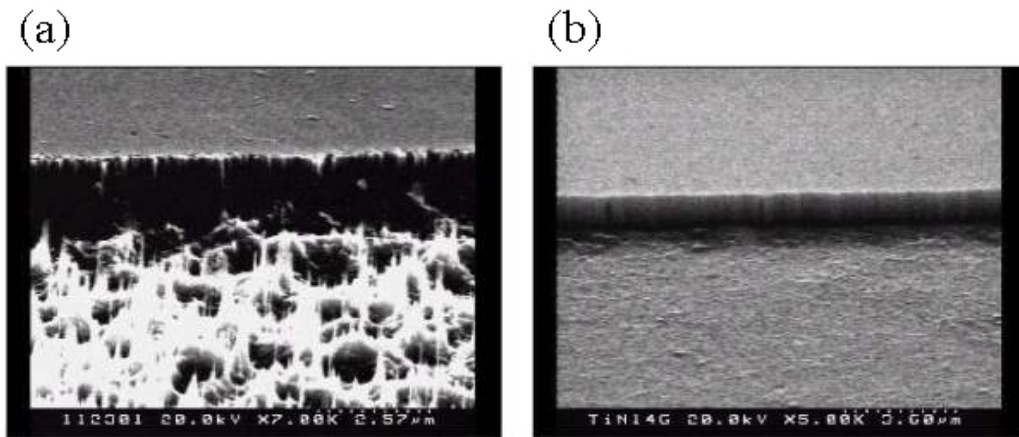
Figure 2.3.3.3 PEC etching (a) with dislocation and striped sidewall (b) without dislocation and striped sidewall by boiled KOH solution post-treatment (From Hwang's group)

2.3.4 Etching damage of PEC etched GaN

There had rarely discussion about etching damage in PEC etching. Although it is the mild etching method with damage the lattice structure, but the electron structure on the etching surface must be considered. The surface state was an important issue for contact and device. Hwang et al. [2.3.4.1] find that after PEC etching GaN in KOH solution, the surface will create the surface state. The defect complex V_{Ga}-O_N relative to yellow luminescence was present. The complex defect was proposed as V_{Ga}-O_N, The thin damage layer could be removed by short time boiled KOH treatment. The PEC etching induced yellow luminescence (YL) was reduced after post-treatment as shown in Figure 2.3.4.1
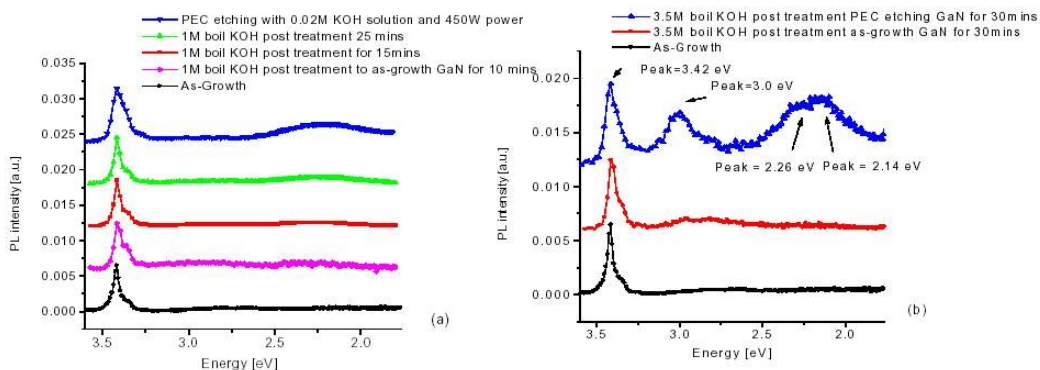
Figure 2.3.4.1 Etching Damage removed by Boiled KOH treatment with (a) low concentration of bolied KOH to remove the damage layer producing YL by short

29

time treatment. (b) High concentration of boiled KOH, treatment will creat damage to GaN surface (From Hwang's group)

With high concentration or long time boiled KOH treatment, the surface state will be created. Reshchikov et al. [2.3.4.2] also find the surface state with H_3PO_4 at 160 °C for 0.5–10 min on the as-growth GaN. It could not be applied to remove the PEC etched damage in GaN. The damage also could remove by photon cryogenic etching with Cl_2 gas. After photon cryogenic etching treatment, the surface became smooth and yellow luminescence was disappear as shown in Figure 2.3.4.2

PAC etching on PEC etched GaN :
240 mJ, 8 Hz, 1.2 mTorr for 10 min.
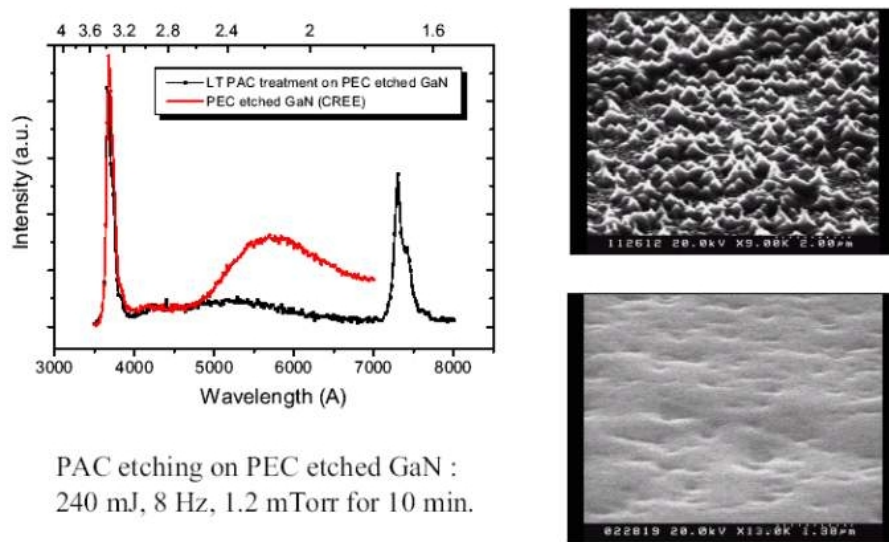
Figure 2.3.4.2 a photoluminescence study in which the damage removal using PAC treatment on PEC etched GaN was examined. The corresponding SEM pictures were taken from as-PEC etched and after PAC treatment of PEC etched GaN (From Hwang's group)

2.3.5 Photon excited cathode effect in PEC etching GaN

The anode photocurrent of PEC etching should be equal to the cathode reduction current. The cathode reduction reaction with Pt electrode was shown in equation (2.3.5.1).

Cathode: $H_2O + e^- \rightarrow OH^- + H_2$; $\Delta E = 0.82eV$ (in V vs SCE)   (2.3.5.1)
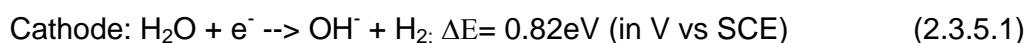
The photocurrent was linear proportional to cathode area. If the cathode was illuminated with energetic photons, the excited electron will enhance reduction. The

exchange current was increasing. The effect was called photon excited cathode effect as shown in Figure 2.3.5.1
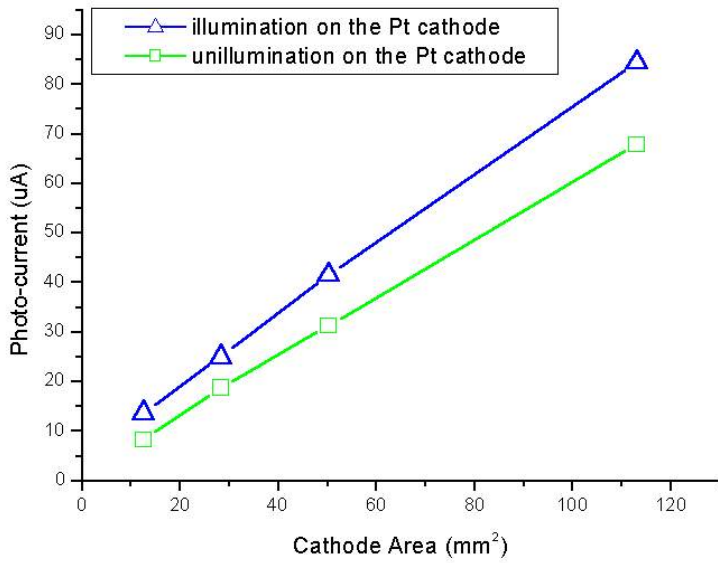
Figure 2.3.5.1 Photocurrent increasing by reduction current enhancement (From Hwang's group)

2.3.6 PEC etching of $In_xGa_{1-x}N$

Hwang et al. [2.3.6.1] study the PEC etching in $In_xGa_{1-x}N$. The indium oxide was grown during PEC etching and slowing the PEC etching rate. The etching rate of $In_xGa_{1-x}N$ depended on the indium oxide dissolution rate and Indium mole fraction in InGaN alloy as shown in Figure 2.3.6.1
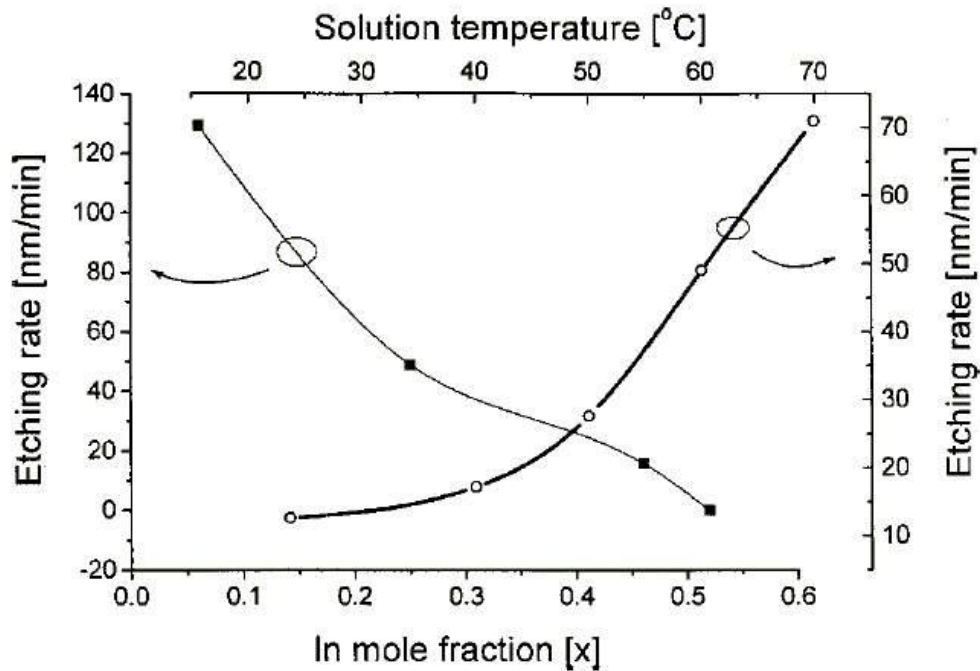
Figure 2.3.6.1 (left scale) Etching rates vs various indium mole fractions at 60 ^{0}C. (Right scale) Etching rates vs various solution temperatures for the In$_x$Ga$_{1-x}$N sample (x=0.25). All the PEC etchings are performed in the unstirred 0.12M KOH with a UV power intensity of 240 mW/cm^2. (From Hwang's group)

The activation energy of the PEC etching for In$_{0.25}$Ga$_{0.75}$N has a value between those obtained for GaN (1.6 kcal/mol) and InN (22.6 kcal/mol) films. The growth of indium oxide layer could be removed clearly by hot HCl treatment.

2.3.7 PEC etching p-GaN

The p-type III-nitrides was inert for PEC etching. [2.3.7.1] It is explained with a mechanism in which the photo-generated electron drifts to the surface between p-GaN and electrolyte, whereas the photo-generated hole moves to the bulk. The accumulation of electrons near the surface strengthens the Ga-O bonding of surface Ga oxides and results in chemical resistance to the etching solution. Borton et. al. [2.3.7.2] showed that an electrical bias applied to p-GaN lowered the Fermi level at the surface and increased the hole density at the interface between p-GaN and electrolyte, resulting in enhancement of PEC etching. That is, the etching rate of p-GaN is strongly dependent on the chemical potential on the surface. The etching rate was 4.4nm/min with 0.1M KOH at 2V as shown in Figure 2.3.7.1
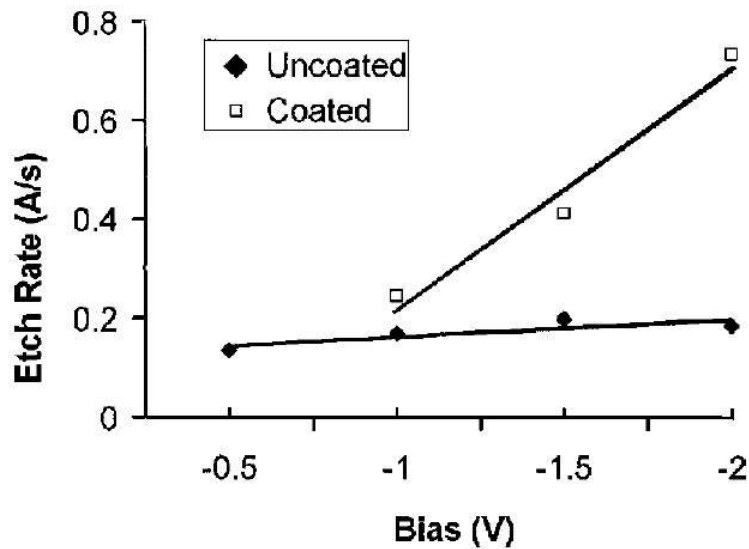
Figure 2.3.7.1 Etch rate *vs* bias for sample with and without Ti exposed to the etchant solution. The figure is reproduced from C. J. E. Borton (2000).

The etching surface was rough and non-uniform in etched profile. Yang et al. [2.3.7.3] applied high electrical bias between semiconductor and electrolyte. The p-GaN near the surface was type reversion under high voltage applied. The highest etching rate was 2.1μm/min with -10V and 0.08mol KOH as shown in Figure 2.3.7.2
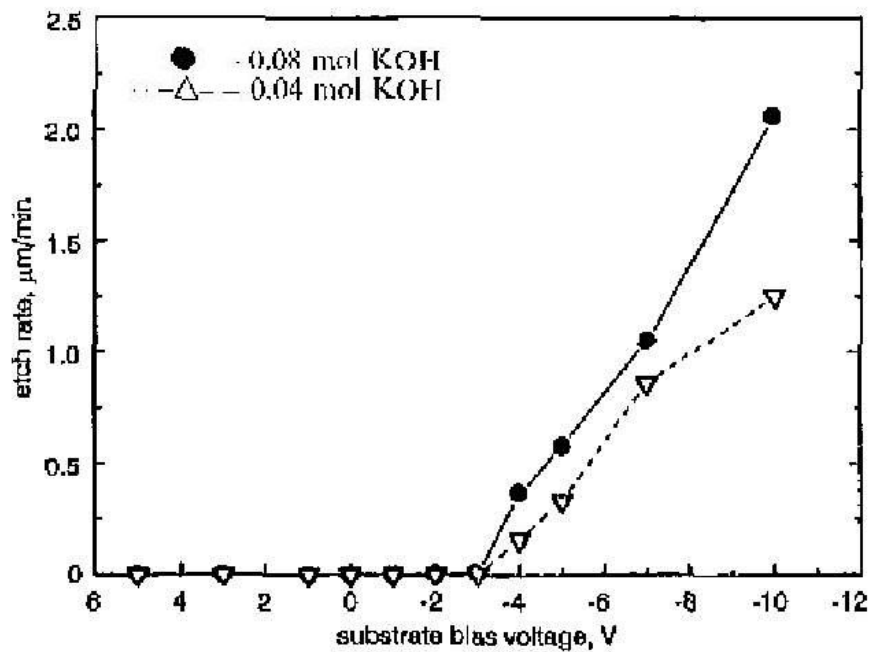

Figure 2.3.7.2 Bias dependence of etched rates for p-GaN measured at locations close to masked region. The figure is reproduced from J.W. Yang (2000).

Reference:

2.3.1.1 M.S. Minsky, M. White and E.L. Hu, Appl. Phys. Lett. 68, 1531 (1996).

2.3.1.2 T. Rotter, J. Aderhold, D. Mistele, O. Semchinova, J. Stemmer, D. Uffmann, J. Graul, Materials Science and Engineering B59 (1999) 350–354

2.3.1.3 J.W. Seo, C.S. Oh, J.W. Yang, G.M. Yang, K.Y. Lim, C.J. Yoon, and H.J. Lee, phys. stat. sol. (a) 188, No. 1, 403– 406 (2001)

2.3.1.4 H. Cho, S.M. Donovan, C.R. Abernathy, S.J. Pearton, F. Ren, J. Han and R.J. Shul, MRS Internet J. Nitride Semicond. Res. 4S1, G6.40(1999)

2.3.1.5 C. Youtsey, I. Adesida and G. Bulman, Appl. Phys. Lett. 71, 2151 (1997)

2.3.1.6 C. Youtsey, I. Adesida,L. T. Romano and G. Bulman, Appl. Phys. Lett. 72, 560 (1998)

2.3.2.1 E Harush, S Brandon, J Salzman and Y Paz, Semicond. Sci. Technol. 17 (2002) 510–514

2.3.3.1 B.S. Shelton, T.G. Zhu, M.M. Wong, H.K. Kwon, C.J. Eiting, D.J.H. Lambert, S.P. Turini, and R.D. Dupuis, Electrochem. Solid-State Lett. 3, 87 (2000)

2.3.3.2 J. T. Hsieh, J. M. Hwang, H. L. Hwang, J. K. Ho, C. N. Huang, C. Y. Chen, and W. H. Hung, *Electrochemical and Solid-State Letters,* **3** (8) 395-398 (2000)

2.3.3.3 C. Youtsey, L.T. Romano and I. Adesida, Appl. Phys. Lett. 73, 797 (1998).

2.3.3.4 C.H. Ko, Y.K. Su, S.J. Chang, W.H. Lan, J. Webb , M.C. Tu, Y.T. Cherng, Materials Science and Engineering B96 (2002) 43-47

2.3.3.5 J.M. Hwang, J. T. Hsieh, H. L. Hwang and W. H. Hung, MRS Internet J. Nitride Semicond. Res. 5S1, W11.73 (2000)

2.3.4.1 J. T. Hsieh, *J.M. Hwang*, H. L. Hwang and W. H. Hung MRS Internet J. Nitride Semicond. Res. 4S1, G10.6 (1999)

2.3.4.2 M.A. Reshchikov, P. Visconti, and H. Morkoc, Appl. Phys. Lett. 78, 177 (2001).

2.3.6.1 J. M. Hwang, J. T. Hsieh, C. Y. Ko, and H. L. Hwang, Appl. Phys. Lett. 76, 3917 (2000)

2.3.7.1 C. Youtsey, G. Bulman, and I. Adesida, J. Electron. Mater. 27, 282(1998).

2.3.7.2 J. E. Borton, C. Cai and M. I. Nathan, P. Chow, J. M. Van Hove, and A. Wowchak, H. Morkoc, Appl. Phys. Lett. 77, 1227 (2000)

2.3.7.3 J.W. Yang, Electronics letters, vol 36, 88, (2000)

2.4 Electroless photoelectrochemical (ELPEC) etching III-Nitride

The disadvantages of PEC etching encountered in device fabrication are the _lateral potential gradient on the GaN film_, _the narrow region of operation for a smooth etched surface_ and _the incapability of etching p-GaN_. The lateral potential gradient was present along the distance from the conducting Pt electrode to the III-Nitride film; a non-uniform depth of etching then occurred along the potential gradient. ELPEC etching was developed to solve this problem, with an oxidizing agent peroxydisulfate ($S_2O_8^{2-}$) replacing the Pt electrode. The localized consume the photoexcited electrons by the photon exctited peroxydisulfate and the localized etching was occurred. The photochemistry of peroxydisulfide are summarized in Figure 2.4.1[2.4.1]

$GaN + photon \rightarrow GaN + e^- + p^+$	Occurs only for $\lambda \leqslant 365$ nm: photoexcitation of GaN, production of electron-hole pair	(1)
$GaN + 3p^+ \rightarrow Ga^{3+} + 1/2N_2$	Overall etching reaction for GaN, consumption of holes	(2)
$S_2O_8^{2-} + 2e^- \rightarrow SO_4^{2-}$	Reduction of peroxydisulfate, consumption of electrons	(3)
$S_2O_8^{2-} + photons \rightarrow 2SO_4^{-\bullet}$	Occurs only for $\lambda \leqslant 310$ nm: photolysis of peroxydisulfate, production of sulfate ion radical	(4)
$SO_4^{-\bullet} + OH^- \rightarrow SO_4^{2-} + OH^\bullet$	Production of the hydroxyl radical, consumption of sulfate ion radical	(5)
$SO_4^{-\bullet} + e^- \rightarrow SO_4^{2-}$	Reduction of the sulfate ion radical, consumption of electrons	(6)
$OH^\bullet + e^- \rightarrow OH^-$	Reduction of the hydroxyl radical, consumption of electrons	(7)
$OH^\bullet + O_2 \rightarrow O_3^- + H^+$	Only in presence of dissolved oxygen in solution, production of ozonide ion, consumption of hydroxyl radical	(8)

Figure 2.4.1 the relevant reaction in the UV enhanced wet etching of GaN

At wavelengths shorter than ~310 nm, the photon excited peroxydisulfate will result in the initial production of the sulfate radical ($SO_4^{-\bullet}$) as reaction (4). Depending on the pH of the solution, this radical either recombines, or results in production of the hydroxide radica l (OH$^-$) in alkaline deaerated solutions as reaction (5), or production of the ozonide (O_3^-) in alkaline aerated solutions as reaction (8). Both the sulfate radical ion and the hydroxide radical are very strong oxidizing agents, and thus could be involved in the photoenhanced wet etching of GaN, through reactions (6) and (7). It should be noted that $S_2O_8^{2-}$ does not absorb at 365 nm.

2.4.1 ELPEC etching rate of GaN

According to Bardwell's results,[2.4.1.1] the morphology of GaN etched with a SiO_2 mask showed grain boundaries and needle-like dislocations. A catalytic Pt mask was then found to produce a rate of etching about ten times as great as that with a SiO_2 mask. The rate of ELPEC etching might attain 40-50 nm/min for GaN, but the resulting morphology was still not smooth with a RMS roughness 20 nm. The etch rate was larger near the Pt mask up to ~30nm/min, and only ~13 nm/min far from the mask. Maher et al. [2.4.1.2] find the PH value of the $KOH/K_2S_2O_8$ electrolyte was change with etching time. It is due to the photolysis of the peroxydisulfate. The etching solution should be continually changed to avoid the PH massive change. The PH change with the etching time was shown in Figure 2.4.1.1
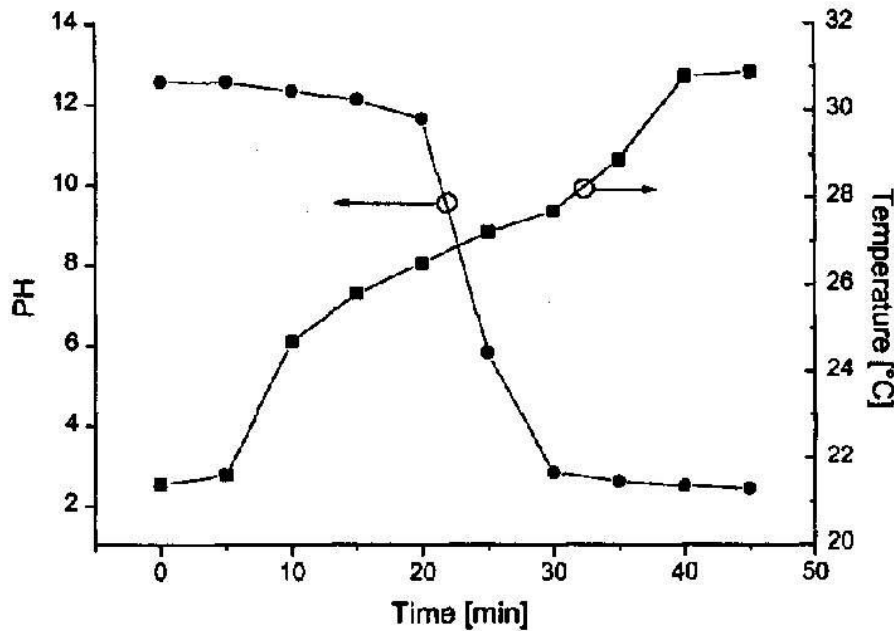
Figure 2.4.1.1 Evolution of solution PH due to photolysis by UV exposure. The figure is reproduced from H. Maher (2000).

The etched morphology of ELPEC etched we Ti and Ti/Pt mask was shown in Figure 2.4.1.2
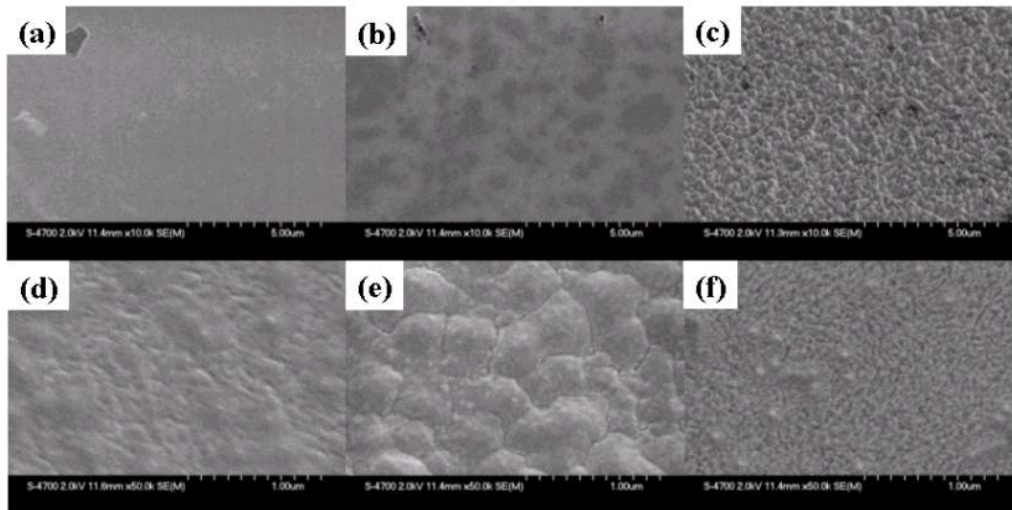
Figure 2.4.1.2 SEM micrographs of GaN surfaces obtained from ELPEC etching with varied duration of UV exposure with a Ti mask: (a) 20 min; (b) 40 min; (c) 60 min, and with a Ti/Pt mask: (d) 20 min; (e) 40 min; (f) 60 min. (From Hwang's group)

Figures 2.4.1.2 (a)-(c) show the SEM micrographs of GaN surfaces obtained after ELPEC etching at room temperature for 20-60 min. The GaN sample was deposited with the Ti mask and was etched in solution (0.05 M KOH, 0.05 M $K_2S_2O_8$) under irradiation with a continuous UV light source having a flux of 16 mW/cm^2. The as-grown GaN samples used in this study exhibited a smooth surface with a RMS roughness 0.22 nm before etching. As shown in Figures 2.4.1.2 (a)-(c), the surface morphology becomes gradually rough with increased duration of etching. Close examination revealed that the surface covered with hexagonal pyramids as shown from the top view of a SEM micrograph in Figure 2.4.1.3
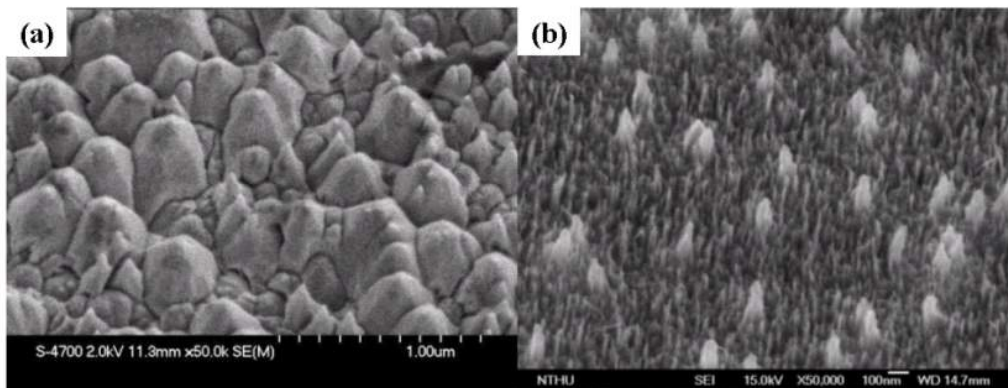
Figure 2.4.1.3 High-magnification SEM micrographs of a GaN surfaces obtained after 60 min ELPEC etching with (a) a Ti mask and (b) a Ti/Pt mask, respectively (From Hwang's group)

the dimension of the base of a pyramid is in a range 300-500 nm. Based on the SEM micrographs, the density of pyramids was determined to be in the range of 10^8-10^{10} cm^{-2}.

Figures 2.4.1.2 (d)-(f) show the SEM micrographs of GaN surfaces obtained after ELPEC etching for 20-60 min, in which the mask on GaN was a Ti/Pt bi-layer metal. The etching condition was the same as that described above with a Ti mask. Like the results from ELPEC etching with a Ti mask, the GaN surface become rough after ELPEC etching with a Ti/Pt mask. The Ti/Pt mask provides a higher etching rate because the catalytic Pt layer can enhance the PEC reaction. The illumination of UV photon on the Ti/Pt mask induces excited-electrons (photoelectron) from the Pt metal, which subsequently moves to the interface between GaN and solution. The excited-electrons then involve in reduction of $S_2O_8^{2-}$ and result in an increase of reduction current (photocurrent). This behavior is similar to the observation that illumining UV light on the Pt cathode of PEC etching causes the increase of etching rate.

As shown in Figure 2.4.1.2 (e), two structural features are present on the GaN surface obtained after 40min ELPEC etching; One is the pyramidal grain with a scale of 300-500nm, and the other is the small texture with the diameter smaller than 100nm and is distributed between the grains. The grain disappeared after etching of longer duration (60 min), and the small texture became predominant on the etched surface. The GaN surface was closely examined with a high-magnification SEM micrograph as shown in Figure 2.4.1.3 (b). Two types of nano-structures are present on the etched surface, which are apparently different in size; one is the larger obtrusive pricks with a density 10^8-10^{10} cm^{-2} and a diameter ~100 nm, and the other is the nano-rod structure with a density ~10^{11} cm^{-2} and a diameter 30-50nm.

PEC etching in KOH solution was reported to cause formation of a GaN surface with spiky whiskers; [2.3.3.2] these whiskers were located on threading dislocations of the GaN film, which act as sites for highly efficient non-radiation recombination of electron-hole pairs during the photo-excited etching reaction. The density of whiskers is comparable with the densities of pyramids in ELPEC etching with a Ti mask and pricks in ELPEC etching with a Ti/Pt mask; for this reason the origin of these pyramids and pricks could be related to the threading dislocations of GaN. The spiky whiskers (diameter 30-50 nm) obtained from PEC etching was simply removed in a boiling KOH solution because chemical binding of Ga-N is weak near the dislocation, whereas the pyramid and prick structures that we obtained in this study were little altered after treatment in the boiling KOH solution. Hence these pyramids and pricks possess the property of crystalline GaN in resisting vigorous chemical conditions. In addition, the pyramid and prick are significantly larger than the whiskers in size. We accordingly

propose that these pyramids and pricks are composed of crystalline GaN enclosing a dislocation defect. The nano-rod obtained from ELPEC etching with a Ti/Pt mask may originate from another type of dislocation defect in the GaN film. The possible mechanism of selective ELPEC etching between dislocation and crystalline GaN in a $K_2S_2O_8$/KOH solution is discussed below.

At the steady state, the total current across an interface between semiconductor and electrolyte is attributed to both isoenergetic and inelastic charge transfer during the PEC reaction. [2.4.1.3] The isoenergetic process can proceed whether or not surface states are involved during the PEC etching. The current density *J'* at the semiconductor-electrolyte junction is expressed as equation (2.4.1.1)

$$J'=P_{tr}(E).J \tag{2.4.1.1}$$

in which P_{tr} is the probability of charge transfer that occurs at energy *E*, and *J* represents the current density at the semiconductor-electrolyte interface when charge-transfer kinetics at the interface is neglected. The current density has contributions from photocurrent (J'_{ph}), space-charge recombination current (J'_{SCR}), and dark currents due to hole and electron (J'_h and J'_n).

$$J'= J'_{ph} + J'_{SCR}+ J'_h + J'_n \tag{2.4.1.2}$$

During ELPEC etching of GaN in the $K_2S_2O_8$/KOH solution, the photo-generated hole was swept to the surface and participates in the oxidation reaction, corresponding to the first term in Equation (2.4.1.2). The Ga oxides formed in this oxidation reaction subsequently dissolve into solution, resulting in the etching effect.

The carrier transport during the ELPEC etching is similar to that in a photoelectrochemical solar cell under the open-circuit condition. [2.4.1.3] The oxidizing agent provides holes to the valence band, whereas the UV photons serve as a source of photo-generated carriers. The kinetics of the photo-generated carrier is proposed to proceed in three steps. The first step is generation of an electron-hole pair upon exposing GaN to the UV radiation. In the following step the resulting hole in the space-charge region drifts towards the interface between GaN and electrolyte, which initiates oxidation of GaN into the Ga oxides. Finally, the photo-voltage gradually develops with an accumulation of carrier charge and subsequently begins relaxation of the carrier by Shockley-Read-Hall (SRH) recombination. The electrons and the holes are drawn to recombine through the deep-level states in the space-charge region or surface states at the interface between GaN and the electrolyte. The photo-generation of electron-hole pairs occurs on a time scale of femtosecond, whereas both accumulation and relaxation of charge carriers proceed on a time scale of millisecond.

[2.4.1.4] The latter processes depend on the impedance of the semiconductor and solution junction and on the incident photon intensity. The overall rate of PEC etching is determined by, which is proportional to the hole density at the interface of GaN and electrolyte. The rate of recombination is greater at a dislocation defect than for the crystalline GaN and thus decreases the rate of etching near a dislocation due to a smaller or hole density. This process results in formation of a surface pyramid in ELPEC etching with a Ti mask, in which a dislocation defect is enclosed by the unetched crystalline GaN.

Similar to previous Bardwell's results, our ELPEC etching with a Ti/Pt mask produced an etched GaN surface with two features of pricks (pyramids) and nano-rods (needle-like). [2.4.1.1] The pricks obtained from ELPEC etching with a Ti/Pt mask has the same order in density as that obtained with a Ti mask and is also attributed to origin from a depression of etching rate at defect site. The nano-rod feature was not observed on ELPEC etching with a Ti mask and however, might also origin from the depression of etching rate at a different type of the defect site. However, this defect was not a carrier recombination center as effective as the threading dislocation causing the formation of pyramids in ELPEC etching. The chemical binding of Ga-N near this defect (called "nano-rod" defect) is relatively weak compared to other regions in GaN and favors a high PEC etching rate at this region. Combination of these two opposing factors results in a low etching slelctivty between nano-rod defect and crystalline GaN in ELPEC etching with a Ti mask. For ELPEC etching with a Ti/Pt mask, the Pt metal enhances the reaction of crystalline GaN with $S_2O_8^{2-}$ as described previously and enlarges the difference of etching rates at crystalline GaN and GaN near the nano-rod defect. As shown in Figure 2.4.1.2 (d)-(f), the nano-rod feature is gradually formed and become evident after a long etching period.

A smooth etching surface sample and a dislocation revealed rough etching surface sample with Ti/Pt patterned was used to verify the broad etching surface on the GaN as shown in Figure 2.4.1.4

(1) Smooth surface

RMS=1.1nm

2.0kV 13.4mm x80.0k 4/22/03 08:56   500nm
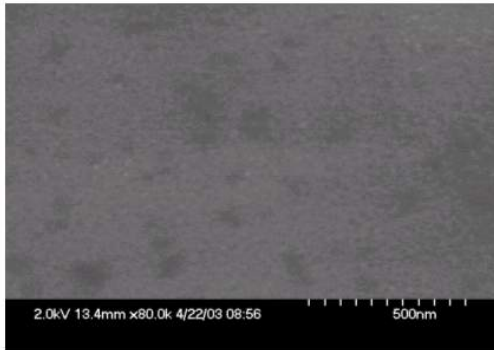
KOH=0.01M;K2S2O8=0.05M;
16mW/cm2

(2) Rough surface

RMS=4.3nm

NTHU   SEI   15.0kV   X50,000   100nm   WD 15.0mm
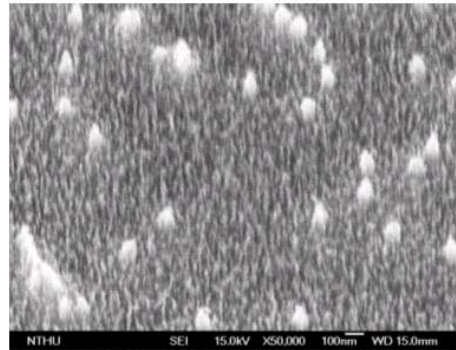
KOH=0.1M;K2S2O8=0.05M;
32mW/cm2

Figure 2.4.1.4 The ELPEC etching with Ti/Pt mask (a) smooth etched surface (b) rough etched surface (From Hwang's group)

The smooth etched surface with RMS roughness 1.1nm was produced under diffusion limited condition. The diffusion limited etching condition are KOH=0.01M, $K_2S_2O_8$=0.05M and 16mW/cm^2. The rough etched surface was due to the dislocation induced morphology without disffusion limited condition. The etching condition are KOH=0.1M, $K_2S_2O_8$=0.05M and 32mW/cm^2. There have two ways to produce a smooth and broad area etched surface. One is etched the GaN under the diffusion limited region. Another is post treatment in hot KOH solution. After smooth surface was produced by ELPEC etching with Ti/Pt mask, the etching depth uniform with broad area could be get as shown in Figure 2.4.1.5.
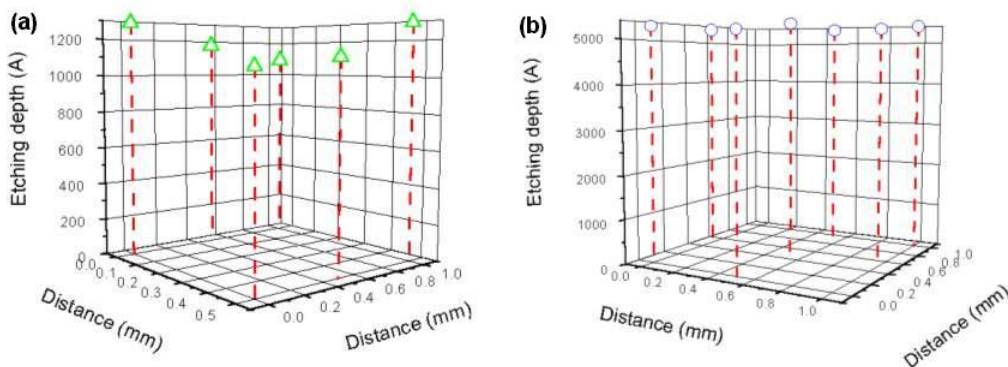
Figure 2.4.1.5 The etching time was 15 minutes with Ti/Pt mask (a) Smooth etching surface (b) Rough etching surface after hot KOH treatment The average

etching depths of the smooth and rough samples were 116.7nm and 529.8nm. The etching rates were 7.78nm/mins and 35.3nm/mins. The etching depths rms were 4.1nm and 2.73nm. (From Hwang's group)

The average etching depths of the smooth and rough samples were 116.7nm and 529.8nm. Both of the etching time was 15 minutes. So the etching rates were 7.78nm/mins and 35.3nm/mins. The etching depths rms were 4.1nm and 2.73nm. The smooth and broad etched surface and anisotropic and uniform etching depth profile was achieved by ELPEC etched or post-treatment method.

Reference

2.4.1.1 J.A. Bardwell, J.B. Webb, H. Tang, J. Fraser, and S. Moisa, J. Appl. Phys. 89, 4142 (2001)

2.4.1.2 H. Maher, D. Disanto, G. Soerensen, M.W. Dvorak, T.W. MacElwee, J.B. Webb and C.R. Bolognesi, Proc. Int. Workshop on Nitride Semiconductor, 965 (2000)

2.4.1.3 S. Chandra, S.L. Singh, and N. Khare, J. Appl. Phys. 59, 1570 (1986).

2.4.1.4 D.J. Fu, T.W. Kang, S.U. Yuldashev, N.H. Kim, S.H. Park, J.S. Yun, and K.S. Chung, Appl. Phys. Lett. 78, 1309 (2001).
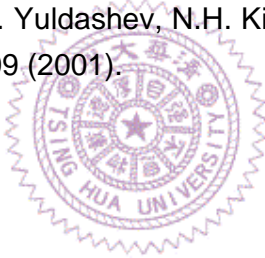
2.5 Electroless photoelectrochemical etching III-Nitride with a chopped source (ELPEC-CS)

2.5.1 ELPEC-CS etchings of GaN

On the basis of the argument above, we performed an innovated ELPEC etching (ELPEC-CS), in which a smooth etched surface can be achieved on decreasing the recombination current at the dislocation site and on creating a uniform density of holes at the interface between GaN and electrolyte with discontinuous UV irradiation. Accordingly, ELPEC etching requires GaN to be exposed to periodic UV illumination with a millisecond period, which is the time scale of the separation of photo-generated carriers. The carrier transport and energy band diagram during ELPEC etching with discontinuous irradiation appear in Figure 2.5.1.1
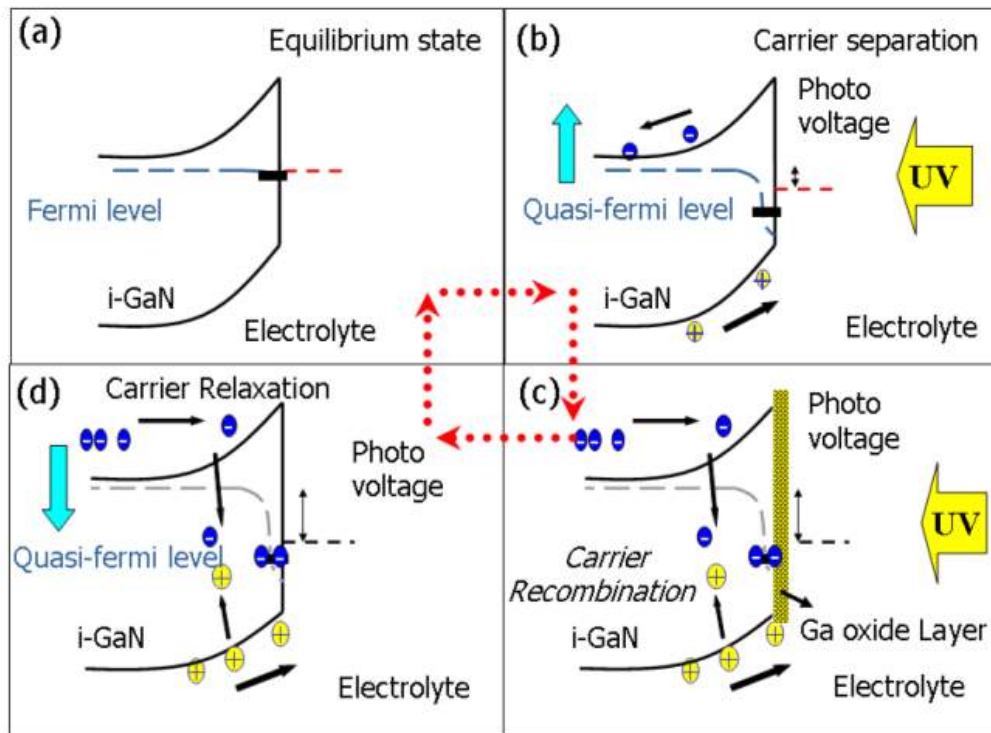
Figure 2.5.1.1 Carrier transport and energy-band diagram of GaN during ELPEC etching under periodic UV illumination: (a) an equilibrium state before UV irradiation, (b) separation of photogeneration carriers under UV irradiation, (c) Ga-oxide growth and carrier recombination upon increase of photovoltage, (d) dissolution of Ga oxides and carrier relaxation without UV illumination. (From Hwang's group)

Holes move to the GaN-electrolyte interface and initiate oxidation of GaN into Ga oxides before a large photo-voltage is built to enhance the recombination of electrons and holes as shown in Figure 2.5.1.1(c). In a subsequent dark interval, electrons accumulated in the bulk undergo relaxation and Ga oxides becomes dissolved as shown in Figure 2.5.1.1(d). A static equilibrium is retained after the excess electrons are released as shown in Figure 2.5.1.1(a). As a result, the period of UV irradiation is critical to the morphology of an ELPEC-CS etched surface.
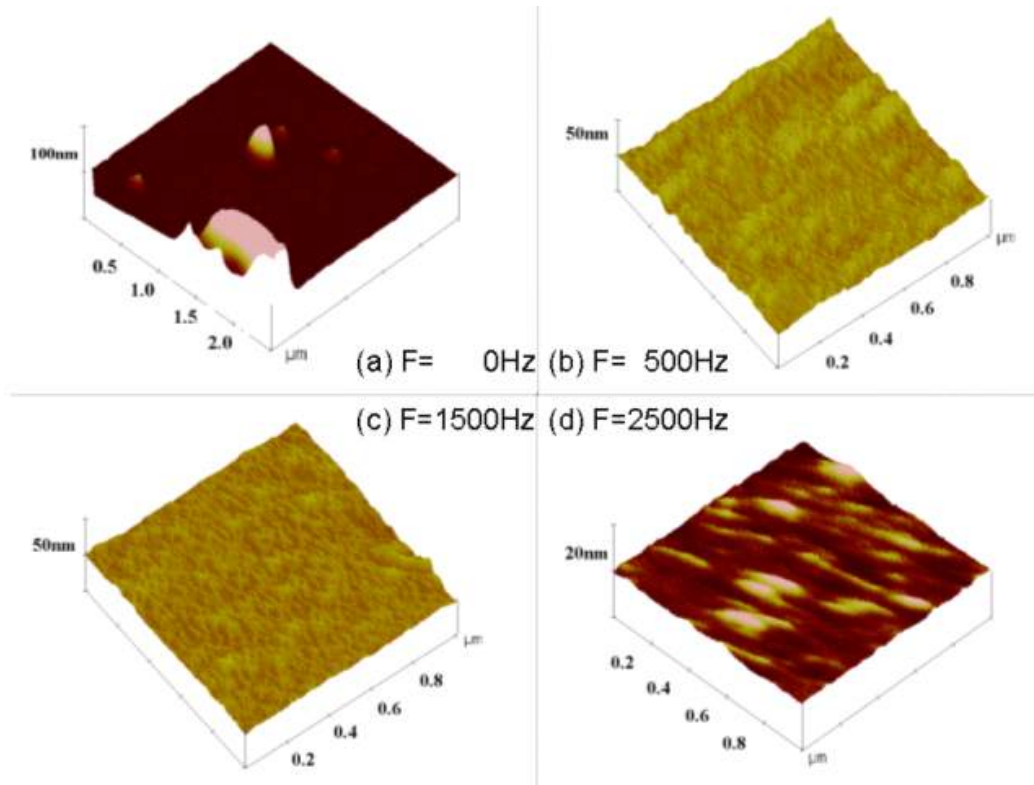
Figure 2.5.1.2 AFM images of a GaN surface obtained from EPPEC etching with varied chopper frequencies: (a) 0 Hz; (b) 500 Hz; (c) 1500 Hz; (d) 2500 Hz. The RMS The RMS roughnesses of resulting GaN are 9.1, 1.34, 0.95, and 0.37 nm, respectively. The GaN samples were etched in solution (0.01 M KOH, 0.05 M $K_2S_2O_8$) for 20 min. (From Hwang's group)

Figure 2.5.1.2 shows a comparison of GaN surfaces obtained from ELPEC-CS etching in solution (0.01 M KOH, 0.05 M $K_2S_2O_8$) for 20 min with varied frequency of the slot chopper, hence varied the period of irradiation. A Ti mask was used on GaN and the intensity of incident photons was 63 mW/cm^2. The surface obtained from ELPEC etching with continuous light (0 Hz) has a RMS roughness of 9.1 nm and was covered with pyramids. The RMS roughnesses are 1.34, 0.95 and 0.37 nm, respectively, for surfaces obtained with the UV source chopped at the frequency of 500, 1500 and 2500 Hz. The greater the frequency of the slot chopper (thus the smaller the

interval of UV irradiation), the smoother is the etched GaN surface. The cross section of ELPEC-CS etched GaN was shown as Figure 2.5.1.3
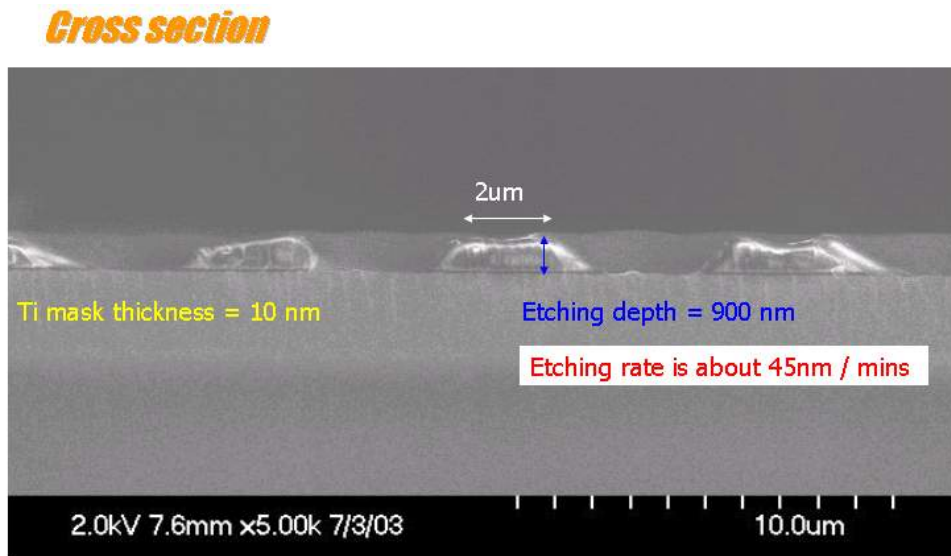
Figure 2.5.1.3 The cross section of ELPEC-CS etched GaN (From Hwang's group)
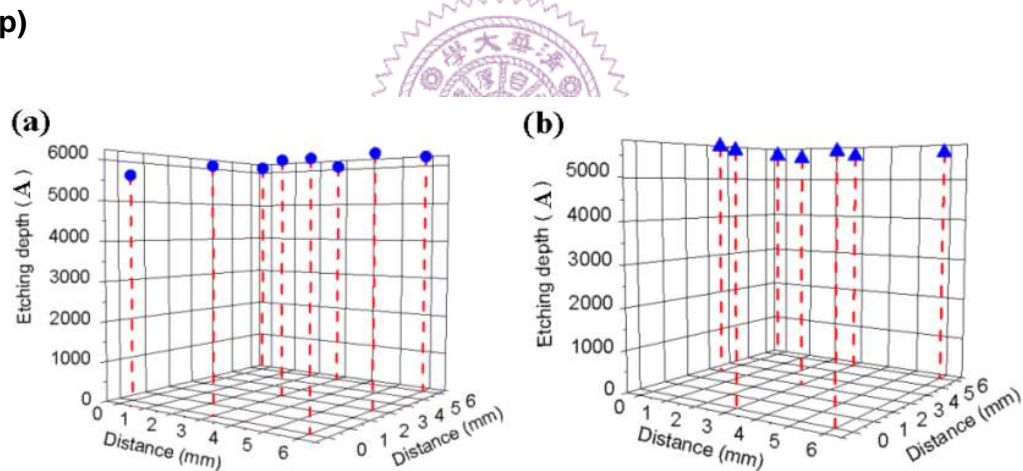
Figure 2.5.1.4 Profiles of etching depth for GaN samples (8×8 mm^2) after ELPEC etching with continuous and chopped (500 Hz) UV sources. GaN samples were etched in solution (0.01 M KOH, 0.05 M K$_2$S$_2$O$_8$) for 20 min. The average and RMS etching depth were 596.2 nm and 6.8 nm for the continuous source, and 567.4 nm and 4.8 nm for the chopped source. (From Hwang's group)

Figure 2.5.1.4 shows the profiles of depth of etching for GaN samples obtained from ELPEC etching for 20 min with continuous and chopped (500 Hz) UV source, respectively, with an etching solution (0.05 M K$_2$S$_2$O$_8$, 0.01 M KOH). With an alpha-step profilometer, we determined the depth of etching randomly on a sample

45

area as large as 8×8 mm^2. The average depth of etching and its RMS are 594.2 and 6.8 nm for continuous illumination, and 567.4 and 4.8 nm for UV light chopped at 500 Hz. It is evident that ELPEC-CS etching leads to a surface smoother than that with continuous irradiation and can provide a uniformly etched GaN surface of large area.
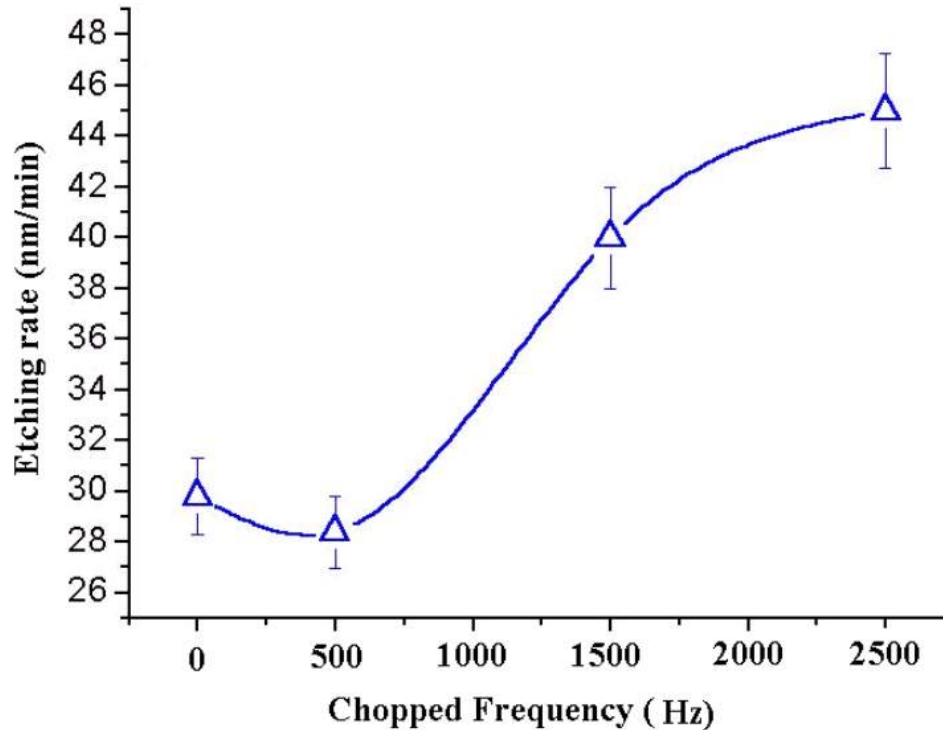
Figure 2.5.1.5 Dependence of etching rate on frequency of the chopper in ELPEC etching. (From Hwang's group)

Figure 2.5.1.5 shows a comparison of ELPEC-CS etching rates in solution (0.01 M KOH, 0.05 M K$_2$S$_2$O$_8$) with varied frequency of the slot chopper. The intensity of incident photons was 63 mW/cm^2. Compared to the etching rate with a continuous UV light, the ELPEC-CS etching rate at 500Hz was decreased. Because the number of photon was reduced to half after the VU light was chopped by a slot chopper with 50 % opening. By increasing the chopper frequency, the recombination current was greatly reduced and the etching rate becomes increased. The higher the frequency of the chopper, the rate of ELPEC-CS etching is greater.

The roughness of the etched GaN surface is very important for the practical application in device fabrication, especially for recess-gate HEMTs and high-power devices. Photo-assisted wet etching with various settings and designs have been developed to improve morphology of the etched GaN.
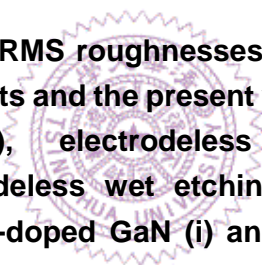
Figure 2.5.1.6 Comparison of RMS roughnesses for PEC etched GaN surfaces from previously reported results and the present work. Etching methods include photoelectrochemical (PEC), electrodeless PEC (Elec. PEC) and chopped-UV-assisted electrodeless wet etching (Chopped Elec. PEC). The samples were unintentionally-doped GaN (i) and n⁺-GaN (n⁺). (From Hwang's group)

Figure 2.5.1.6 [2.5.1.1-2.5.1.4] shows the comparison of the etched GaN surface obtained from various PEC methods. As compared to the previously reported results, ELPEC etching with a chopped UV source can provide an etched GaN surface with smoothness near that of as-grown GaN.

2.5.2 ELPEC-CS etchings of p-GaN
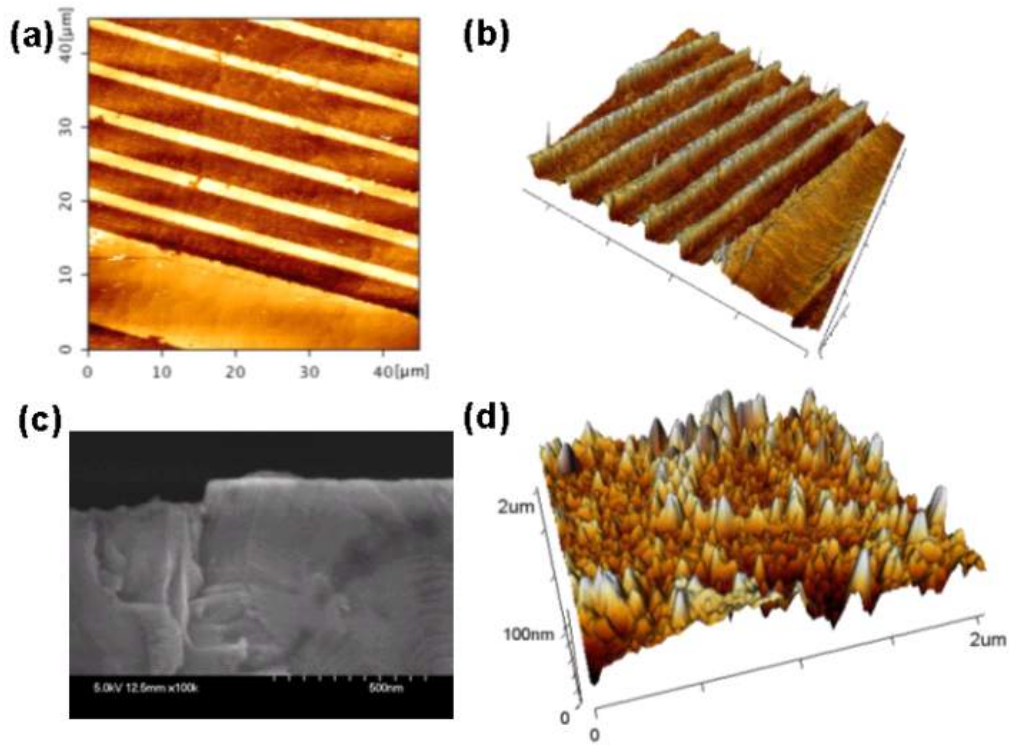
Figure 2.5.2.1 (a) 2-D AFM image (b) 2-D AFM image of an ELPEC-CS etched p-GaN surface with a 2μm-wide striped pattern. (c) SEM micrograph of cross section of an ELPEC-CS etched p-GaN sample (d) high-resolution AFM image of ELPEC-CS etched p-GaN surface. (From Hwang's group)

In this study, we have also applied ELPEC-CS etching to p-GaN. Figure 2.5.2.1 (a) and (b) show the 2-D and 3-D images of atomic force microscopy (AFM) for a p-GaN sample with ELPEC-CS etching. The etching was performed in solution (0.5 M KOH, 0.05 M $K_2S_2O_8$) with a chopper frequency 3000 Hz and a power intensity 63mW/cm^{-2}. The p-GaN sample was etched with a 10nm-thick Au mask with a 2mm-wide striped pattern. The etched depth after 40 min ELPEC-CS etching was ~110 nm as shown in Figure 2.5.2.1 (a) and accordingly the etching rate was determined to be 2.8 nm/min. The SEM micrograph of the cross section for the etched p-GaN profile is shown in Figure 2.5.2.1 (c). The p-GaN sample displays a vertical etching edge after ELPEC-CS etching, without an undercut or shallow profile.
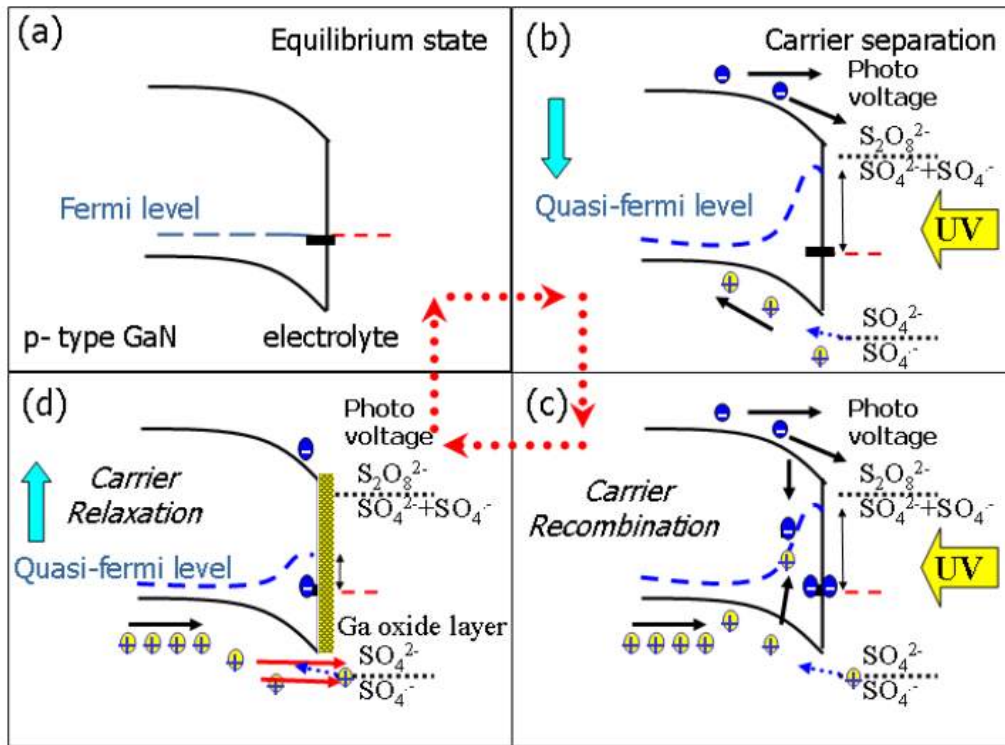
Figure 2.5.2.2 Carrier transport and energy-band diagram of p-GaN during ELPEC etching under periodic UV illumination: (a) an equilibrium state before UV irradiation, (b) separation of photogeneration carriers under UV irradiation, (c) Electron reduction and carrier recombination upon increase of photovoltage (d) Ga-oxide growth and dissolution of Ga oxides without UV illumination. (From Hwang's group)

Figure 2.5.2.2 depicts the dynamics of photo-generated carriers during ELPEC-CS etching of p-GaN, which is similar to that for GaN. The photo-generated electrons at the conduction band drift to the surface due to the band bending as shown Figure 2.5.2.2 (b). These electrons subsequently transfer into etching solution via two pathways; (1) involving a reduction reaction of $S_2O_8^{2-}$ and other electrolyte and (2) flowing into the solution as hot electrons. In ELPEC etching, photodissociation of $S_2O_8^{2-}$ can produce $SO_4^{\cdot-}$ which has the energy level lower than the valence band of p-GaN. Beside the photo-generated hole, the hole is also formed at the interface after the electron transfers from the valence band of p-GaN into $SO_4^{\cdot-}$ and results in the reduction of $SO_4^{\cdot-}$ into SO_4^{2-}. In ELPEC, photodissociation of $S_2O_8^{2-}$ produces $SO_4^{\cdot-}$ which has the energy level lower than the valence band of p-GaN. These holes move toward the bulk due to the band bending and increase the photo-voltage near the surface. When the photo-voltage is built high enough, the photo-generated carriers (hole and electron) start to recombine as shown in Figure 2.5.2.2 (c). This is the reason that the UV source is chopped to provide the dark interval in ELPEC etching. In the

dark interval, the recombination of electron-hole can be reduced or suppressed and the hole is driven the surface by the photo-voltge and induces the oxidation of p-GaN with OH^- and H_2O to form Ga oxides as shown in Figure 2.5.2.2 (d). The Ga oxides are subsequently dissolved into the solution; that is the effective step of ELPEC-CS etching of p-GaN. Thus, the etching rate is proportional to the reduction current via relaxation of hole in the dark interval.

In order to obtain large etching rate, the KOH concentration used in ELPEC-CS etching of p-GaN is relatively higher than that for GaN, at which the etching of p-GaN may not proceed at a diffusion-limited condition and not favor the smoothness and uniformity of etched p-GaN. However, our results show that the ELPEC-CS etching of p-GaN can still produce a uniform etching depth as shown in the 3-D AFM image of Figure 2.5.2.1 (c). Figure 2.5.2.1 (d) shows the roughness variation of the etched p-GaN surface, which is less than 50nm. In addition, we found that the etching rate is dependent on the material of the mask. With the same etching condition as described above, the etching rate with Au and Ti metal masks were ~2.8 and ~1 nm/min, respectively.

Since the ELPEC-CS etching can provide the smooth and uniform etched p-GaN surface, we extend its application to the fabrication of a GaN p-n mesa structure. A sample of 0.7mm-thick p-GaN film grown on a 3mm-thick i-GaN was etched in $K_2S_2O_8$/KOH solution under the irradiation of chopped UV light. The sidewall of an etched sample is shown in Figure 2.5.2.3
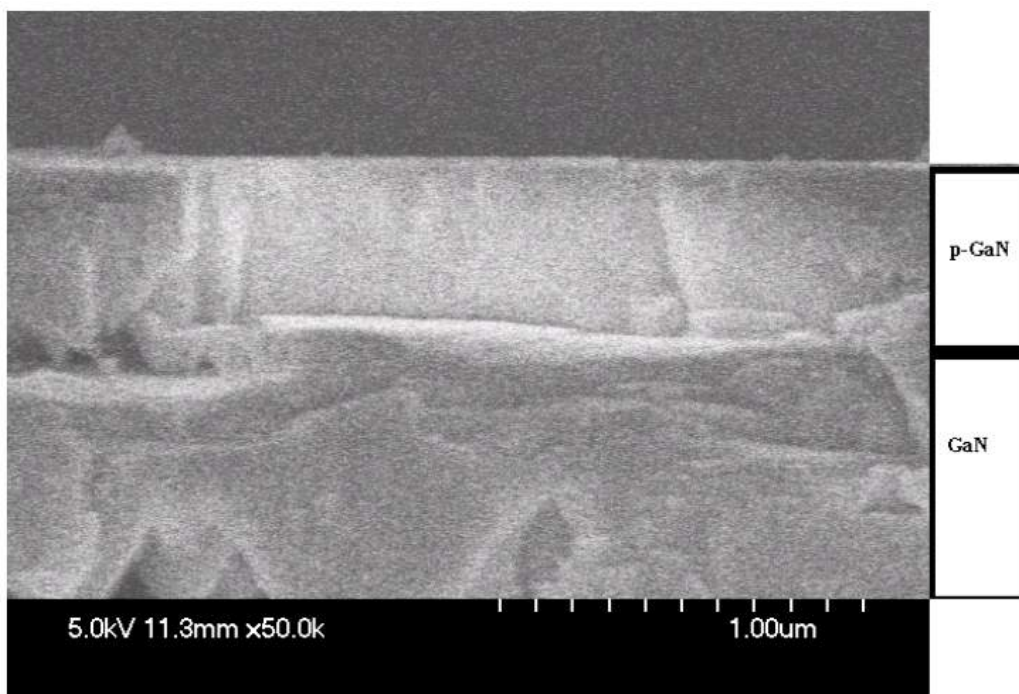
Figure 2.5.2.3 SEM micrograph of the sidewall of a p-n mesa structure obtained from ELPEC-CS etching. (From Hwang's group)

, on which the p-GaN film is etched through to the i-GaN layer. The sample was 0.7 μm p-GaN grown on 3 μm GaN. With prolonging etching, there was start to lateral etching GaN under the p-GaN with ELPEC-CS.
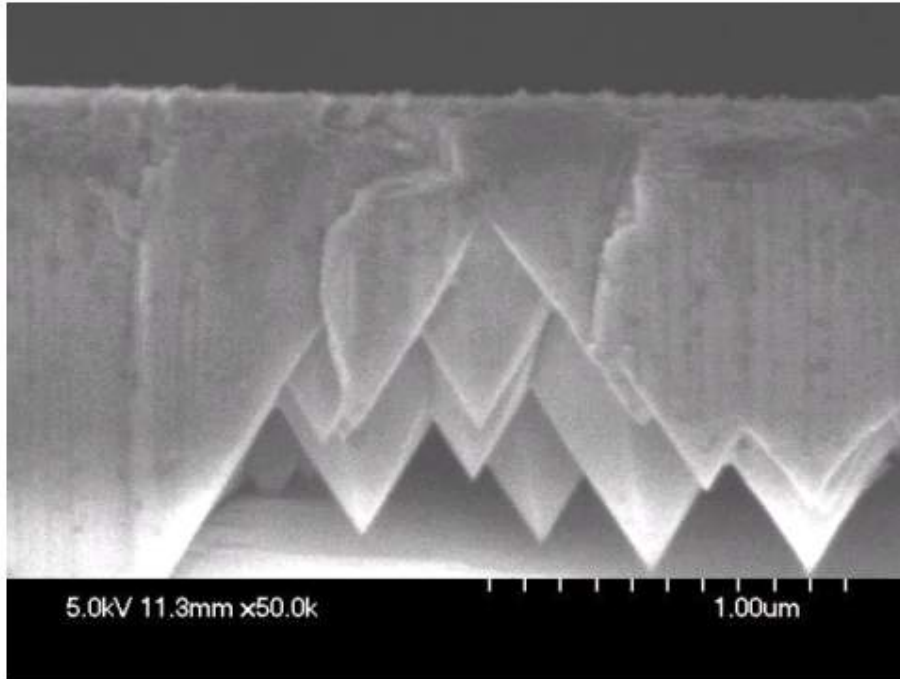
Figure 2.5.2.4 The poor quality GaN was preferred etched under ELPEC-CS etching. (From Hwang's group)

The lateral etching GaN under p-GaN from the interface of GaN and sapphire was shown in Figure 2.5.2.4. The interface of GaN and sapphire had poor crystal quality, so the lateral etched rate near the interface was higher.

2.5.3 ELPEC-CS etchings of multi quantum well structure diode

The diode structure with MQWs had composed of p-GaN, p-AlGaN, GaN, InGaN and n-GaN layer. The Pt metal mask was used for etching blue emission diode. The SEM of etched profile was shown in Figure 2.5.3.1(a).
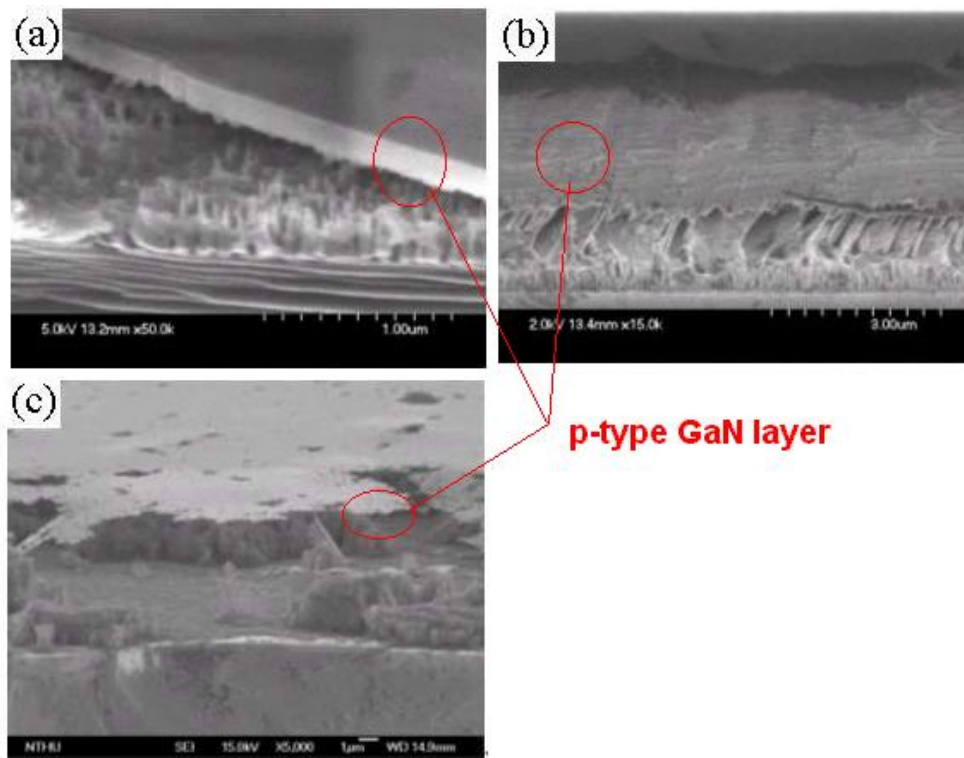
Figure 2.5.3.1 The undercut formation by ELPEC-CS etching (a) high concentration KOH (0.1M) (b) prolong etch (c) floating of the p-type layer. (From Hwang's group)

The p-type III-Nitride was etched with a vertical sidewall, the etched bottom surface had the dislocation revealed on GaN surface, there was lateral etched of InGaN and GaN layer below the p-GaN layer. The lateral etching effect was due to none collimated photon beam. With prolonging etching to sapphire, the cross-section SEM of the etching surface was shown as Figure 2.5.3.1 (b), The side wall of p-type layer and MQWs layer had no lateral etched under better light collimation. But there still had high lateral etched rate in GaN near the interface due to it poor quality of crystalline. The green light emission diode was etched with an irregular Pt metal mask. After ELPEC-CS etching, the lateral etched could be shown very clearly as Figure 2.5.3.1 (c). The diode was not etched though to sapphire, there had thin GaN layer on the etching bottom from the SEM image. The lateral etching distance under p-type material was larger then 3μ m measured by SEM image. In some location of p-GaN surface had broken, these region was covered by Pt metal mask during etching. In this case, after the p-type material was etched through by ELPEC-CS, the vertical etching and lateral etching was simultaneously. With better collimated light, the lateral etching could be reduced as Figure 2.5.3.1 (b). Without better collimated light, the photon could be reflected into the region under Pt mask region. The n-GaN and MQWs layer was etched. Some location of p-type material was etched through even under the Pt mask.

From the Figure 2.5.3.1 (c), the p-type material was floating on the air with depth lateral etching effect. After the etched through p-type material of the blue emission diode, two probes were touching on p-GaN and n-GaN. The bias was applied. In Figure 2.5.3.2, the first blue LED was fabricated successfully by the ELPEC-CS method.
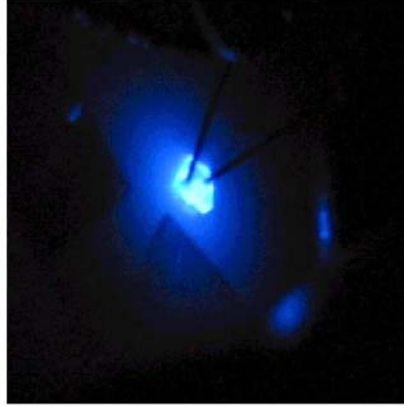
Figure 2.5.3.2 The blue emission from LED. (From Hwang's group)

In summary, the chopped photon was used to suppress the recombination current at dislocation. The smooth, uniform, and broaden etching surface in GaN by ELPEC-CS was achieved. The ELPEC-CS in p-GaN was due to the strong hole relaxation current while the light off during the chopped light with 2μm strip pattern. The Au and Pt catalytic metal mask could enhance the etching rate of p-GaN. The vertical etching profile and no lateral etching depth distribution were achieved. There had the lateral etching effect in P/N diode or MQWs structure for blue and green emission, the better collimated light could reduced the lateral etching. The p-GaN, p-AlGaN, GaN, InGaN, n-GaN could be etched by ELPEC-CS method. A new practical tool for III-Nitride based optical or electrical device fabrication process was invented in my work as shown in Figure 2.5.3.3.

type	Etching Method Ability	PEC	ELPEC	ELPEC-CS
n、i	Anisotropic etching profile	o	o	o
n、i	Broaden etching area	o	o	o
n、i	Lattice damage free	o	o	o
n、i	Cheap etching facility	o	o	o
n、i	High etching rate	o	o	o
n、i	Smooth etching surface	o (n+ only)	o (rms=1.1nm)	o (rms=0.37nm)
n、i	Uniform etching depth	x	o	o
p	p-type material etching	x	x	o
n、i、p	MQW LED Device fabrication	x	x	o

Figure 2.5.3.3 Comparison of the etching ability between conventional PEC, ELPEC and ELPEC-CS method. (From Hwang's group)

Reference

2.5.1.1 C. Youtsey, I. Adesida,L. T. Romano and G. Bulman, Appl. Phys. Lett. 72, 560 (1998).

2.5.1.2 B.S. Shelton, T.G. Zhu, M.M. Wong, H.K. Kwon, C.J. Eiting, D.J.H. Lambert, S.P. Turini, and R.D. Dupuis, Electrochem. Solid-State Lett. 3, 87 (2000)

2.5.1.3 J.A. Bardwell, J.B. Webb, H. Tang, J. Fraser, and S. Moisa, J. Appl. Phys. 89, 4142 (2001).

2.5.1.4 H. Maher, D. Disanto, G. Soerensen, M.W. Dvorak, T.W. MacElwee, J.B. Webb, and C.R. Bolognesi, Proc. Int. Workshop on Nitride Semiconductor, 965 (2000).

Chapter 3.

Device fabrication by roughing technology

3.1 Roughing for the Device

3.1.1 Total rough structure for GaN based blue LED

We developed a technique of ELPEC with a chopped UV source (ELPEC-CS) that achieves an etching rate 45 nm/min with a uniform etching depth [3.1.1.1]. This ELPEC-CS technique was successfully extended to etch *p*-type of GaN [3.1.1.2]. The ELPEC-CS method was applied to rough the GaN-based LED with a mesa structure fabricated by photolithography and inductively coupled plasma (ICP) etching. We report their results of etching surfaces and sidewalls. The roughening mechanism was discussed. After ELPEC-CS treatment, the transparent conductive layer (TCL) of Ni/Au oxidation, p-type contact pad and n-type contact were deposited. The property of this GaN-based LED was reported.

Experiments

The LED samples used in this studing were grown on (0001)-oriented sapphire substrates by metalorganic chemical vapor phase epitaxy. The LED structure consists of a 30-nm-thick GaN low-temperature buffer layer, a 2-μm-thick undoped u-GaN layer, a 2-μm-thick highly conductive n-type GaN (n=5×10^{18} cm^{-3}) layer, a MQW region consisting of six-period 3/10-nm-thick InGaN/GaN multiple quantum well, and a 0.15-μm-thick p-type GaN (p=5×10^{17} cm^{-3}) layer. The LED sample were prepared before processing by first using standard solvent clean, dipping into HCl solution (HCl:H_2O=1:1) for 1min, immersed into boiling aqua regia (HCl:HNO_3=3:1) for 10 min, and rinsed in running deionized water.

A GaN-based mesa structure was fabricated with conventional photolithography and ICP etching. The p-type layer was etching through to n-type layer. The etching depth by ICP etching is 0.6~0.7μm. ELPEC-CS treatment was applied to the GaN-based mesa structure. Before treatment, the samples were treated in methanol and acetone with ultrasonic vibration to remove residual contamination from the surface, rinsed with de-ionized water, and dried in flowing N_2 gas.

All ELPEC-CS treatment were performed in a Teflon electrochemical cell with a quartz window to transmit UV light. The concentrations of KOH was 0.1 M and $K_2S_2O_8$ electrolytes was 0.05M. A mercury-arc lamp (Oriel, 1000 W) with 800W (UV~100mW/cm^2) was served as a source of UV light. A water filter was mounted before the sample to decrease infrared irradiation that might heat the sample. For the periodic illumination with ELPEC-CS etching, a slot chopper with 50% opening was located between the mercury lamp and the electrochemical cell.

After treatment, the TCL layer of Ni/Au oxidation was deposited and alloyed. The Au contact pad of p-type layer was deposited on TCL. The n-type contact was formed

with Ti/Al and alloyed.

The current to voltage and current to intensity was measurement with the probe station system.

Results and discussion

Mesa LED structures (290 × 290 μm^2) were fabricated on a GaN-based sample with photolithography and ICP etching. The structure was etched through *p*-GaN and MQW layers to a *n*-GaN layer with an etching depth about 0.6-0.7 μm. The diagram of the mesa LED after ICP etching was shown in Figure 3.1.1.1(c). Afterwards, the ELPEC-CS method was used to treat the surface of the mesa LED structure; etching was performed for 30 min in solution (KOH 0.1 M, $K_2S_2O_8$ 0.05M) under irradiation (power density 100 mW/cm^2 and chopper frequency 3 kHz). Figure 3.1.1.1(a), 1(d), 1(b) show tilt angle (45 degree) SEM images of etching morphologies of *p*- and *n*-GaN layers, and the edge of the mesa structure, respectively. Nano-rod structures were densely formed on the *n*-GaN surface as shown in Figure 3.1.1.1(d). The *p*-GaN layer formed the etched pit with a dimension ~1 μm and preferred etched at dislocation sites and grain boundaries as shown in Figure 3.1.1.1(a). Figure 3.1.1.1(b) shown the edge between p-GaN and n-GaN was distorted after ELPEC-CS treatment.
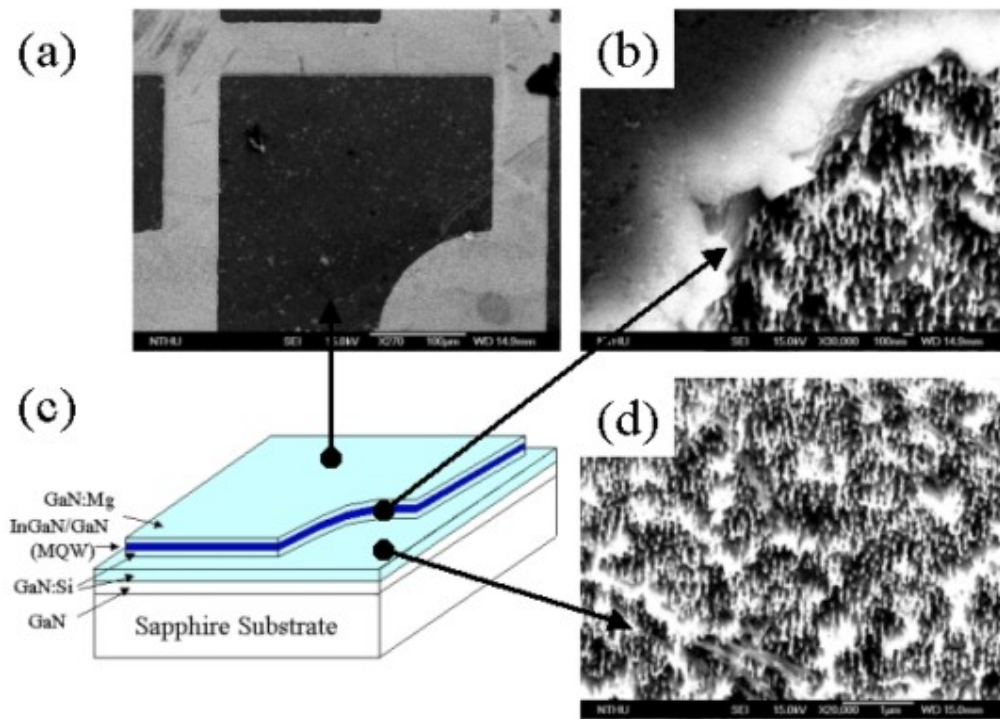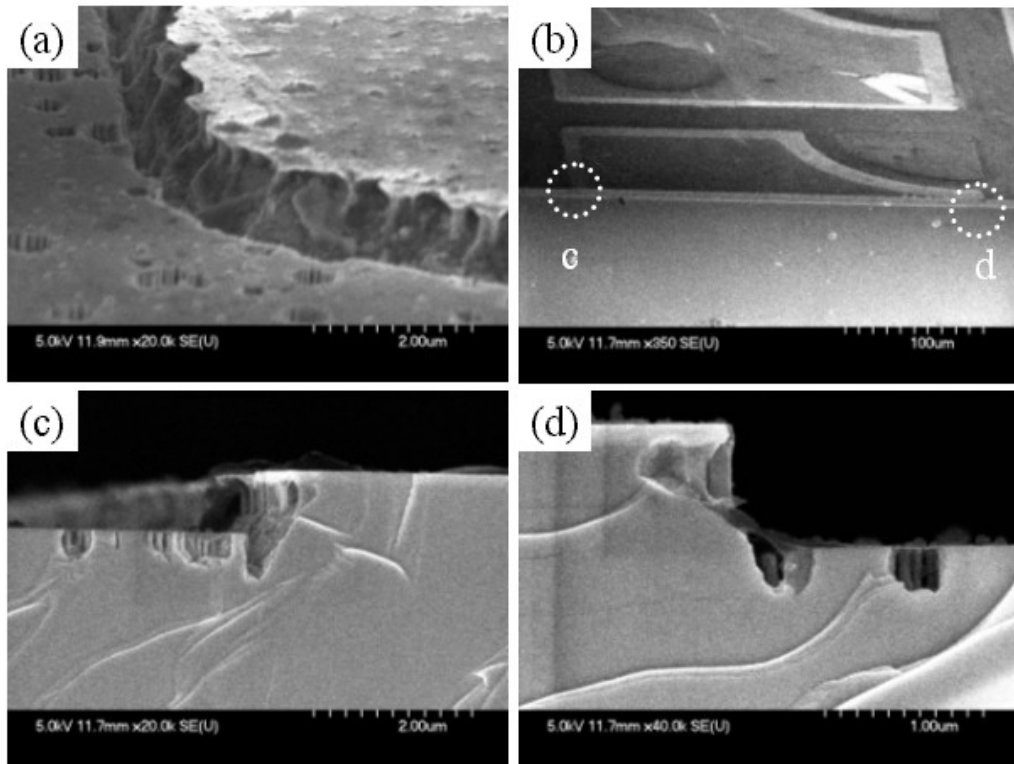

Figure 3.1.1.1. SEM micrographs of various regions of a mesa GaN-based structure after post-treatment with ELPEC-CS etching at a power density 100 mW/cm^2. (a) *p*-GaN etched surface (b) mesa edge between p-GaN and n-GaN (c) diagram of the mesa after ICP etching (d) *n*-GaN etched surface. (From Hwang's group and cooperate with S. C. Hsu)

After ELPEC-CS treatment, the TCL of the NiAu oxidation , p-type contact pad and

n-type contact was deposited and alloyed. The device was fabricated completely. For discuss the sidewall roughness, the LED was cut through the center of the device as shown in Figure 3.1.1.2(a). The tilt angle SEM was used to display whole device after cutting. The white circle c and circle d region were the device edge. The corss-section of the sidewall at circle c and circle d was shown in Figure 3.1.1.2(c) and Figure 3.1.1.2(d). Figure 3.1.1.2(c) shown the cross-section of the nano-rod on the n-type GaN etched surface. The cross-section of the hillock at the bottom of the n-type GaN etched surface was also shown in Figure 3.1.1.2(c) and Figure 3.1.1. 2(d). The undercut near the p-GaN region was due to the preferred etching between p-GaN and InGaN/GaN MQW/n-type GaN. During undercut formation, the p-GaN will collapse. The collapsed p-type GaN on the n-type GaN etched surface was shown in Figure 3.1.1.2(d). The diagram of the etched sidewall was shown in Figure 3.1.1.2(b). The undercut near the p-GaN layer was form and the p-GaN layer collapsed during treatment. Finally the n-GaN sidewall profile become the curve line.
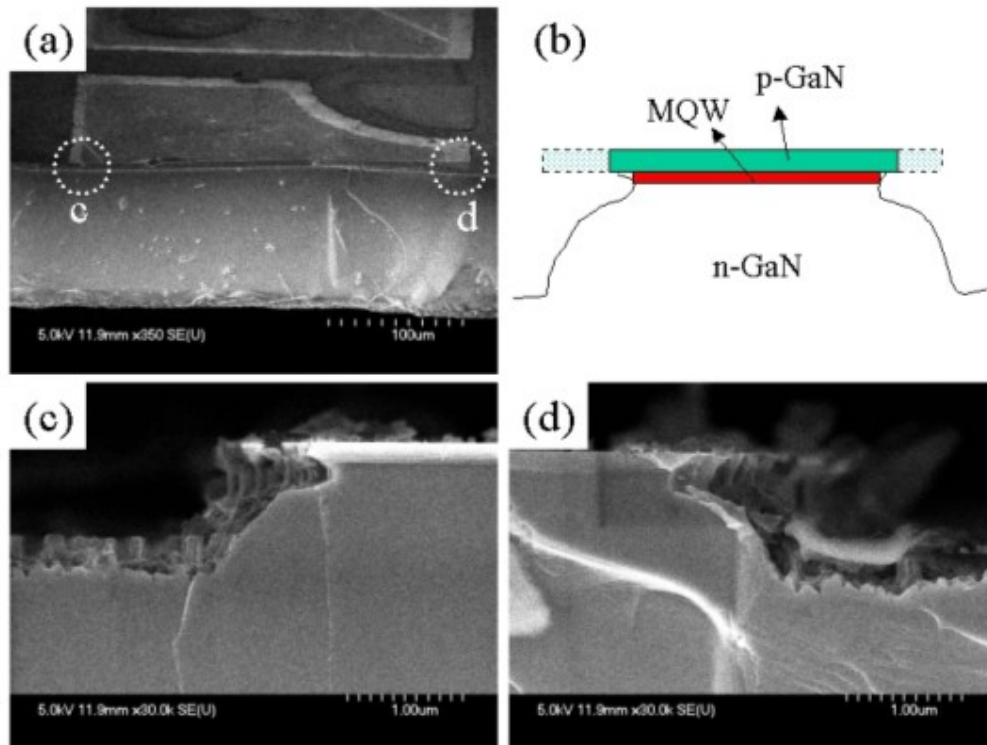
Figure 3.1.1.2. SEM micrographs of various regions of a GaN-based LED after cutting through the center of the device (a) tilt angle image of the half device (b) diagram of the cross-section profile of (a) (c) the cross-section profile of circle c region in (a) (d) the cross-section profile of circle d region in (a) (From Hwang's group and cooperate with S. C. Hsu)
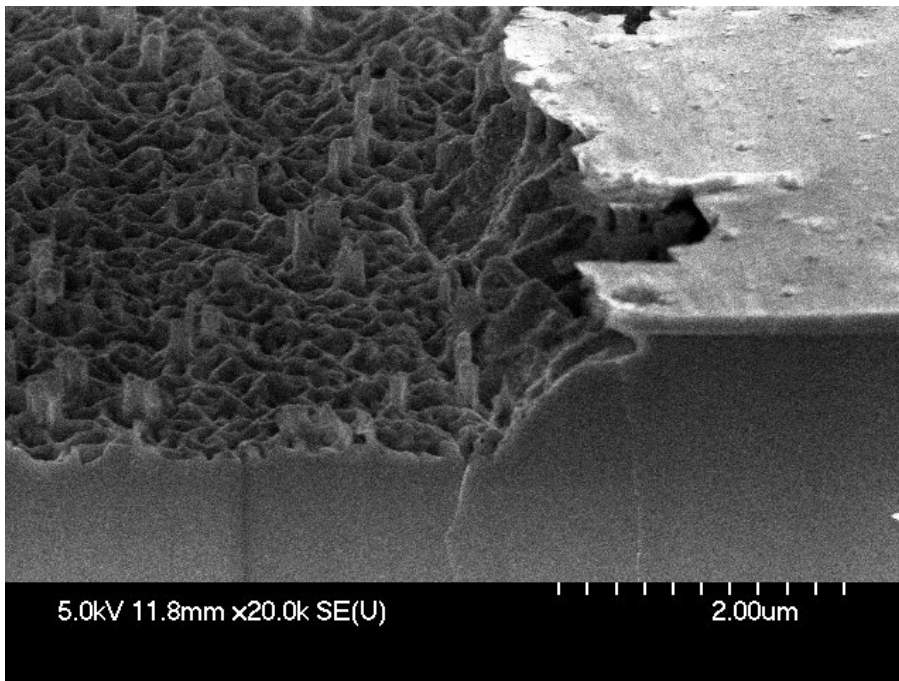
Figure 3.1.1.3. Tilt angle SEM micrographs of Figure 3.1.1.2 (c) (From Hwang's group and cooperate with S. C. Hsu)

The tilt angle SEM micrographs of Figure 3.1.1.2 (c) was shown in Figure 3.1.1.3. The nano-rod and surface morphology of the n-GaN etched surface was shown. The morphology of the device rough with low photon intensity was shown in Figure 3.1.1.4. No obvious etching pit in p-type layer in low photon intensity condition. The nano-rod was not observed at the n-GaN surface with low photon intensity condition.

Figure 3.1.1.4. SEM micrographs of various regions of a GaN-based LED after post-treatment with ELPEC-CS etching at a power density < 10 mW/cm². (a) tilt angle SEM of (c) (b) tilt angle image of the half device (c) the cross-section profile of circle c region in (b) (d) the cross-section profile of circle d region in (b). (From Hwang's group and cooperate with S. C. Hsu)

The light emission mapping under low and higher current injection was recorded by color CCD as shown in Figure 3.1.1.5. The device structure was shown in Figure 3.1.1.2 .The emission mapping with inject current of 30μA at 2.7V was shown in Figure 3.1.1.5(a-1). The emission light transmitted through rough p-GaN layer and TCL from the active layer. The emission intensity was uniform. Under higher current injection of 470μA at 3.2V, the emission light was enhance extraction from the rough edge of the LED as shown in Figure 3.1.1.5(a_2). The edge of LED was indicated by white line. The current to voltage and current to light intensity within 1mA was shown in Figure 3.1.1.5(b). The light started to detect by photodiode at 2.5V. The voltage was 3.27V at 1mA. The linear between current to light intensity under low injection current was suggested that the low non-radiative recombination and high extraction efficiency with this total rough device structure. Under high current injection at 20mA with 5.5V as shown in Figure 3.1.1.5(c), the driver voltage was to high compared with conventional LED (3.1~3.6V) at 20mA. It was due to the high contact resistance of the TCL deposition. The series resistance was 91.7Ω. The current to intensity was linear within 5mA. While the injection current higher than 5mA, the external quantum efficiency was reduced. It was due to the thermal heating effect with the poor thermal conductivity of

the sapphire substrate.

(a) 30uA,2.7V   470uA, 3.2V   (b)

(c)
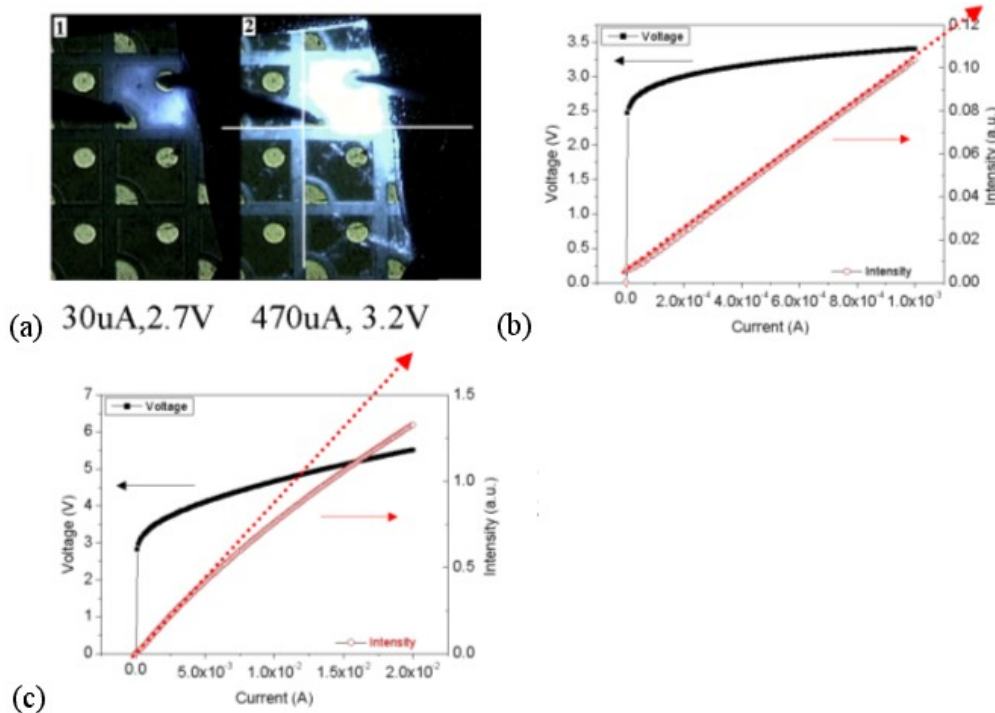
Figure 3.1.1.5. The total rough device properties (a) (1) The light intensity mapping under low current injection (2) The light intensity mapping under higher current injection (b) The current to voltage and current to light intensity within 1mA injection current (c) The current to voltage and current to light intensity within 20mA injection current. (From Hwang's group and cooperate with S. C. Hsu)

The performance of three LEDs was compared.

DEVICE 1 : **Flat** surface cavity LED without roughing by photon assisted wet etching method.

DEVICE 2 : **Surface rough** LED with photon assisted wet etching method before mesa formation by ICP etching.

DEVICE 3 : **Total rough** LED with photon assisted wet etching method after mesa formation by ICP etching.

The DEVICE 1 had flat p-type GaN surface and sidewall after ICP etching. The DEVICE 2 had rough p-type GaN surface after photon assisted wet etching treatment and smooth sidewall after mesa formation by ICP. The DEVICE 3 had rough p-type GaN surface and rough sidewall after photon assisted wet etching treatment. The p-type GaN surface of the DEVICE 2 wafer after photon assisted wet etching treatment was shown in Figure 3.1.1.6. The concentrations of KOH was 0.1 M and $K_2S_2O_8$ electrolytes was 0.05M. A mercury-arc lamp (Oriel, 1000 W) with 800W (UV~100mW/cm^2) was served as a source of UV light. The chopped frequency of the

60

photon was 3kHz. The treatment time was 30mins. The grain boundary was preferred etched after treatment as shown in Figure 3.1.1.6 (a) &(b). The roughness was about 0 ~ 6nm from the cross section data as shown in Figure 3.1.1.6 (c).
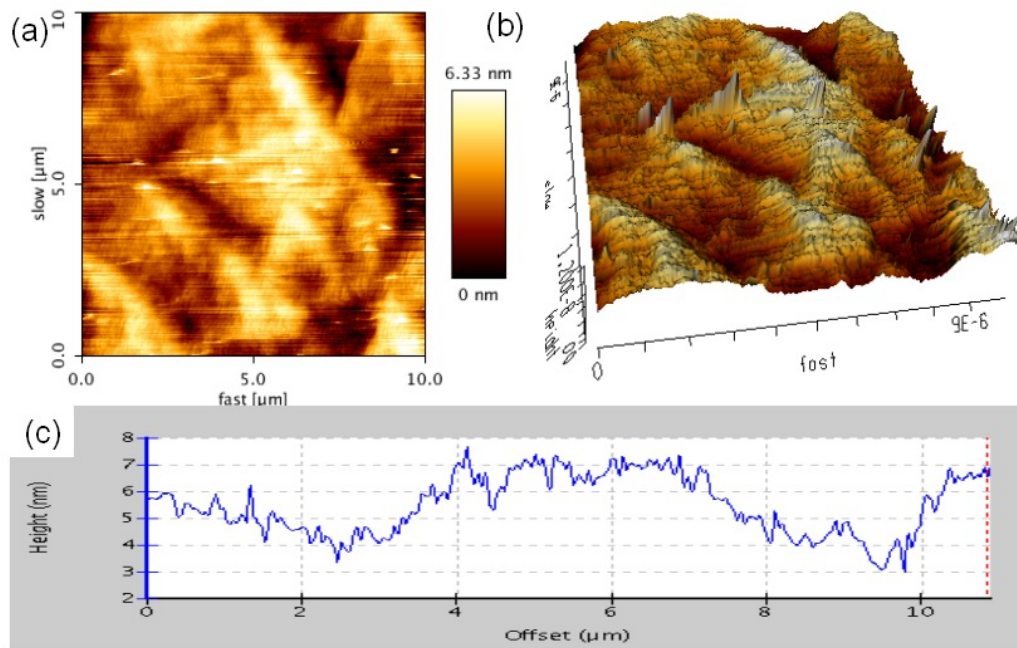
Figure 3.1.1.6. The surface morphology of the Device 2 after photon assisted wet etching treatment (a) 2D morphology image with AFM (b) 3D morphology image with AFM (c) Cross-section of the treated surface. (From Hwang's group and cooperate with S. C. Hsu)

The current to voltage (I-V) and current to emission power (I-L) were measured after chip bonding as shown in Figure 3.1.1.7. The Flat, Surface rough and Total rough in Figure were represented as Flat surface cavity LED, surface rough LED and Total rough LED, respectively. The output power started to saturate at high current injection higher then 60mA and decrease at injection current higher then 80mA. The total rough LED had produce higher max optical output (~4.6mW) than the surface rough LED (~1.8mW) and the Flat surface cavity LED (~1.2mW). The operation voltage was higher then the 5V while the injection current high then 20mA. It shown that the series resistance was very high. The operation properties of the three Devices were list in Table 3.1.1.1
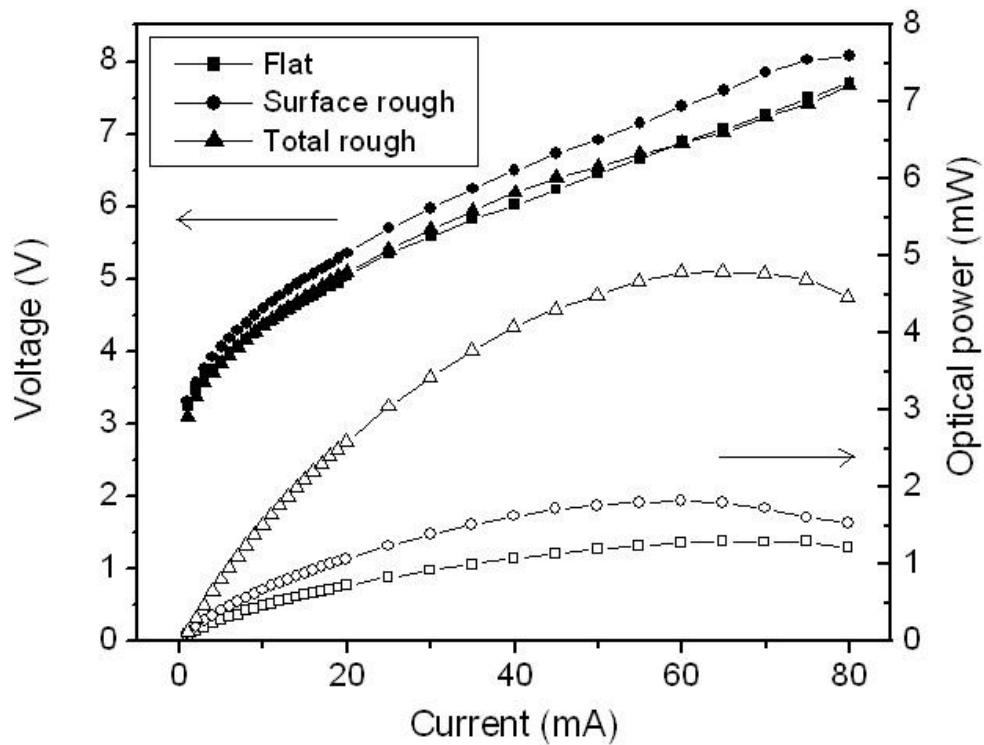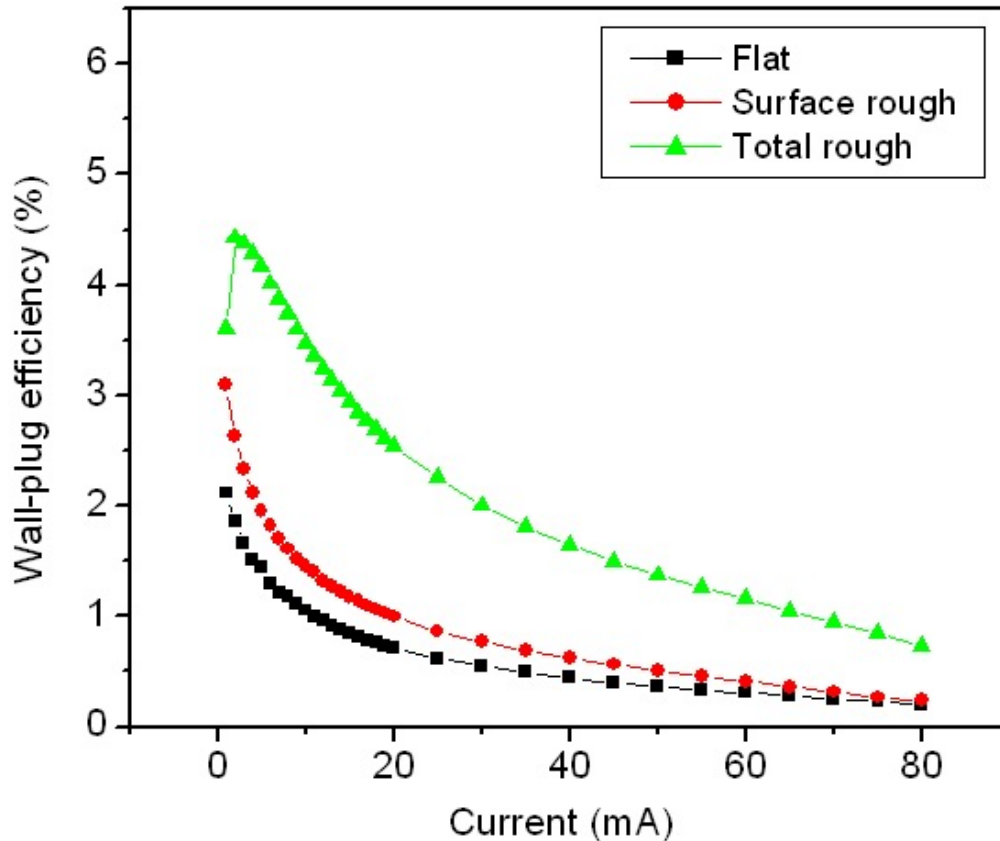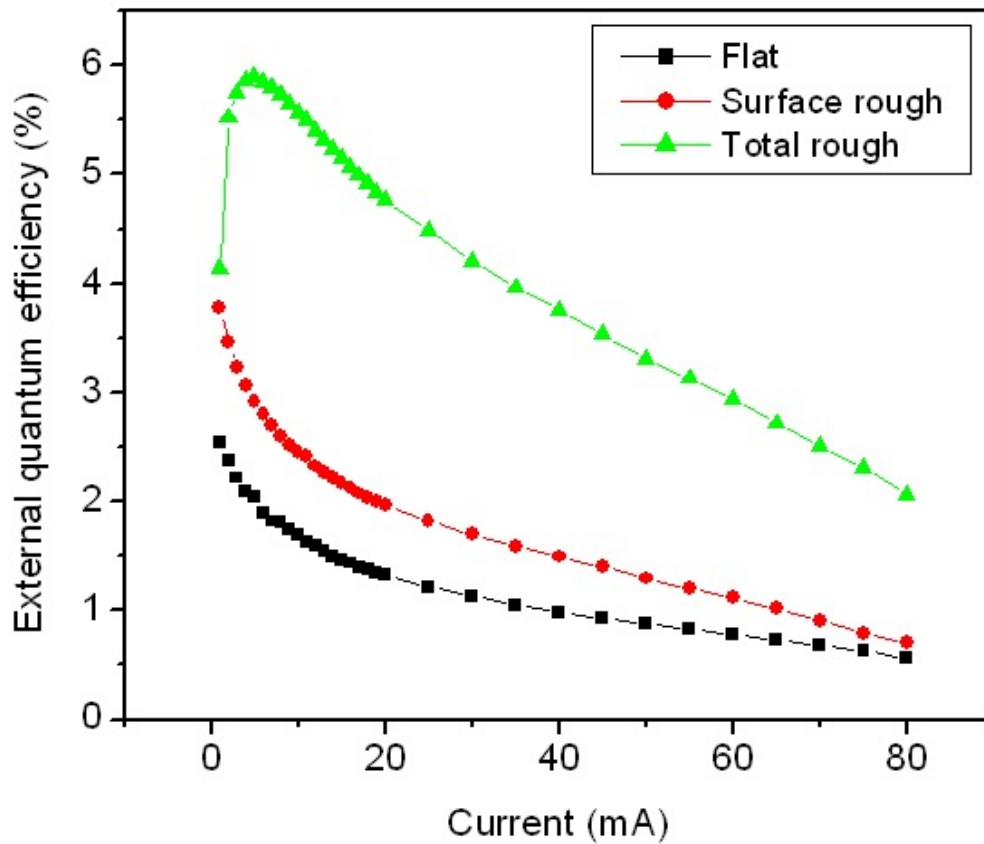
Figure 3.1.1.7. The I-V-L result of flat surface cavity LED, surface rough LED and Total rough LED. (From Hwang's group and cooperate with S. C. Hsu)

The transition current was defined as the current while the linearity of the current to emission intensity was lost. The transition current will increasing while the thermal resistance reduce, suppress piezoelectrical effect and series resistance reduce. The higher optical output power and max output of the total rough LED was due to the higher light extraction efficiency and lower series resistance.

Table 3.1.1.1 Comparison of the properties with three devices

LED type	Operation current	Operation voltage	Output power	Series resistance	Transition current
Flat surface cavity	20mA	5.04V	0.72mW	42.4Ω	5.0mA
Surface rough	20mA	5.35V	1.07mW	44.4Ω	5.0mA

Total rough	20mA	5.09V	2.59mW	38.7Ω	6.1mA

The Wall-plug efficiency could be extracted from the I-V and I-L data in Figure 3.1.1.7. The Wall-plug efficiency was extracted without epoxy resin encapsulation. The max efficiency was 4.5% at lower injection current and 2.5% at 20mA of the total rough LED.

Figure 3.1.1.8. The Wall-plug efficiency of flat surface cavity LED, surface rough LED and Total rough LED. (From Hwang's group and cooperate with S. C. Hsu)

The external quantum efficiency was extracted from the Figure 3.1.1.8. The max external quantum efficiency was ~6% at low injection current and 4.7% at 20mA of the total rough LED. The low external quantum efficiency was due to the low internal quantum efficiency of the LED (poor quality sample). We focus on the light extraction efficiency enhanced ratio by comparing the three LEDs with and without roughing tech. The enhanced ratio of the external quantum efficiency was shown in Figure 3.1.1.10.

Figure 3.1.1.9. The external quantum efficiency of flat surface cavity LED, surface rough LED and Total rough LED. (From Hwang's group and cooperate with S. C. Hsu)

The surface rough LED could improve ~1.5 time efficiency then flat surface cavity LED by roughing the p-type GaN of the surface rough LED. The Total rough LED could improve ~3.5-3.75 time efficiency then flat surface cavity LED while the injection current larger then the 20mA. The lower enhanced ratio of the total rough LED was suggested due to the current crowding effect of this device. Under higher current injection, the most light could be emission under the TCL. The light absorption of the contact pad was dominated at low current injection.
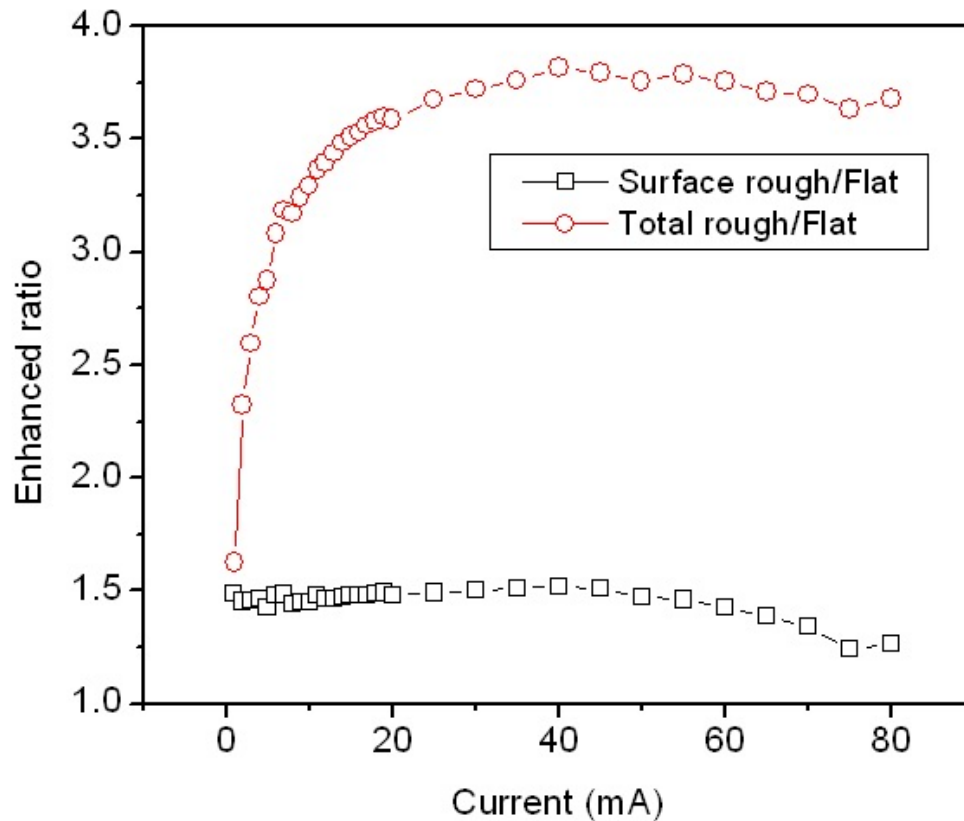
Figure 3.1.1.10. The enhanced ratio of the external quantum efficiency with flat surface cavity LED, surface rough LED and Total rough LED. (From Hwang's group and cooperate with S. C. Hsu)

The current increasing will increase the power. The spectrum stability under lower optical output power was shown in Figure 3.1.1.11. The lm (light intensity) of the LEDs were proportional to the optical output power. The total rough LED had higher spectrum stability at higher output power. While the injection current is higher then 60mA at total rough LED, the output power start to decrease and the lm (light intensity) was also decrease. The device efficiency at various current injected was shown in Figure 3.1.1.12. The lm/W was decreasing gradually following the injection current increasing.
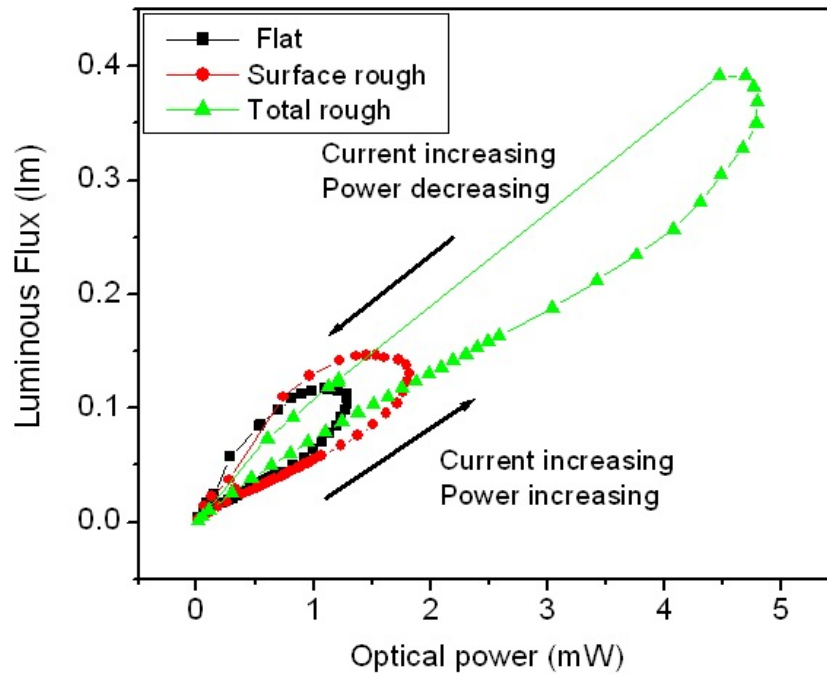
Figure 3.1.1.11. The optical properties of the power to luminous at various current injection with flat surface cavity LED, surface rough LED and Total rough LED. (From Hwang's group and cooperate with S. C. Hsu)
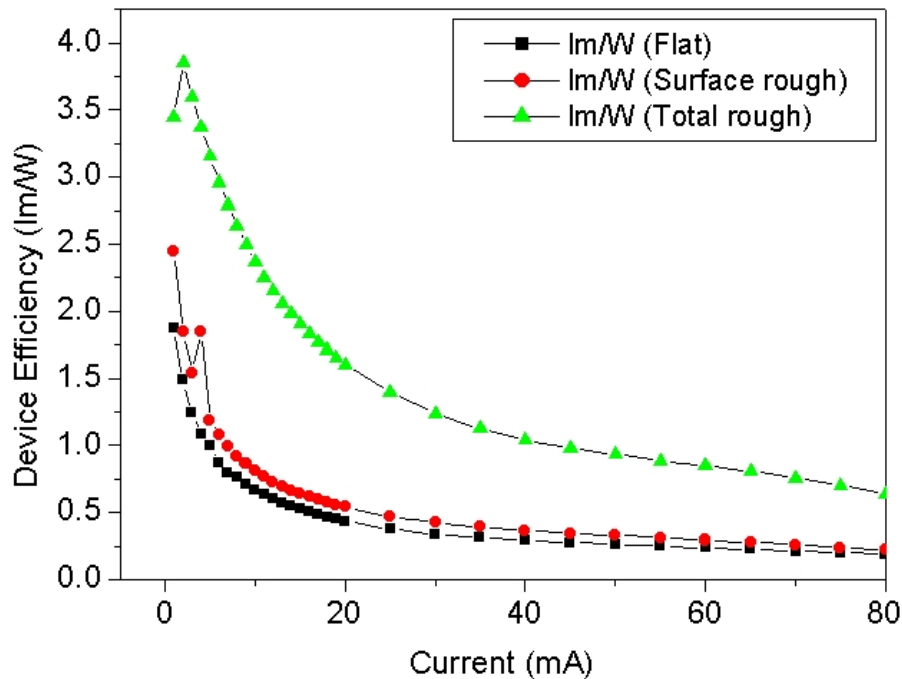
Figure 3.1.1.12. The device efficiency at various current injection with flat surface cavity LED, surface rough LED and Total rough LED. (From Hwang's group and cooperate with S. C. Hsu)

The field pattern was at 20mA and 50mA was shown in Figure 3.1.1.13. The field pattern was similar while the injection current higher than 20mA. The forward light

intensity was increasing in total rough LED. Most light was extracted from the forward. The field pattern was stable with in 20mA-50mA at total rough LED. Three field patterns were compared in Figure 3.1.1.14.
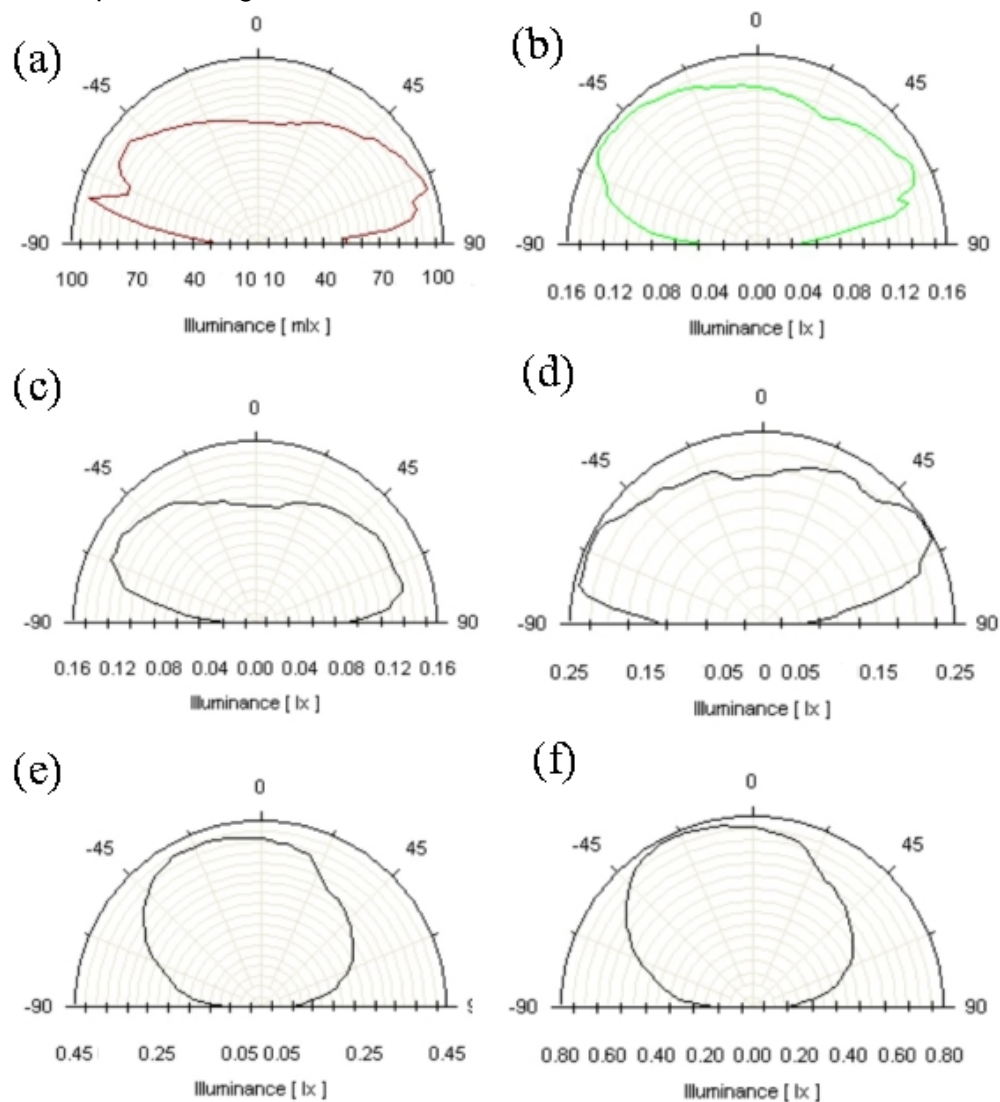
Figure 3.1.1.13. The field pattern (a) Flat surface cavity LED at 20mA (b) Flat surface cavity LED at 50mA(c) Rough surface LED at 20mA (d) Rough surface LED at 50Ma (e) Total rough LED at 20mA (f) Total rough LED at 50mA. (From Hwang's group and cooperate with S. C. Hsu)
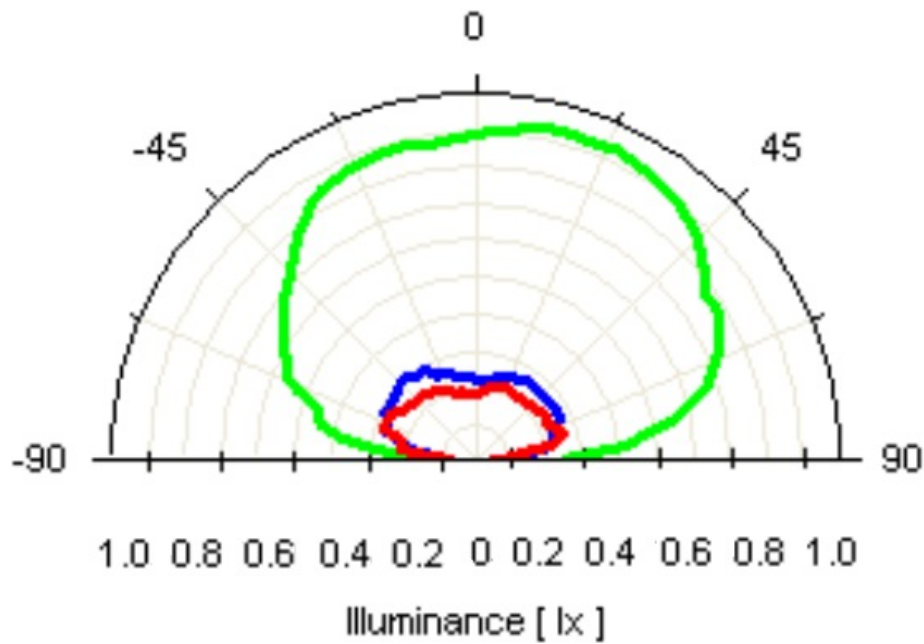
Red line - Flat, Blue line - Surface rough, Green line - Total rough

Figure 3.1.1.14. Comparison of the field patterns with three devices. (From Hwang's group and cooperate with S. C. Hsu)

Conclusion

The GaN-based mesa structure was forming by photolithography and ICP etching. The ELPEC-CS was applied to rough the top p-type surface and sidewall. An undercut is observed near the *p*-GaN and the curve line of the n-GaN sidewall was formed. The n-GaN etched surface with nano-rod and hillock structure was presented after treatment. After roughening, the transparent conductive layer (TCL) of Ni/Au oxidation, p-type contact pad and n-type contact were deposited. The total rough device was fabricated completely. The linearity between current and light emission intensity in low injection current was demonstrated. It was suggested than the total rough device structure could efficiently enhanced the light extraction. From the emission intensity mapping at higher current, the light could be enhanced extracted from the rough sidewall of the device edge.

The three devices performance were analysis by electrical and optical properties. The light extraction efficiency was increasing by roughing with photon assisted method was identified from the efficiency analysis.

References

3.1.1.1 Z. H. Hwang, J. M. Hwang, W. H. Hung and H. L. Hwang, Appl. Phys. Lett. 84, 3759 (2004).

3.1.1.2 J.M. Hwang, K.Y. Ho, Z.H. Hwang, W.H. Hung ,Kei May Lau, H.-L. Hwang,

Chapter 4.

Device scale-down for III-Nitride LED

4.1 The micro and nano structure of III-Nitride fabricated by photon assisted wet etching method

The abbreviation of the etching parameter was shown in the Table 4.1.1. The methods of the photon assisted wet etching were also shown in the table. For simplify expression of the etching condition, the condition will be shown as the form of [*M:* ,*P:* ,*E:* ,*O:* ,*Ma:* ,*Ti:* ,*F:* ,*T:* ,*B:* ,*El*]. The example of the condition was [*M:* **LED** ,*P:* **900W** ,*E:* **0.1**,*O:* **0.1** ,*Ma:* **Ni/Au (10/10nm)**,*Ti:* **30**,*F:* **3k**,*T:* **90** ,*B:* **1**,*El:* **Pt**]. The material was LED structure. The lamp power was 900W. The etchant was 0.1M KOH. The oxidizer was $K_2S_2O_8$. The mask was Ni/Au. The etching time was 30mins. The chopped frequency was 3kHz. The solution temperature was 90^0C. The applied bias was 1V. The electrode was Pt electrode.

Table 4.1.1 The condition of the photon assisted wet etching

Condition	Material	Photon intensity (mW/cm^2) or lamp power (W)	Etchant (M) (KOH)	Oxidizer (M)($K_2S_2O_8$)	Mask
Abbreviation	*M*	*P*	*E*	*O*	*Ma*
Condition	Time (minute)	Frequency (Hz)	Temperature (^{o}C)	Bias (V)	Electrode
Abbreviation	*Ti*	*F*	*T*	*B*	*El*

*Condition [*M:* ,*P:* ,*E:* ,*O:* ,*Ma:* ,*Ti:* ,*F:* ,*T:* ,*B:* ,*El*]

*Photoelectrochemical (PEC)

*Bias photoelectrochemical (BPEC)

*Electroless photoelectrochemical (ELPEC)

*Electroless photoelectrochemical with chopped photon source (ELPEC-CS)

*Bias-Electroless photoelectrochemical with chopped photon source (BELPEC-CS)

* Bias-Thermal-Electroless photoelectrochemical with chopped photon source (BTELPEC-CS)

4.1.1 Micro scale structure fabrication

The fabrication of micro scale material will be shown in this section. The methods including the PEC, ELPEC-CS, BELPEC-CS, BTELEPC-CS and Inductively-coupled plasma (ICP) etching III-Nitride will be presented. The mechanism was discussed in Chapter 3.

4.1.1.1 PEC etching

The etching condition was [*M:* **GaN**,*P:* ,*E:* ,*O:* ,*Ma:* **Titanium**,*Ti:* , *F:* ,*T:* , *B:* ,*El:*]. The

selected etching crystalline GaN near the line pattern will reveal the dislocations as shown in Figure 4.1.1.1.1 (a). The dimension of the etched line pattern was 2μm. The rectangle hole-pattern array with 4μm width and 100μm length was shown in Figure 4.1.1.1.1 (b). The square hole-pattern with 50μm width and 50μm length was shown in Figure 4.1.1.1.1 (b).
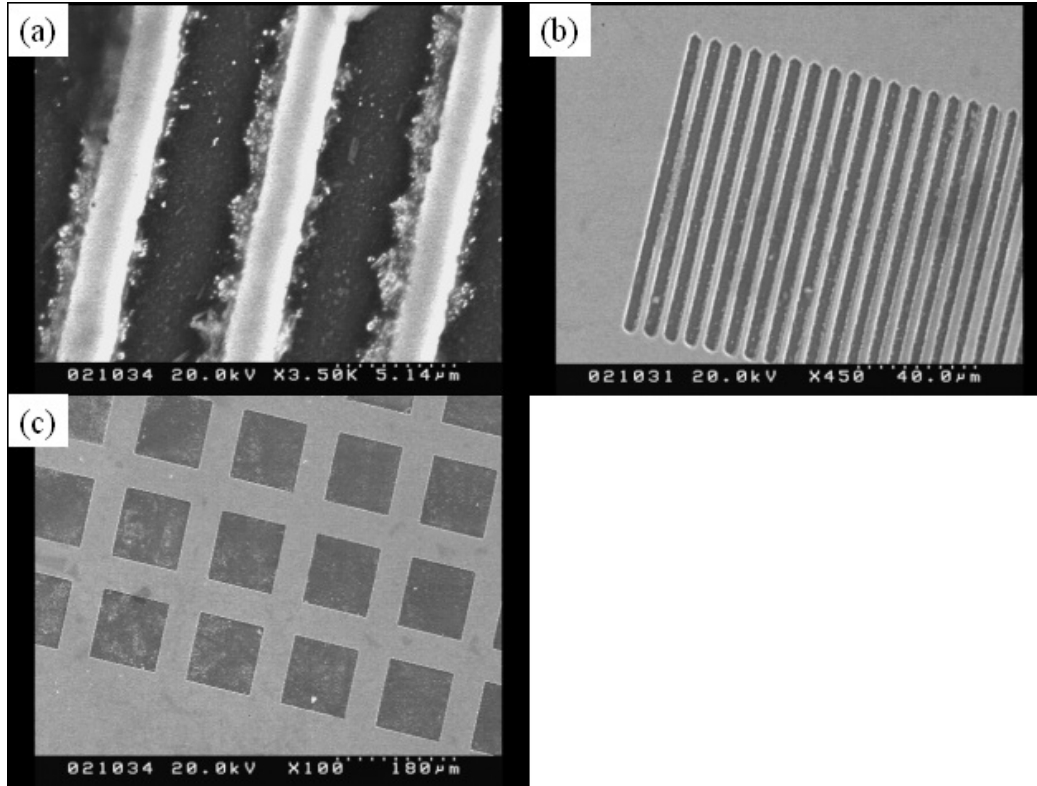

Figure 4.1.1.1.1 The SEM photography of PEC etched GaN. (a) strip pattern (b) rectangle hole-pattern (c) square hole-pattern

The etching condition was [*M:* GaN ,*P:* ,*E:* ,*O:* ,*Ma:* Titanium,*Ti:* ,*F:* ,*T:* ,*B:* ,*El*]. The etched GaN pattern was post-treatment with boiled KOH solution as shown Figure 4.1.1.1.2. The residual dislocation after PEC etching was removed as shown in Figure 4.1.1.1.2 (a). The 3μm GaN mesa with smooth and vertical cavity was formed after post-treatment as shown in Figure 4.1.1.1.2 (b). The smooth etched surface of the square hole-pattern with 50μm width and 50μm length was shown in Figure 4.1.1.1.1 (c).
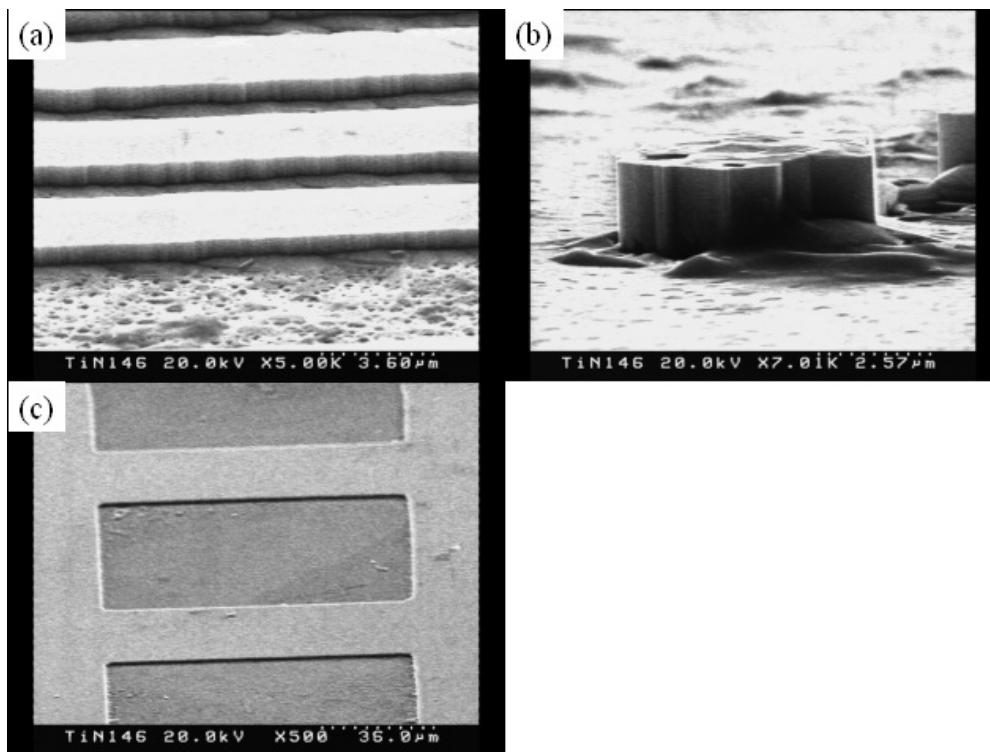
Figure 4.1.1.1.2 The SEM photography of PEC etched GaN with 1M boiled KOH treatment. (a) strip pattern (b) isolated mesa (c) square hole-pattern

4.1.1.2 ELPEC-CS etching

The etching condition was [*M:* **GaN** ,*P: 63*,*E:* **0.01**,*O:* **0.05** ,*Ma:* **Titanium**,*Ti:* ,*F: 2.5k*,*T:***RT** ,*B:* ,*E*l]. The cross-section fo the 2.5μm strip pattern was shown in Figure 4.1.1.2.1. There had a trapezoid etching profile. Very uniform etched depth was achieved and no whisker was found in the etched surface.
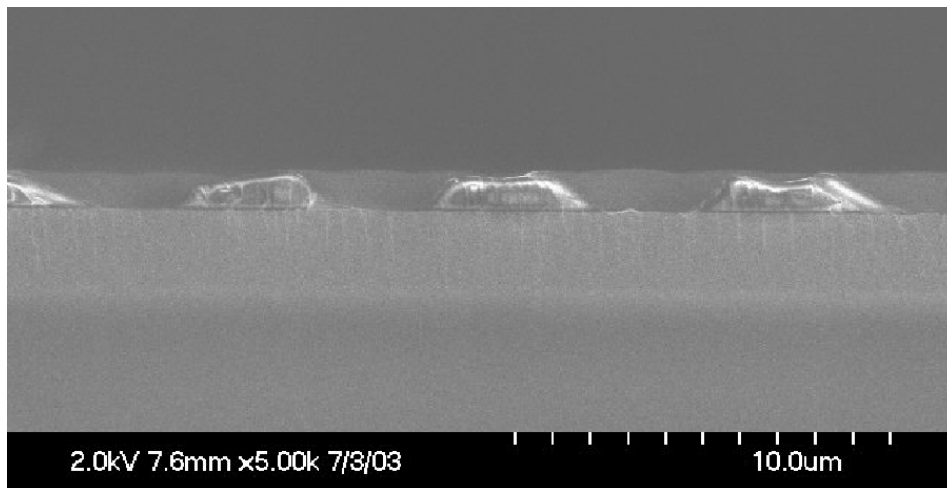
Figure 4.1.1.2.1 The cross-section of the ELPEC-CS etched GaN pattern.

The etching condition was [*M:* **GaN** ,*P: 900W* ,*E:* **0.1**,*O:* **0.05** ,*Ma:* **Ni/Au (10/10nm)**,*Ti: 30*,*F:* **3k**,*T:***RT** ,*B:* ,*E*l]. The etching profile was shown in Figure 4.1.1.2.2. The reduction

current was suppressed due to the high contact resistance of the Ni/Au metal mask. The etching depth was very shallow near the 2μmx5μm mask. The width of the shallow etched region was about 3~4μm.

NTHU   SEI   15.0kV   X3,500   1μm   WD 14.1mm
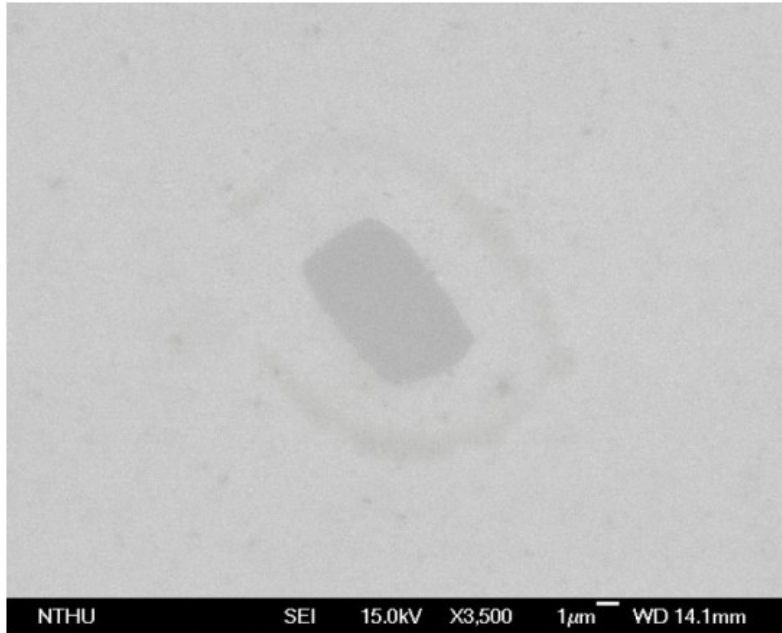
Figure 4.1.1.2.2 Mask effect in ELPEC-CS etching GaN

The etching condition was [*M:* **p-GaN/GaN** ,*P:* **63** ,*E:* **0.1**,*O:* **0.05** ,*Ma:* **Au (10nm)**,*Ti:* ,*F:* **3k**,*T:***RT** ,*B:* ,*El*]. The 2μm strip pattern was shown in Figure 4.1.1.2.3 (a). The p-type GaN was not etched through. The p-type GaN was etching through as shown in Figure 4.1.1.2.3 (b). The etching condition was [*M:* **p-GaN/GaN** ,*P:* **110** ,*E:* **0.01**,*O:* **0.05** ,*Ma:* **Au (10nm)**,*Ti:* ,*F:* **3k**, *T:* **RT** ,*B:* , *El:* **Pt]**. The needle structure of the GaN was observed on the etched surface. The undercut of the GaN under p-type GaN was also observed. Another etching condition with no undercut was observed as shown in Figure 4.1.1.2.3 (c). The etching condition was [*M:* **p-GaN/GaN** ,*P:* **110** ,*E:* **0.01**,*O:* **0.05** ,*Ma:* **Au (10nm)**,*Ti:* ,*F:* **1k**,*T:***RT** ,*B:* ,*El:* **Pt]**. The dislocation and hillock was observed after etching through p-type GaN. The width of the strip was about 1 μm. The hole-pattern after etching through p-type GaN was shown in Figure 4.1.1.2.3 (d). The serious undercut of p-type GaN was observed.
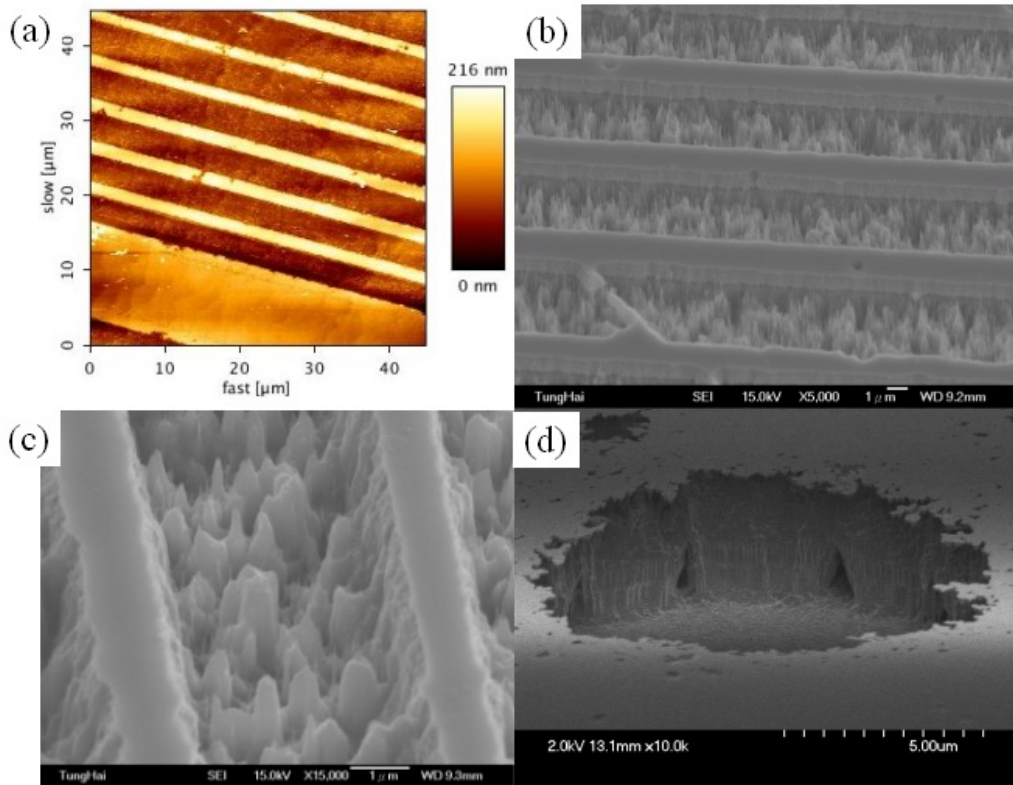
Figure 4.1.1.2.3 The etched profile of the p-type GaN on GaN. (a) AFM image (b) SEM image (c) SEM image (d) SEM image of The hole-pattern.

After etching through p-type GaN of p-type GaN on GaN, the sample was post-treatment with boiled KOH. The dislocation was removed after post-treatment as shown in Figure 4.1.1.2.4 (a). The 2μm strip pattern was achieved after etching as shown in Figure 4.1.1.2.4.
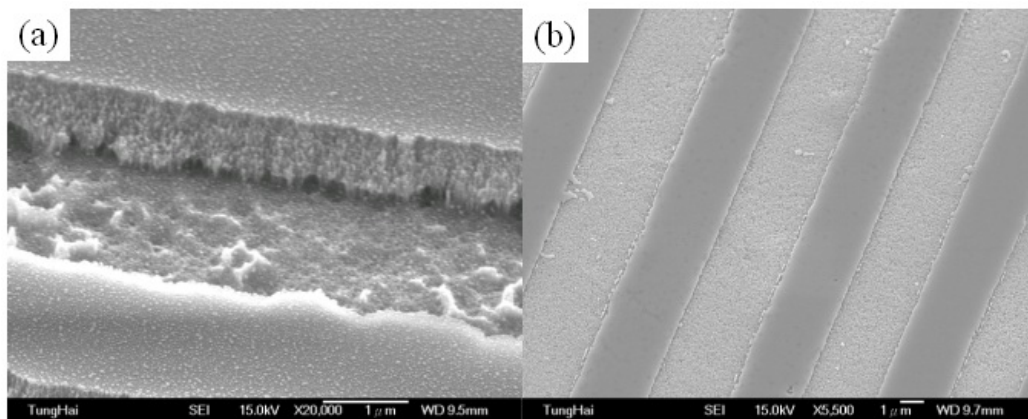

Figure 4.1.1.2.4 The etched profile after post-treatment (a) SEM image of p-type GaN sidewall and GaN etched surface (b) Top view of the etched pattern.

The LED sample was etched with isolated mesa metal mask. The etching condition was [*M:* **LED** *,P:* **900W** *,E:* **0.1**,*O:* **0.05** ,*Ma:* **Ni/Au (10/10nm)**,*Ti:* **30x2**,*F:*

3k,*T:***RT** ,*B: ,El*]. The mask effect also observed as shown in Figure 4.1.1.2.5. The pattern size was 2 μm x 5 μm. The shallow etching depth near the mask was observed. The etching rate was very low due to the low reduction current. The width of the shallow etching region was about 1μm.
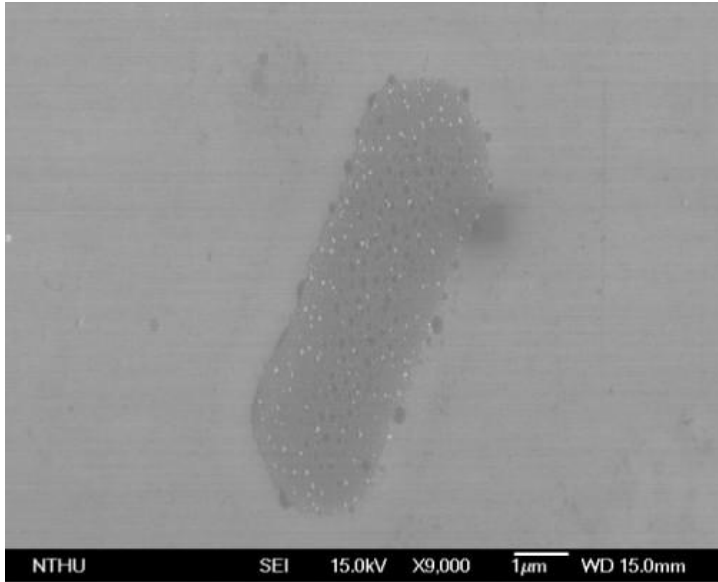
Figure 4.1.1.2.5 The SEM image with tilt angle (45^{0}).

4.1.1.3 BELPEC-CS etching

The BELPEC-CS etching was applied for etching GaN with isolated NiAu metal mask. The GaN was etched with NiAu mask. The etching condition was [*M:* **GaN** ,*P:* **900W** ,*E:* **0.1**,*O:* **0.05** ,*Ma:* **Ni/Au (10/10nm)**,*Ti:* **30**,*F:* **3k**,*T:***RT** ,*B:* **2.5**,*El:* **Pt**]. There had a lateral potential gradient along the Pt electrode. There had no etching apart from Pt electrode as shown in Figure 4.1.1.3.1 (a). The hole-pattern in the etching region was shown in the Figure 4.1.1.3.1 (b). The etching surface was rough under BELPEC-CS etching. There had some hillock with size <300nm on the etched surface.
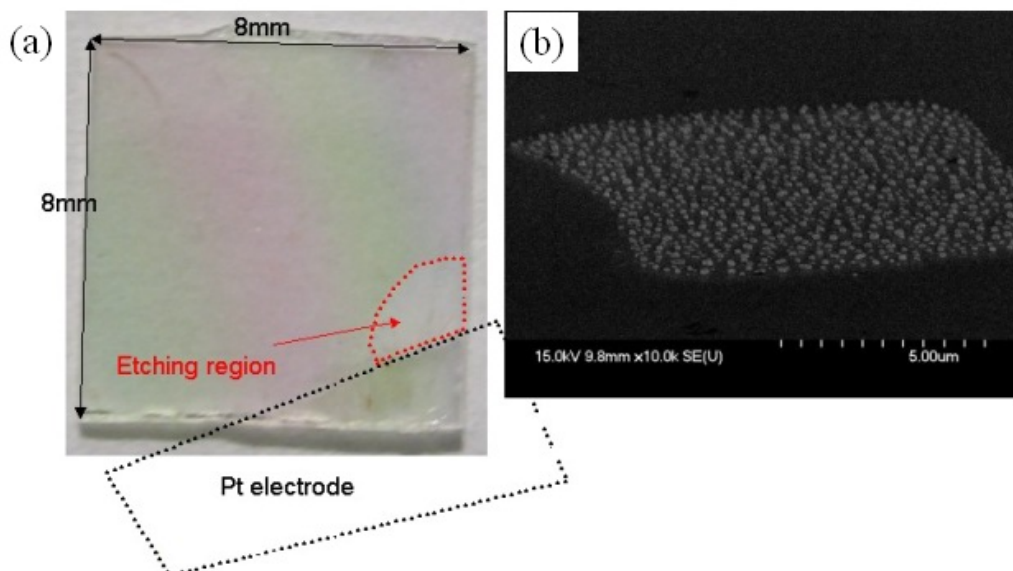
Figure 4.1.1.3.1 (a) optical microscopy after etching (b) SEM image of the hole-pattern after etching

The isolated mesa metal mask in the etching region was shown in Figure 4.1.1.3.2 (a). The etching condition was [*M:* **GaN** ,*P:* **900W** ,*E:* **0.1**,*O:* **0.05** ,*Ma:* **Ni/Au (10/10nm)**,*Ti:* **30**,*F:* **3k**,*T:***RT** ,*B:* **2.5**,*El:* **Pt**]. The dimension of the mask was about 10μm. The etching surface was very rough by this etching method as shown in Figure 4.1.1.3.2 (b). The cross-section profile from AFM measurement was shown in Figure 4.1.1.3.2 (c). The etching depth was about 50nm, but the roughness was higher than 50nm.
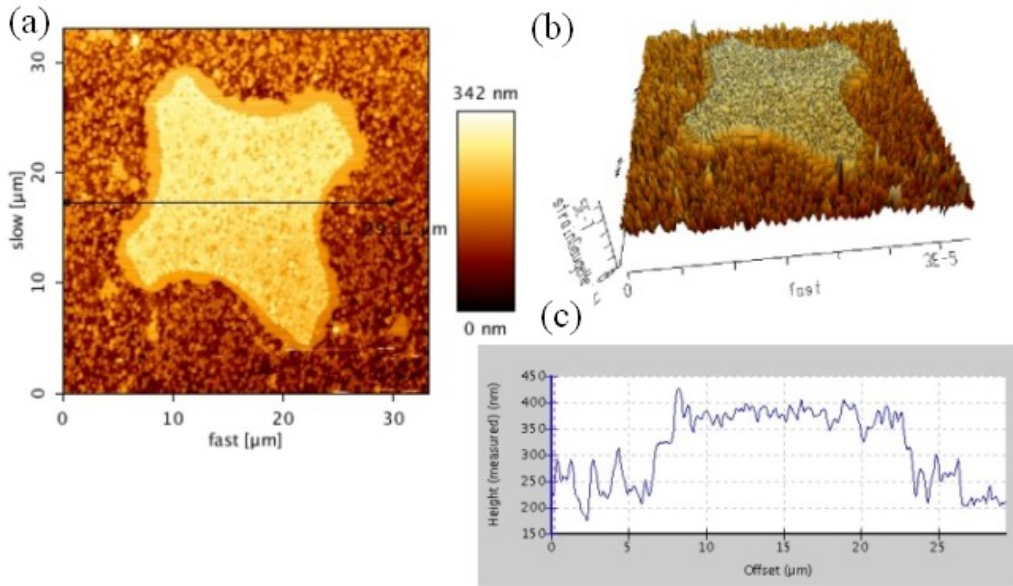
Figure 4.1.1.3.2 The etched profiles (a) AFM photography (b) 3D AFM image (c) profile of etched isolated pattern in (a)
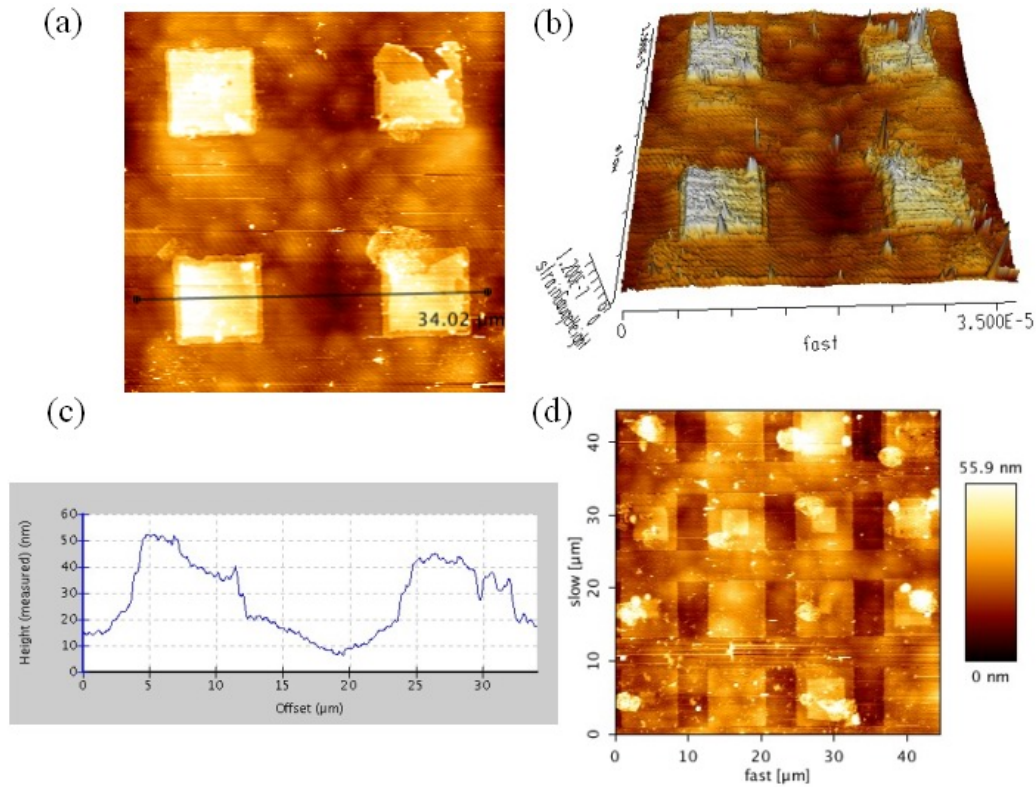
Figure 4.1.1.3.3 The surface morphology after etching (a) The AFM image of morphology (b) 3D AFM image (c) profile of etched pattern (d) The impurity deposition on Au pad.

The isolated mesa metal mask with 8μm x 8μm was shown in Figure 4.1.1.3.3 (a). The etching condition was [*M:* **LED** ,*P:* **900W** ,*E:* **0.1**,*O: ***0.1** ,*Ma:* **Ni/Au (10/10nm)**,*Ti:* **30**,*F:* **3k**,*T:***RT** ,*B:* **2.5**,*El:* **Pt**]. The p-type GaN preferred etching in grain boundary was shown in Figure 4.1.1.3.3 (a) and (b). The etching depth was about 10nm. The etching rate is very smooth with the isolated metal mask due to the low reduction current. There had some thing deposited on the Ni/Au metal mask as shown in Figure 4.1.1.3.3 (d).

4.1.1.4 BTELPEC-CS etching

The mesh mesa metal mask was design for BTELPEC-CS etching. The diagram of the BTELEPC-CS etching was shown in Figure 4.1.1.4.1 (a). The pattern of the photo mask with four different mesa sizes was shown in Figure 4.1.1.4.1 (b). The metal mesh was connected with a metal wire for voltage applied. The design of the photo mask was shown in Figure 4.1.4.1 (c).
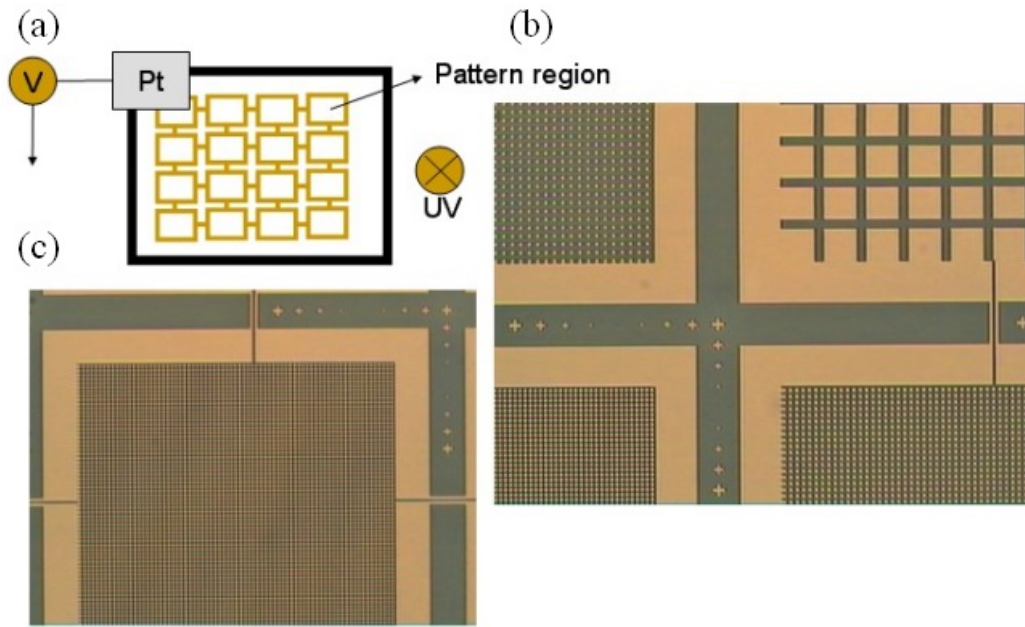
Figure 4.1.1.4.1 The mesh-metal design for BTELPEC-CS etching. (a) diagram (b) four mesa size on photo mask (c) connecting wire between mesh on the photo mask

The LED structure was used for micro LED fabrication. The etching condition was [*M:* **LED** ,*P:* **900W** ,*E:* **0.1**,*O:* **0.1** ,*Ma:* **Ni/Au (10/10nm)**,*Ti:* ,*F*: **3k**,*T: 90* ,*B:* **1.2**,*El:* **Pt**], stir=100rpm. The Ni/Au metal mask was mesh-mesa metal mask. There had large scale etching hole on the LED. The hole size larger than $50\mu m$ as shown in Figure 4.1.1.4.2 (a) and Figure 4.1.1.4.2 (b). This large size of etched hole was an special phenomenon for photon assisted wet etching. The etching depth was larger than $2\mu m$. The p-type GaN layer and InGaN MQW was etching through. This effect was guessed at the "**bubble effect**". We find that there had much more bubble at the LED surface during etching. The Ni/Au mask was doesn't remove during etching as shown in Figure 4.1.1.4.2 (c). There had some etching hole on the un-masked region. The etching depth was larger than $1\mu m$. The etching rate is very high at the etched region. The p-type GaN layer was not etched with uniform etching depth.
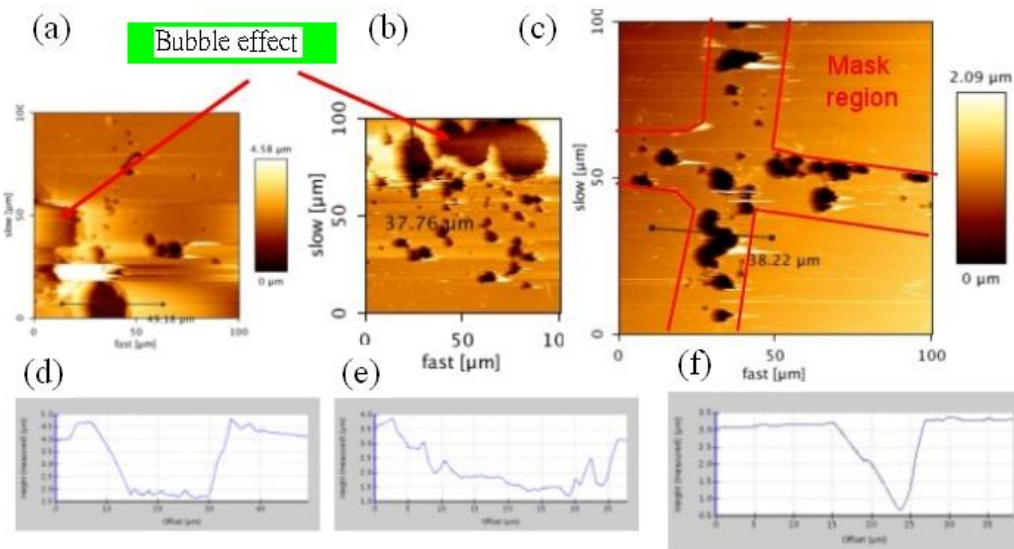
Figure 4.1.1.4.2 The etched profile of BTELPEC-CS etching (a) bubble effect (b) bubble effect (c) etching hole (d) cross-section of (a) (e) cross-section of (f) cross-section of (c)

The sample as shown in Figure 4.1.1.4.2 was used for etching again. The etching condition was [*M:* **LED** ,*P:* **900W** ,*E:* **0.1**,*O:* **0.1** ,*Ma:* **Ni/Au (10/10nm)**,*Ti:* ,*F:* **3k**,*T:* **90** ,*B:* **1.2**,*El:* **Pt**] stir=100rpm. After etching, the sample was scanned by AFM. There had very etching hole In large area scan as shown in Figure 4.1.1.4.3 (a). The etching depth about 1.4μm from the cross-section measurement of the etching hole was shown in Figure 4.1.1.4.3 (d). In small scan region, the metal mask was revealed by error signal from the AFM measurement as shown in Figure 4.1.1.4.3 (b). The 8 μm Ni/Au metal mask was shown in Figure 4.1.1.4.3 (c). The etching holes were observed between the masked regions. There had no etching occurred in none etching region as shown in Figure 4.1.1.4.3 (e). The p-type GaN layer on LED was etched in some regions. After some location of the p-type layer was etched, the etching rate was suppressed at close region of the p-type GaN. The holes will diffuse to the InGaN MQW and n-type GaN. The etching rate of the p-type GaN with UV photon irradiation will be suppressed.
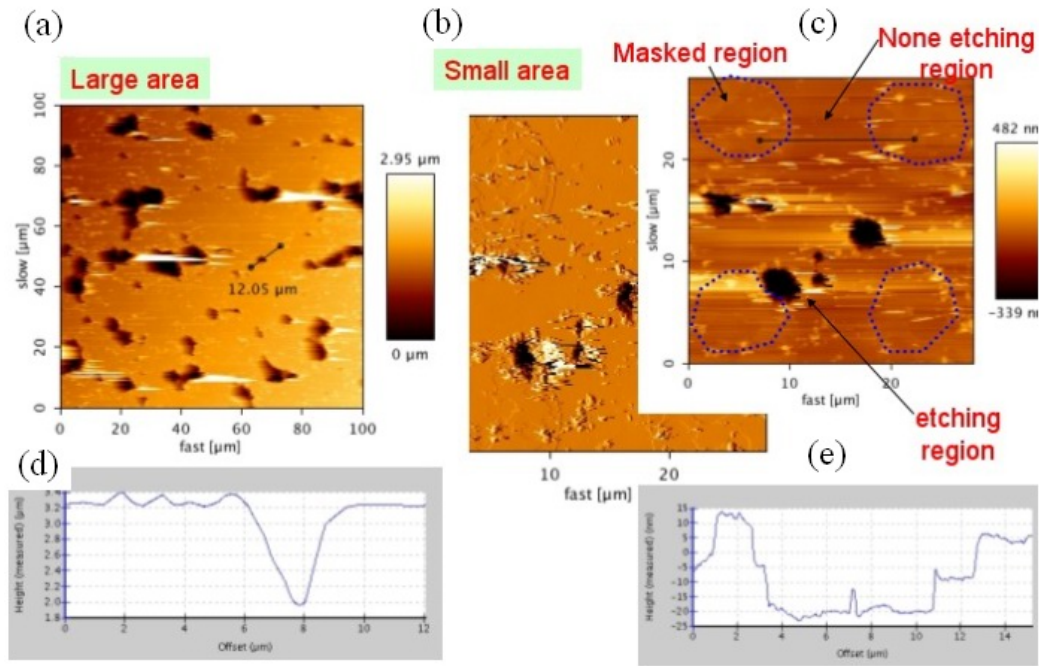
Figure 4.1.1.4.3 The etched profile of BTELPEC-CS etching measured by AFM (a) large scan area (b) small scan area (c) etching hole (d) cross-section of (a) (e) cross-section of (c)

The hole-pattern was used for BTELPEC-CS etching III-Nitride LED. The etching condition was [*M:* **LED** ,*P:* **900W** ,*E:* **0.1**,*O:* **0.1** ,*Ma:* **Ni/Au (10/10nm)**, *Ti:* ,*F:* **3k**,*T:* **90** ,*B:* **1.2**,*El:* **Pt**] stir=100rpm. The mask distortion was shown in Figure 4.1.1.4.4 (a) after etching. The mask distortion was due to the error in metal mask formation process. The periodic etched hole was shown in Figure 4.1.1.4.4 (b) and (c). The etching depth was about 3μm from the cross-section of the circle hole pattern etching as shown in Figure 4.1.1.4.4 (f). The error signal image from the AFM measurement was shown in Figure 4.1.1.4.4 (d). The metal mask could be revealed by the error signal image. The p-type layer inside the metal hole-pattern was not etched uniform. There had some was none etched inside the hole- pattern from the cross-section measurement as shown in Figure 4.1.1.4.4 (c). The none etching region will hinder the LED fabrication.
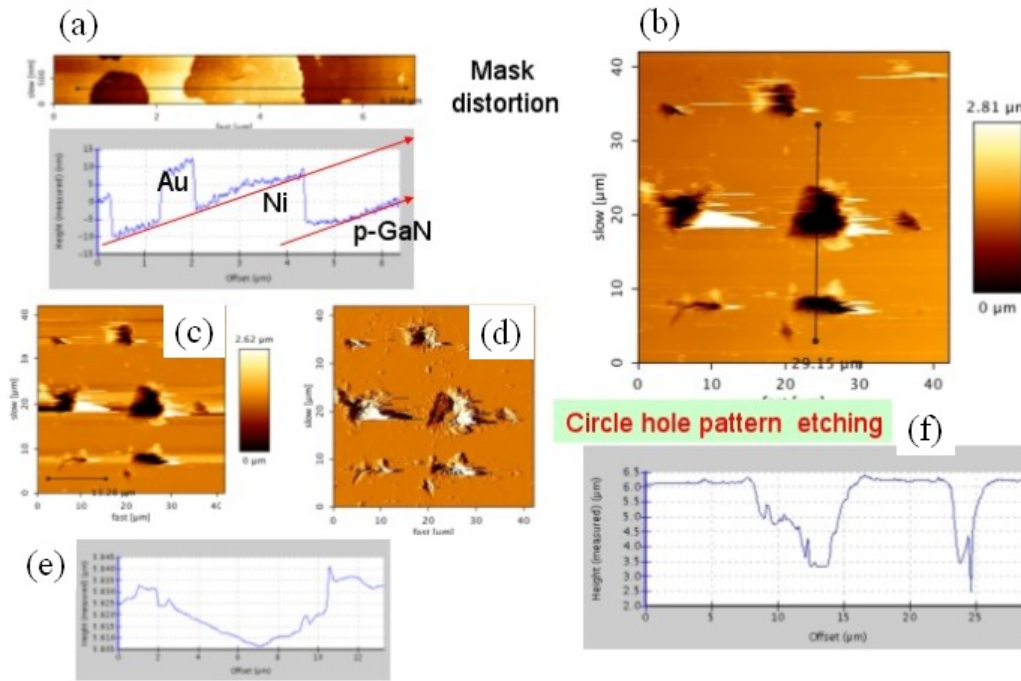
Figure 4.1.1.4.4 The etched profile of BTELPEC-CS etching measured by AFM (a) mask distortion (b) hole-pattern (c) hole-pattern (d) error signal of hole-pattern (e) cross-section of (c) (f) cross-section of (b)

For LED fabrication, the sample as shown in Figure 4.1.1.4.4 was used for etching again. The etching condition was [*M:* **LED** ,*P:* **900W** ,*E:* **0.1**,*O:* **0.1** ,*Ma:* **Ni/Au (10/10nm)**,*Ti:* **30**,*F:* **3k**,*T:* **90** ,*B:* **1**,*El:* **Pt**] stir=100rpm. The etched hole array was fabricated as shown in Figure 4.1.1.4.5 (a). The 3D AFM image was shown in Figure 4.1.1.4.5 (b). The etching depth was 1.5 μm from the cross-section AFM image as shown in Figure 4.1.1.4.5 (a)
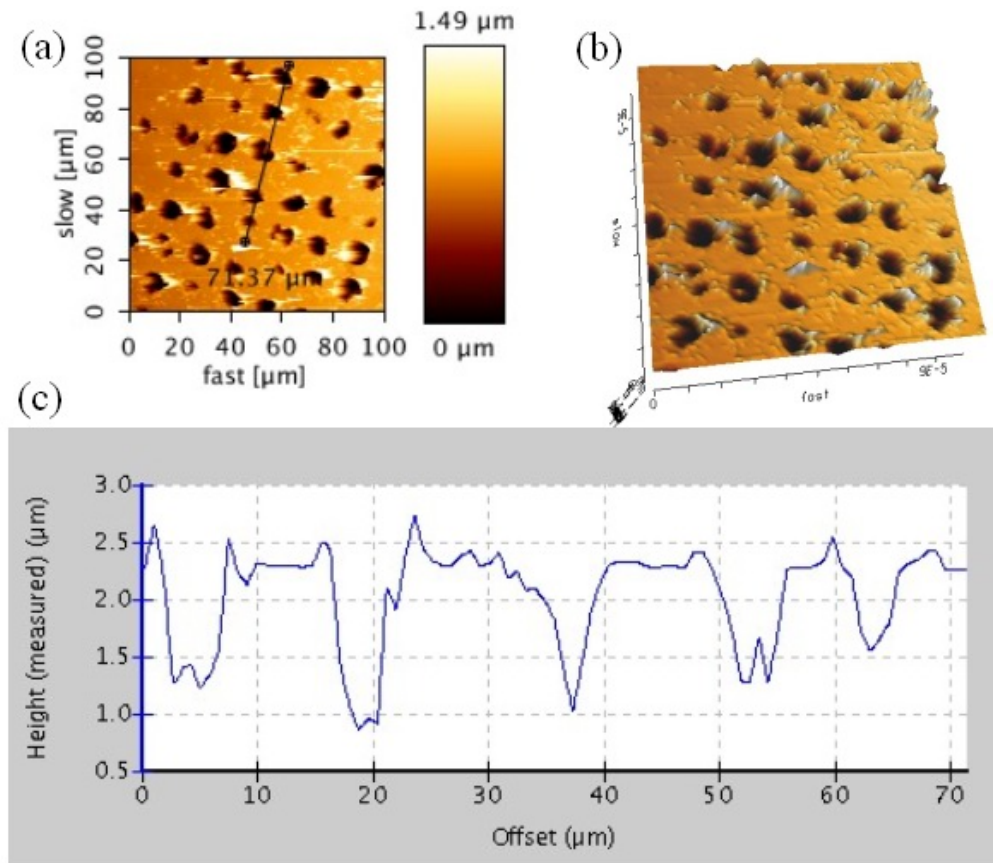
Figure 4.1.1.4.5 The etched profile of BTELPEC-CS etching measured by AFM (a) periodic etched hole (b) 3D AFM image (c) cross-section of (a)

With prolonged etching LED, the p-type GaN layer will be etched with mesh-mesa metal mask. The etching condition was [*M:* **LED** ,*P:* **900W** ,*E:* **0.1**,*O:* **0.1** ,*Ma:* **Ni/Au (10/10nm)**,*Ti:* **30**,*F*: **3k**,*T:* **90** ,*B:* **1**,*El:* **Pt**] stir=100rpm. The p-type GaN layer was not etched clearly between metal masks as shown in Figure 4.1.1.4.6 (a) in 8 μm mesa masks. In 80 μm mesa masks as shown in Figure 4.1.1.4.6 (b), the unmasked p-type GaN layer was not removed clearly also. The etching depth was 3 μm as shown in Figure 4.1.1.4.6 (a)
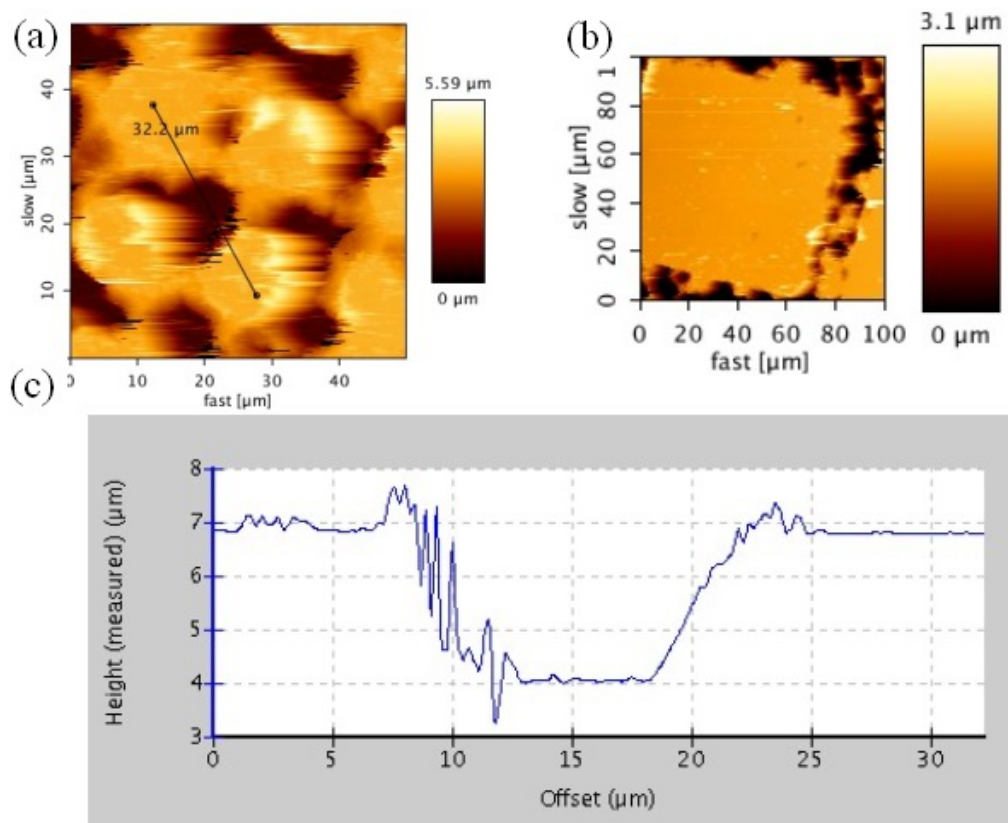
Figure 4.1.1.4.6 The etched profile of BTELPEC-CS etching measured by AFM (a) 8 μm mesa mask (b) 80 μm mesa mask (c) cross-section of (a)

The SEM image of the mesa structure LED was shown in Figure 4.1.1.4.7 (a). The SEM image of the mesa structure LED array was shown in Figure 4.1.1.4.7 (b). The SEM image of the hole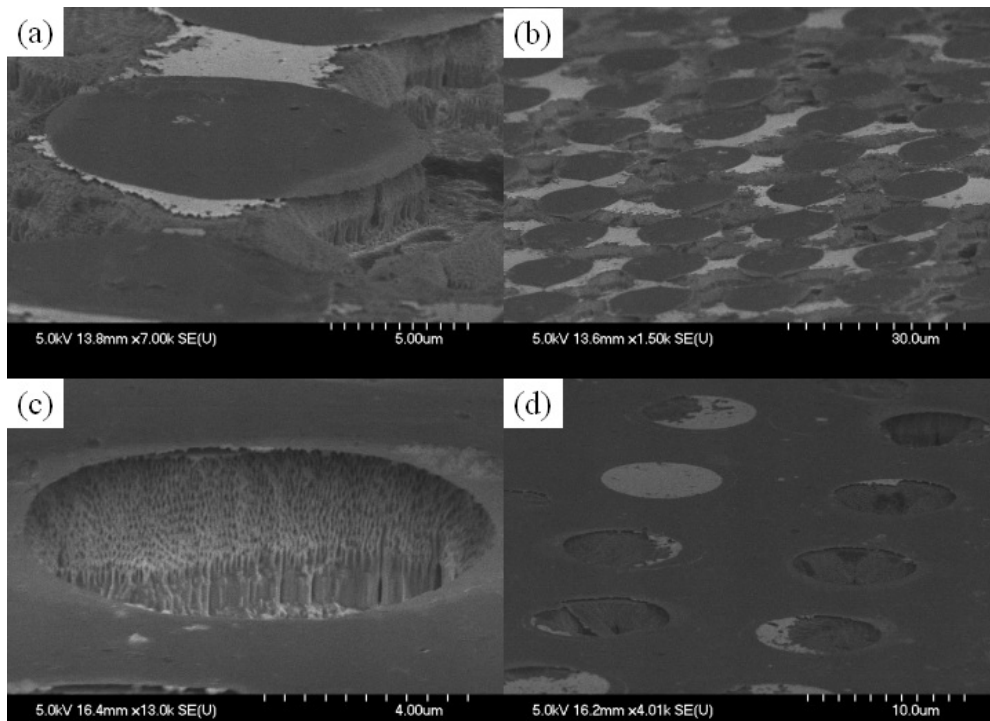-pattern structure of LED was shown in Figure 4.1.1.4.7 (c). The SEM image of the hole-pattern array structure of LED was shown in Figure 4.1.1.4.7 (d).

Figure 4.1.1.4.7 SEM image of etched profile (a) 8 μm mesa LED (b) mesa LED array (c) hole-pattern (d) hole-pattern array.
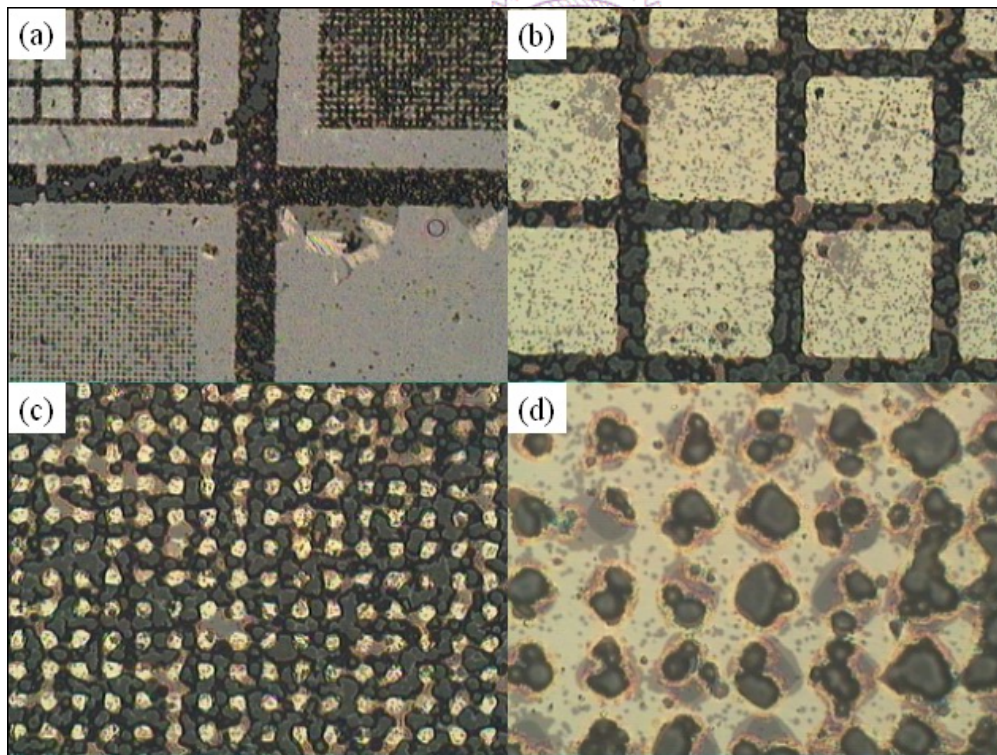
Figure 4.1.1.4.8 The optical microscopy after BTELPEC-CS etching (a) mesh-mesa structure (b) 80μm LED mesa array (c) 8 μm LED mesa array (d) 8 μm hole-pattern array.

The optical microscopy after BTELPEC-CS etching was shown in Figure 4.1.1.4.8. The etched mesh-mesa structure was shown in Figure 4.1.1.4.8 (a). The etched 80μm LED

mesa array was shown in Figure 4.1.1.4.8 (b). There had some none etched p-type GaN between the mesa. The etched 8 μm LED mesa array was shown in Figure 4.1.1.4.8 (c). There had some none etched p-type GaN between the mesa also. The etched 8 μm hole-pattern array was shown in Figure 4.1.1.4.8 (d). Some regions of the p-type GaN layer inside the hole-pattern were not etched.

The sample as shown in Figure 4.1.1.4.7 was post-treatment with 1M, KOH for 1mins with 90^0C solution temperature. After post treatment, the Ti (10nm)/Al(100nm) multi layer metal was deposited. The SEM image of the mesa structure LED was shown in Figure 4.1.1.4.9 (a). The undercut was observed and the sidewall was smooth after post treatment. The hole-pattern array was also achieved. The mesa LED array was observed in Figure 4.1.1.4.9 (c)
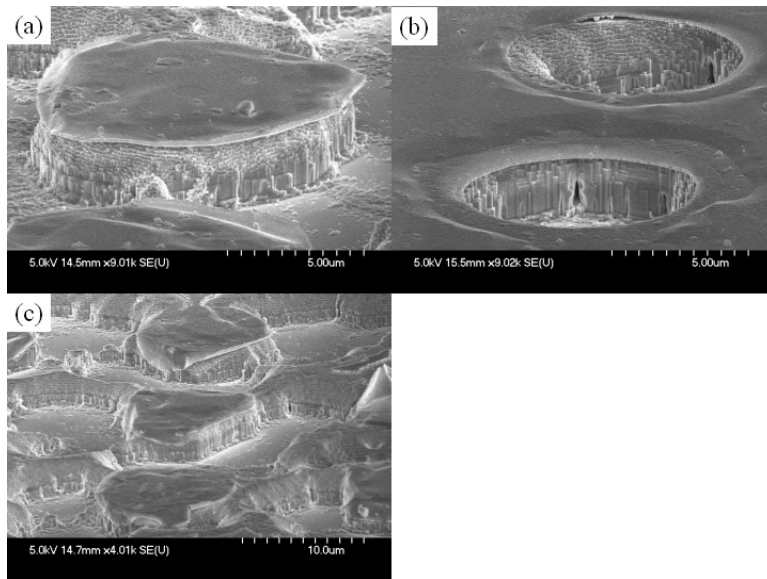
Figure 4.1.1.4.9 SEM image of etched profile with post-treatment (a) 8 μm mesa LED (b) hole-pattern array (c) mesa LED array

During the BTELPEC-CS etching, the solution was filled with bubble near the LED surface. The etching condition was [*M:* **LED** ,*P:* **900W** ,*E:* **0.1**,*O:* **0.1** ,*Ma:* **Ni/Au (10/10nm)**,*Ti:* **30**,*F:* **3k**,*T:* **90** ,*B:* **1**,*El:* **Pt**] stir=100rpm. The bubble was appeared during the BTELPEC-CS etching as shown in Figure 4.1.1.4.10 (b). The bubble was disappeared while the bias was change to zero as shown in Figure 4.1.1.4.10 (a). What is the role playing of the bubble during etching was unclear now. The mechanism was under research. The sample was contact with the Pt electrode as shown in Figure 4.1.1.4.10
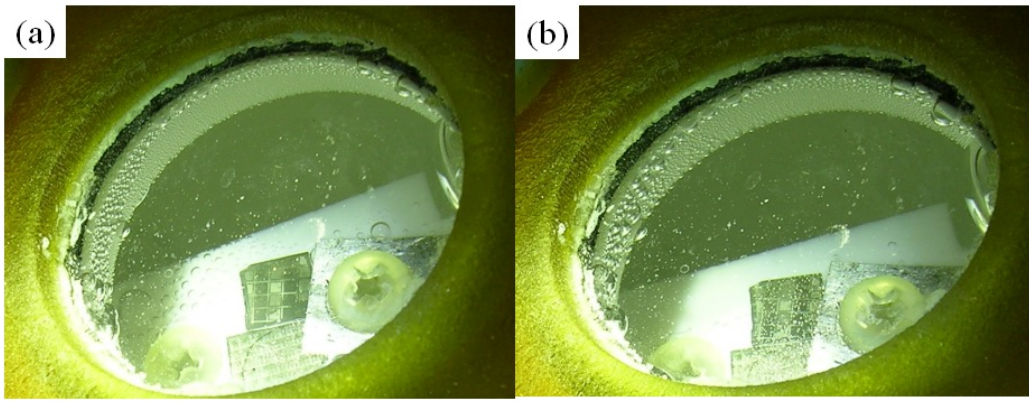
Figure 4.1.1.4.10 The optical microscopy of the LED surface during BTELPEC-CS etching (a) without bias applied (b) with bias applied

The SEM microscopy of the LED after BTELPEC-CS etching was shown in Figure 4.1.1.4.11. The 15μm hole pattern with 500nm grid was shown in Figure 4.1.1.4.11 (a). The under cut of NiAu on p-type GaN in the grid region was shown in Figure 4.1.1.4.11 (b). The hole-pattern array was shown in Figure 4.1.1.4.11 (c). The n-type GaN etched surface had the crystallography etching surface as shown in Figure 4.1.1.4.11 (d) The etching condition was [*M:* **LED** ,*P:* **900W** ,*E:* **1**,*O:* **0.1** ,*Ma:* **Ni/Au (10/10nm)**,*Ti:* **30**,*F:* **3k**,*T:* **90** ,*B:* **1**,*El:* **Pt**] stir=100rpm.
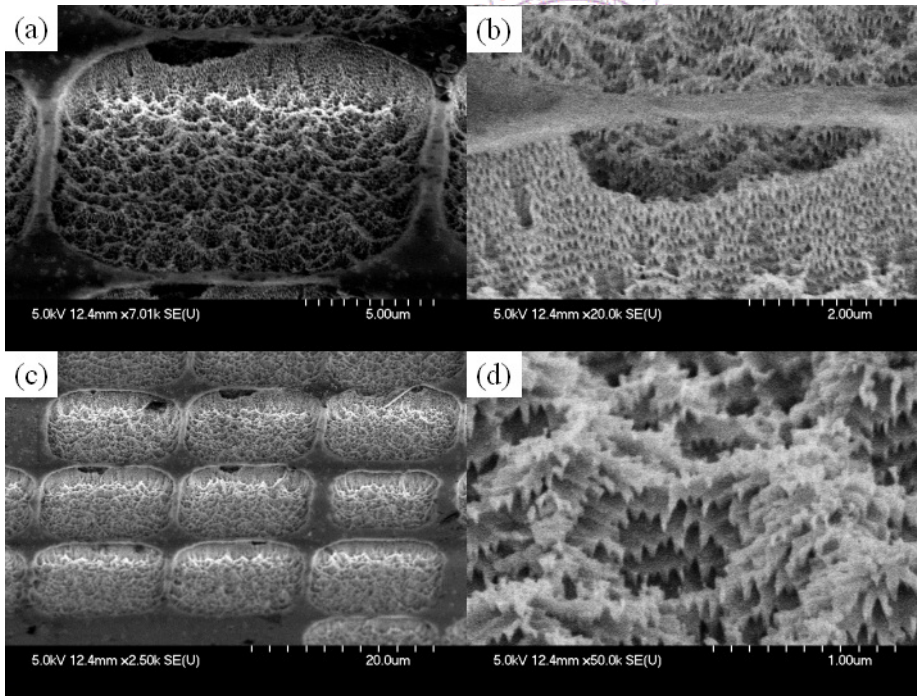
Figure 4.1.1.4.11 The SEM microscopy of the LED after BTELPEC-CS etching (a) hole-pattern (b) under cut of NiAu on p-type GaN. (c) hole-pattern array (d) n-type GaN etched surface
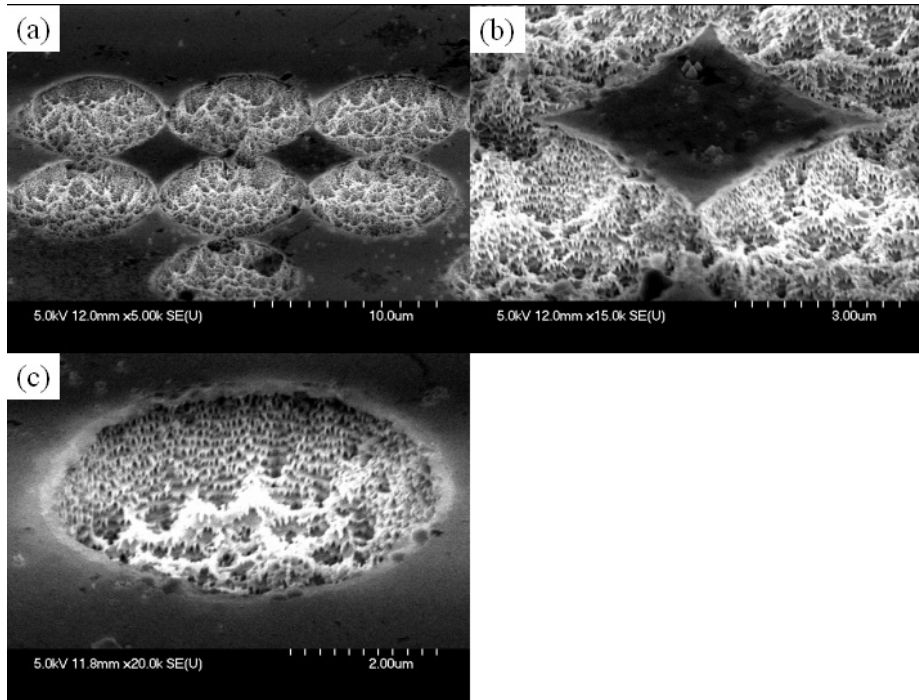
Figure 4.1.1.4.12 The SEM microscopy of the LED after BTELPEC-CS etching (a) mesh-mesa metal mask (b) mesa structure of LED. (c) 4μm hole-pattern

The SEM microscopy of the LED after BTELPEC-CS etching was shown in Figure 4.1.1.4.12. The mesh-mesa metal mask was shown in Figure 4.1.1.4.12 (a). The NiAu mask was formed by over wet etching of NiAu under PR during photolithography process. The under cut of mesa structure LED was shown in Figure 4.1.1.4.12 (b). The micro scale hole-pattern was shown in Figure 4.1.1.4.12 (c). The etching condition was [*M:* **LED** ,*P:* **900W** ,*E:* **1**,*O:* **0.1** ,*Ma:* **Ni/Au (10/10nm)**,*Ti:* **30**,*F:* **3k**,*T:* **90** ,*B:* **1**,*El:* **Pt**] stir=100rpm.
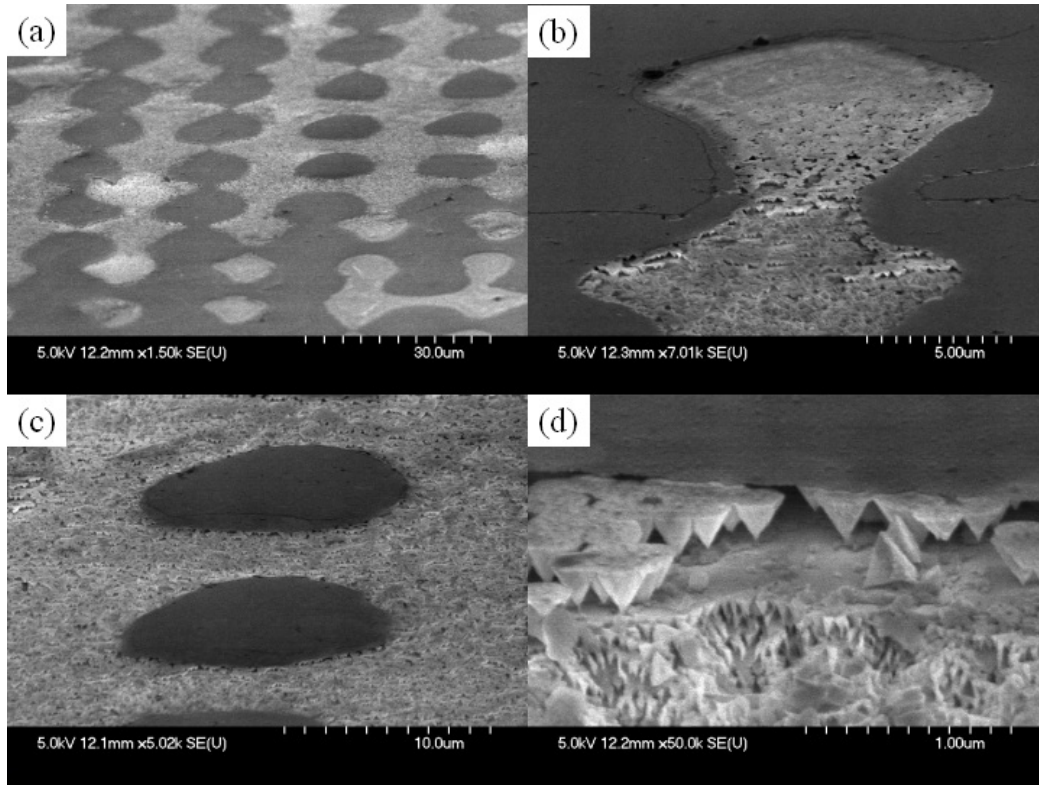
Figure 4.1.1.4.13 The SEM microscopy of the LED after BTELPEC-CS etching (a) mesh-mesa metal mask (b) none isolated in mesh-mesa metal mask (c) isolated mesa LED (d) the etched profile near the metal mask

The SEM microscopy of the LED after BTELPEC-CS etching was shown in Figure 4.1.1.4.13. The mesh-mesa metal mask was shown in Figure 4.1.1.4.13 (a). The non-isolated NiAu mask in mesh mesa metal mask was formed after photolithography process as shown in Figure 4.1.1.4.13 (b). The isolated NiAu mask in mesh mesa metal mask was formed after photolithography process as shown in Figure 4.1.1.4.13 (c). The under cut of mesa structure LED was shown in Figure 4.1.1.4.13 (d). The etching condition was [*M:* **LED** ,*P:* **900W** ,*E:* **1**,*O:* **0.1** ,*Ma:* **Ni/Au (10/10nm)**,*Ti:* **30**,*F:* **3k**,*T:* **90** ,*B:* **1**,*El:* **Pt**] stir=100rpm.

4.1.2 Nano scale structure fabrication

The photon assisted wet etching could produce the nano structure of II-Nitride. The methods including PEC etching, ELPEC etching and ELPEC-CS etching was shown in the section.

4.1.2.1 PEC etching

The dislocation had high recombination velocity then the crystalline GaN. By controlling the photon intensity and solution concentration. The selective etching between dislocation and crystalline could be achieved. The dislocation revealed dislocation was shown in Figure 4.1.2.1.1 (a). The width of the dislocation was <90nm.

From the top view SEM in Figure 4.1.2.1.1 (b), the dislocation was not along the <0001>. The dislocation was mixed type screw dislocation. The selective etching dislocation was shown in Figure 4.1.2.1.1 (c). The etching pits was about 90nm. The dislocation density was about 10^8-10^9cm^{-2}.
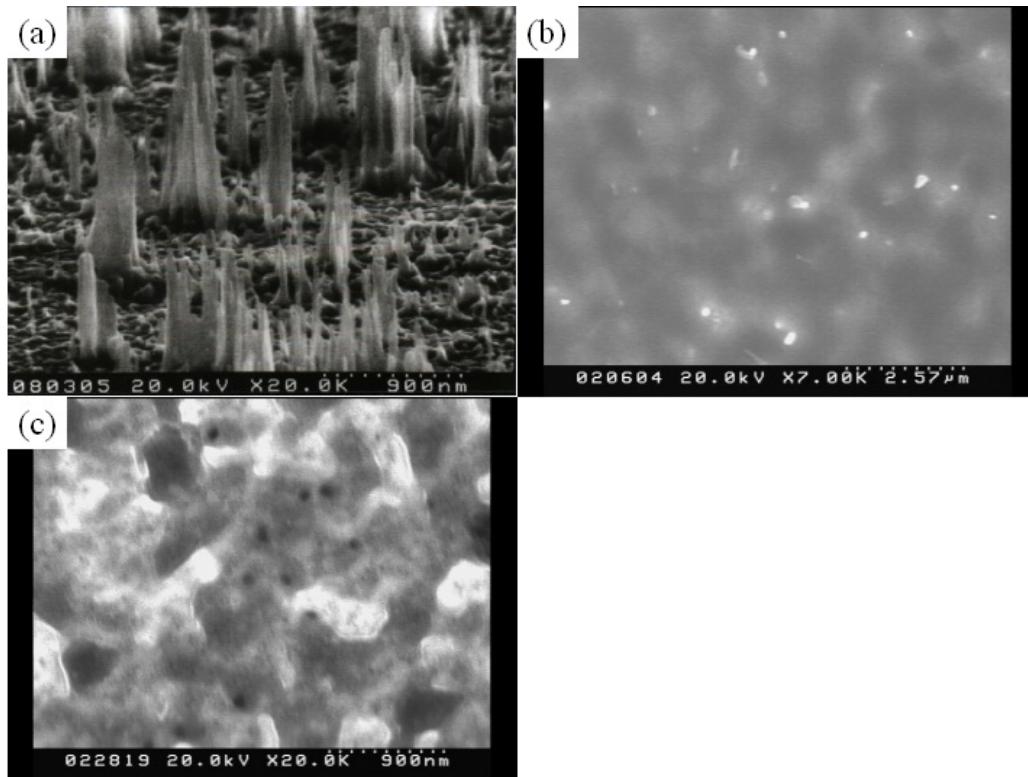

Figure 4.1.2.1.1 Dislocation formation in GaN by selective etching (a) dislocation reveal (b) top view of dislocation (c) etched pits

The nano structure will form at the specific etching condition. There will have small hillocks after etching as shown in Figure 4.1.2.1.2 (a). The based size of the hillocks will grow after prolonged etching as shown in Figure 4.1.2.1.2 (b). The size was about 90nm at the top of hillocks. The density of the hillocks was about 10^{11}cm$^{-2.}$ The origin of the hillocks formation was different from the dislocation reveal. The boiled KOH was used to treat the PEC etching GaN. An nano rod with size 90nm and 1μm height was observed in the experiment as shown in Figure 4.1.2.1.2 (c). The origin of the nano rod formation was unknown. But it had shown the possibility for make a good nano rod by this
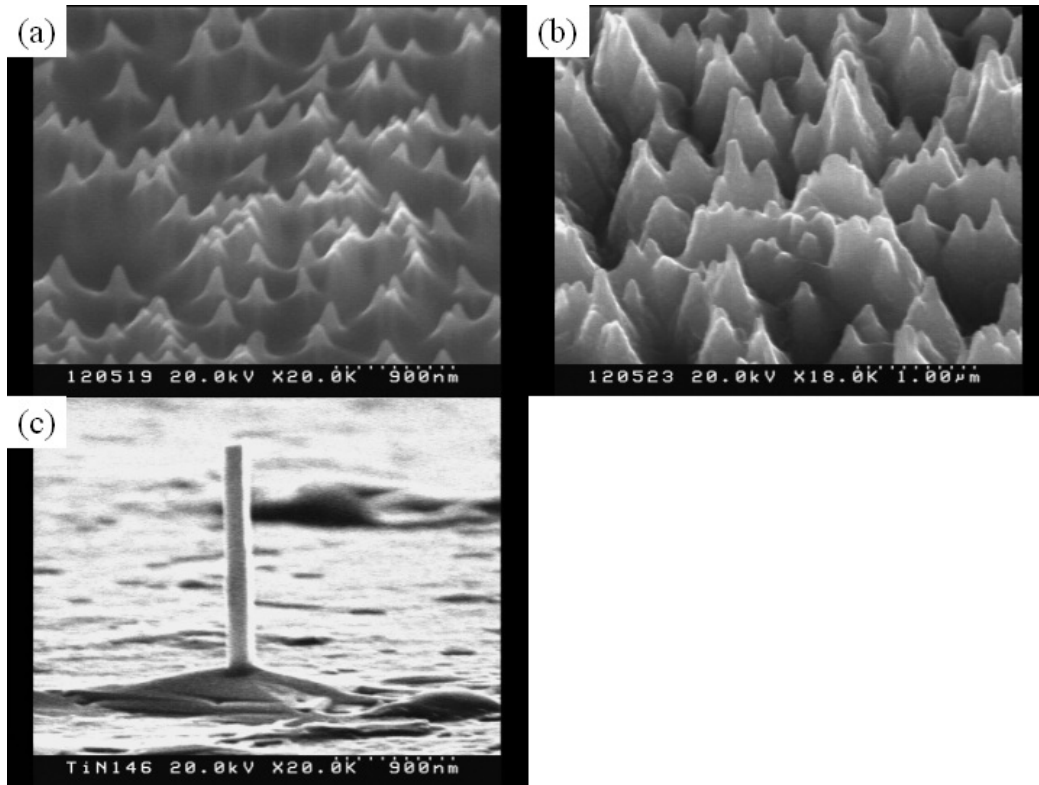method.

Figure 4.1.2.1.2 GaN nano rod formation by PEC etching (a) nano hillock formation (b) prolong etching (c) hot KOH treatment

The selective etching with others of defect was also revealed by PEC etching and boiled KOH treatment. The pinhole defect was observed after PEC etching as shown in Figure 4.1.2.1.3 (a). The size of the pinhole was 300nm. After boiled KOH etching, the hexagonal shape etching pits was observed as shown in Figure 4.1.2.1.3 (b) and (c).
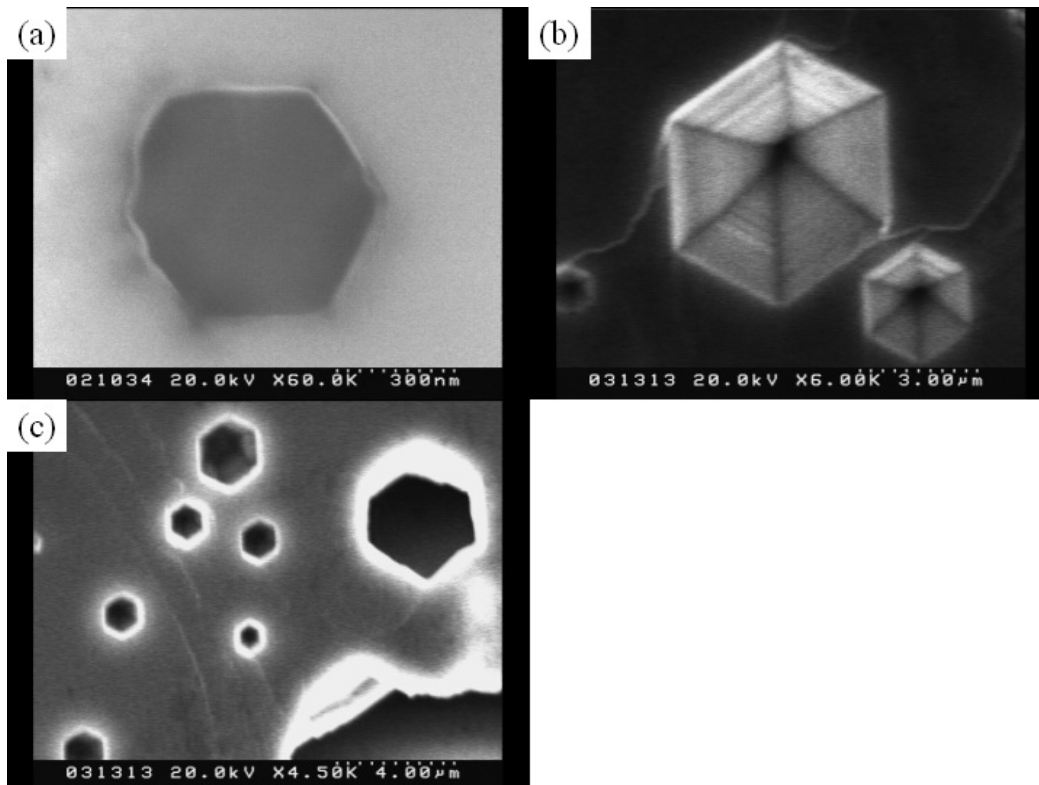
Figure 4.1.2.1.3 Etching pits formation (a) Pinhole formation by PEC etching (b) etching pits formation by boiled KOH (c) etching pits formation by boiled KOH.
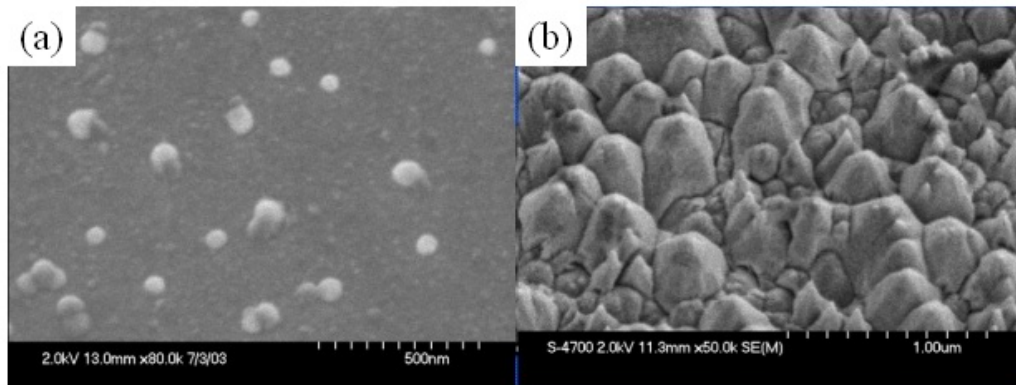
4.1.2.2 ELPEC etching

Figure 4.1.2.2.1 Nano structure formation with Ti mask by ELPEC etching in GaN (a) Pore formation (b) pyramid structure

The ELPEC etching was applied to etching GaN. In the early stage of the GaN etching. The 50-100nm pore was formation by ELPEC etching as shown in Figure 4.1.2.2.1 (a). After prolonged etching, the pyramid structure was form. The 300nm-500nm pyramids was formation as shown in Figure Figure 4.1.2.2.1 (b).

4.1.2.3 ELPEC-CS etching

The ELPEC-CS was used to etching the nano wire of p-type GaN on GaN. The etching condition was [*M:* **p-GaN/GaN** ,*P:* **109** ,*E:* **0.01**, *O:* **0.05** ,*Ma:* **Au (10nm)**, *Ti:*, *F*:

3k,*T:* **RT** ,*B:* ,*El:*]. The nano wire of p-type GaN was formation as shown in Figure 4.1.2.3.1 (a). The p-type GaN was not etching through. The nano wire cross the strip was shown in Figure 4.1.2.3.1 (b)
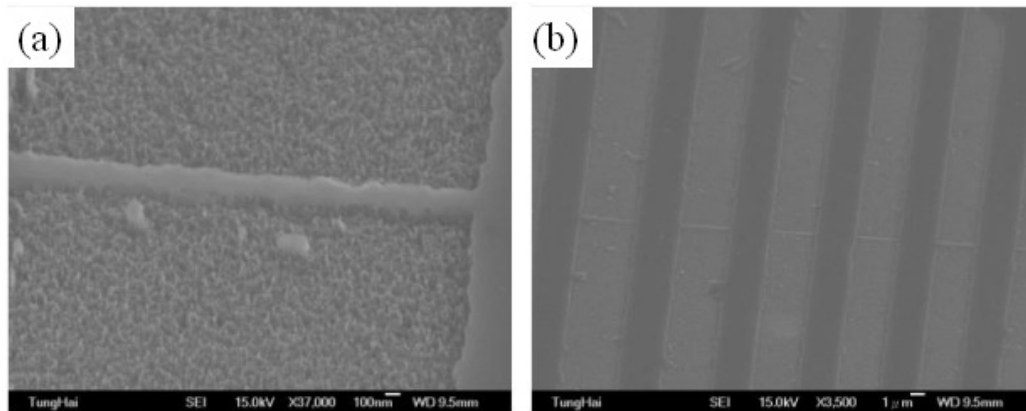

Figure 4.1.2.3.1 150nm Nano scale etching p-type GaN with Au mask by lithography.(a) nano wire (b) nano wire cross strip pattern

4.1.3 Quantum scale structure fabrication

The nano structure ranged between 1-10nm was achieved by ELPEC-CS etching.

4.1.3.1 ELPEC-CS etching

The GaN nano wire ~10nm was formed. The etching condition was [*M:* **GaN** ,*P:* **32** ,*E:* **0.04**,*O:* **0.05** ,*Ma:* **Ti/Pt (10nm/10nm)**,*Ti:***20**,*F:* **3k**,*T:* **RT** ,*B:* ,*El:*]. The etching mechanism was suggested as the porous structure formation principle. The nano-wire was shown in Figure 4.1.3.1.1.
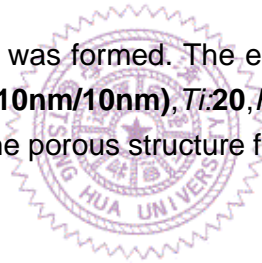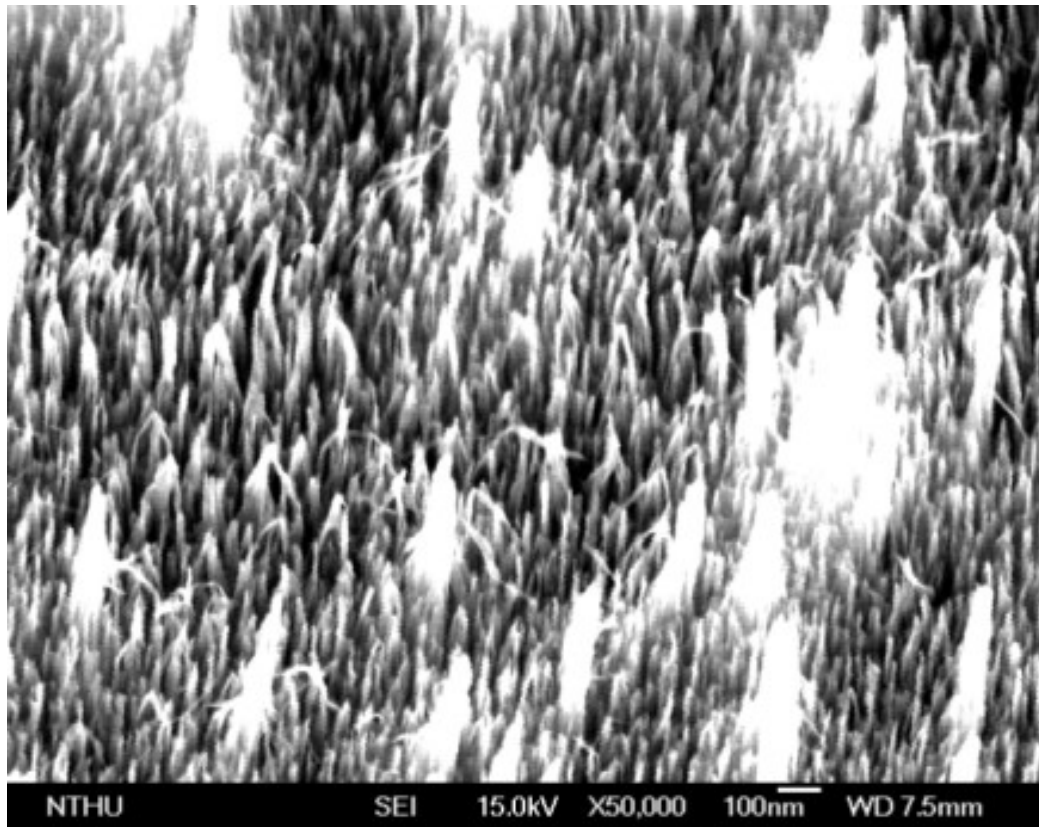
Figure 4.1.3.1.1 The GaN nano-wire formation

The p-type GaN nano rod ~10nm was formed. The etching condition was [*M: GaN* ,*P:* **32** ,*E:* **0.04**,*O:* **0.05** ,*Ma:* **Ti/Pt (10nm/10nm)**,*Ti:***20**,*F:* **3k**,*T:* **RT** ,*B:* ,*El:*]. The etching mechanism was suggested as the porous structure formation principle. The smooth Au mask and etched surface was shown in Figure 4.1.3.1.2. The nano rod was observed by AFM and SEM. The 3D AFM image was shown in Figure 4.1.3.1.2.(b) The SEM image was shown in Figure 4.1.3.1.2.(c)
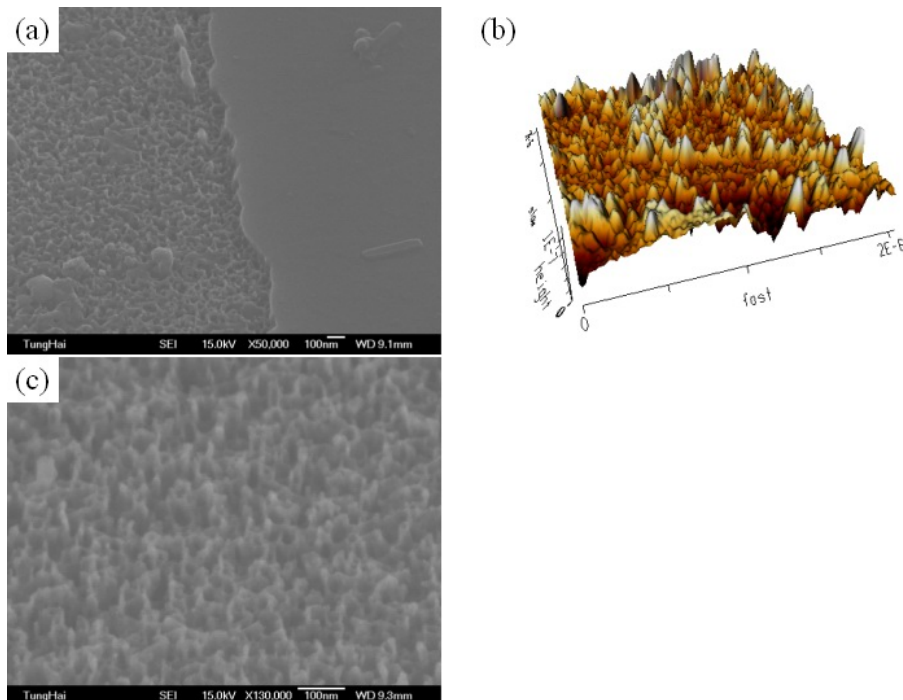
Figure 4.1.3.1.2 The p-type GaN nano-porous formation. (a) SEM image of the etched and Au masked region (b) 3D AFM image of etched surface (c) SEM image of etched surface.

4.2 Summary

In the report, various structure sizes were fabricated by various etching technology. The etching result was shown in Chapter 4.1. The size of III-Nitride based structure was fabricated from $300\mu m$ to 10nm. The LED structure from $300\mu m$ to $4\mu m$ could be formatted by photolithography following by etching. By controlling photolithography in diffraction mode or over etching the metal mask, the size could be reduced from $2\mu m$ to $.5\mu m$. The mesa GaN LED or P/N diode could be fabricated. The nano structure from 100 to 30nm of GaN could be formatted due to the dislocation-induced morphology during etching in photo-assisted wet etching. The structure with 50~10nm nano-wire could be fabricated in GaN or p-GaN during photo-assisted wet etching. The micro-LED was successfully fabricated. How to make the nano-LED with scale-down (100~0.1nm for nano scale) for III-Nitride was the major research in the future.